FUNDAMENTAL STUDY OF ALGINATE-BASED 3D PLATFORMS FOR THE PROPAGATION AND PANCREATIC DIFFERENTIATION OF HUMAN EMBRYONIC STEM CELLS

by

Thomas Charles Richardson

B.S. in Chemical Engineering, Texas A&M University, 2010

Submitted to the Graduate Faculty of

Swanson School of Engineering in partial fulfillment

of the requirements for the degree of

Doctor of Philosophy

University of Pittsburgh

2017

UNIVERSITY OF PITTSBURGH

SWANSON SCHOOL OF ENGINEERING

This dissertation was presented

by

Thomas Richardson

It was defended on

June 20, 2017

and approved by

Sachin Velankar, Ph.D., Associate Professor, Department of Chemical and Petroleum Engineering

Vijay Gorantla, M.D., Ph.D., Assistant Professor, Department of Plastic Surgery

Dissertation Co-Advisor: Prashant N. Kumta, Ph.D., Edward R. Weidlein Chair Professor, Department of Bioengineering

Dissertation Co-Advisor: Ipsita Banerjee, PhD, Associate Professor, Department of Chemical and Petroleum Engineering

FUNDAMENTAL STUDY OF ALGINATE-BASED 3D PLATFORMS FOR THE PROPAGATION AND PANCREATIC DIFFERENTIATION OF HUMAN EMBRYONIC STEM CELLS

Thomas Richardson, PhD

University of Pittsburgh, 2017

Type 1 diabetes (T1D) is an autoimmune disease affecting millions of people worldwide, wherein the insulin producing pancreatic islets are destroyed. Shortage of donor cells, combined with immune rejection, limits transplantation as a viable therapy. However, human pluripotent stem cells (hPSCs) have the capacity to become any cell type, and the potential to provide an unlimited supply of hPSC-derived insulin producing cells. Additionally, immune rejection is still a hurdle which must be overcome before hESC-based therapy for T1D can be brought to fruition. It is therefore necessary to develop suitable culture and differentiation strategies which employ cell encapsulation with an appropriate material which can protect the new insulin producing cells from the body's immune system and is supportive of hPSC biomanufacturing.

Alginate encapsulation has been previously used for providing the needed immune protection of donor insulin-producing cells for transplantation. Therefore, in this work we first showed that alginate encapsulation supports efficient differentiation of hPSCs to insulin producing cells, and also significantly enhanced maturation of hPSCs compared to 2D controls. Previous studies for islet encapsulation have also shown that alginate hydrogel composition significantly affects the capacity for immune isolation. However, such capsule compositions could modify the differentiation of the encapsulated cells. Thus, we next

evaluated the effect of capsule composition on material properties and thus on pancreatic differentiation of encapsulated hESCs. Our results clearly showed that even in the presence of chemical differentiation factors, substrate stiffness greatly affects the efficiency of pancreatic differentiation. Taking this a step further, we developed a high throughput 3D alginate array platform that allowed for multivariate perturbations of insoluble differentiation cues, namely alginate stiffness and cell-cell contact, during pancreatic differentiation. Our results accordingly indicated that while stiffness did influence proliferation and pancreatic differentiation, the effect of cell-cell contact was more significant.

Finally, we developed an e-cadherin mimicking peptide-conjugated alginate substrate which mimics cell-cell contact, to meet the biomanufacturing needs of hPSCs. The designed biomimetic substrate supported single cell survival and propagation, as well as maintained hPSC pluripotency and differentiation potency. Overall, the findings from this dissertation represent a significant advancement in strategies supporting the propagation and pancreatic differentiation for biomanufacturing of hPSCs as an effective cell therapy treatment for T1D.

TABLE OF CONTENTS

TABLE OF CONTENTS VI

LIST OF TABLES XII

LIST OF FIGURES XIII

PREFACE XVI

1.0 INTRODUCTION 1

1.1 TYPE 1 DIABETES 1

1.2 ALGINATE ENCAPSULATION 3

1.3 HUMAN PLURIPOTENT STEM CELLS 6

1.3.1 General Background and pancreatic differentiation 6

1.3.2 Alginate Encapsulation for the culture and differentiation of hPSCs 8

1.4 HUMAN PLURIPOTENT STEM CELL BIOMANUCFACTURING AND LARGE SCALE CULTURE 11

1.4.1 Current approaches for large scale hPSC biomanufacturing 12

1.5 SPECIFIC AIMS 13

1.5.1 Specific Aim 1: To evaluate the feasibility of obtaining hPSC derived pancreatic cell types under encapsulation. 14

1.5.2 Specific Aim 2: To determine the effect of cell physical microenvironment on the pancreatic differentiation of hPSCs. 14

1.5.3 Specific Aim 3: To develop a synthetic biomimetic substrate for supporting single cell viability and biomanufacturing of hPSCs. 15

2.0 ALGINATE ENCAPSULATION OF HUMAN EMBRYONIC STEM CELLS TO ENHANCE DIRECTED DIFFERENTIATION TO PANCREATIC ISLET-LIKE CELLS 16

2.1 INTRODUCTION 16

2.2 MATERIALS AND METHODS 19

2.2.1 Cell Culture 19

2.2.2 hESC Encapsulation 20

2.2.3 Differentiation of Encapsulated hESCs 20

2.2.4 Viability 21

2.2.5 Proliferation 21

2.2.6 Quantitative reverse transcription polymerase chain reaction 21

2.2.7 MagPix 22

2.2.8 Glucose Stimulated Hormone Release 23

2.2.9 Western Blot 23

2.2.10 Flow Cytometry 24

2.2.11 Immunostaining 24

2.2.12 Statistical Analysis 25

2.3 RESULTS 26

2.3.1 Pancreatic differentiation and characterization of hESCs 26

2.3.2 Encapsulation of predifferentiated hESC results in low yield of viable cells 30

2.3.2.1 Viability and Proliferation. 30

2.3.2.2 Effect of Encapsulation on hESC Maturation 33

2.3.3 Encapsulation of undifferentiated hESCs results in high viability and strong islet-specific maturation 34

2.3.3.1 Viability and Proliferation 34

2.3.3.2 Differentiation under Encapsulation 36

2.3.3.3 Intracellular C-peptide and Glucagon content and release 40

2.3.3.4 Enhanced differentation is likely due to increased pSmad/pAKT ratio 42

2.4 DISCUSSION 45

2.5 CONCLUSIONS 51

3.0 CAPSULE STIFFNESS REGULATES THE EFFICIENCY OF PANCREATIC DIFFERENTIATION OF HUMAN EMBRYONIC STEM CELLS 53

3.1 INTRODUCTION 53

3.2 MATERIALS AND METHODS 56

3.2.1 Human embryonic stem cell culture 56

3.2.2 Barium alginate encapsulation of hESCs 56

3.2.3 Barium alginate capsule characterization 57

3.2.4 Differentiation of encapsulated hESCs 58

3.2.5 Cell viability 58

3.2.6 Image analysis 59

3.2.7 hESC proliferation and death 59

3.2.8 qRT-PCR for gene expression analysis 60

3.2.9 MagPix for TGFβ pathway signaling analysis 60

3.2.10 Immunostaining 61

3.2.11 Statistical analysis 61

3.3 RESULTS 62

3.3.1 Barium alginate stiffness, and not diffusion, affects encapsulated hESCs 62

3.3.2 Capsule stiffness suppresses the growth dynamics of encapsulated hESCs. 64

3.3.3 Increasing capsule stiffness supports DE differentiation, while suppressing PP differentiation 68

3.3.4 Capsule Properties impact signaling at both the DE and PP stage 74

3.4 DISCUSSION 80

3.5 CONCLUSIONS 87

4.0 DECOUPLING THE EFFECT OF MULTIPARAMETRIC PERTUBATIONS ON HUMAN PLURIPOTENT STEM CELLS DURING PANCREATIC DIFFERENTIATION 88

4.1 INTRODUCTION 88

4.2 METHODS 91

4.2.1 Human embryonic stem cell culture 91

4.2.2 Alginate array formation and hESC encapsulation 92

4.2.3 hESC differentiation 93

4.2.4 Atomic Force Microscopy 93

4.2.5 Viability 94

4.2.6 DNA and protein immunostaining and quantification using LICOR 94

4.2.7 Regression analysis 94

4.3 RESULTS 96

4.3.1 3D alginate array formation 96

4.3.2 3D alginate array characterization 98

4.3.3 hESC growth and viability in the alginate array during pancreatic differentiation 101

4.3.4 Quantitative analysis of growth and proliferation in the alginate array during pancreatic differentiation 105

4.3.5 Pancreatic differentiation in the alginate array 110

4.3.6 Statistical analysis to identify best predictors of proliferation and differentiation 115

4.4 DISCUSSION 117

4.5 CONCLUSIONS 124

5.0 ENGINEERED PEPTIDE MODIFIED HYDROGEL PLATFORM FOR BIOMANUFACTURING OF HUMAN PLURIPOTENT STEM CELLS 125

5.1 INTRODUCTION 125
5.2 MATERIALS AND METHODS 130
5.2.1 hPSC Culture 130
5.2.2 Thin Alginate Hydrogel formation and peptide conjugation 130
5.2.3 Cell Attachment 131
5.2.4 LIVE/DEAD Assay 131
5.2.5 Cell Expansion 131
5.2.6 Directed Differentiation 132
5.2.7 Quantitative Reverse Transcriptase Polymerase Chain Reaction 132
5.2.8 Immunostaining 133
5.2.9 Statistical Analysis 133
5.3 RESULTS 134
5.3.1 Substrate Design and Characterization 134
5.3.2 hESC Attachment to Peptide Conjugated Alginate hydrogel 135
5.3.3 hESC Viability and expansion potential after propagation 137
5.3.4 hESC Pluripotency on Peptide Modified Substrate 141
5.3.5 hESC Differentiation Potential 143
5.3.6 Cell Attachment and Pluripotency using Peptide combinations 145
5.4 DISCUSSION 148
5.5 CONCLUSIONS 152
6.0 OVERALL CONCLUSIONS AND FUTURE WORK 153
6.1 AIM 1: ALGIANTE ENCAPSULATION AS A PLATFORM FOR THE PANCREATIC DIFFERENTIATION OF HPSCS 153
6.2 AIM 2: THE EFFECT OF ALGIANTE CAPSULE PROPERTIES ON THE PANCREATIC DIFFRENTIATION OF HPSCS 155

6.3 AIM3: PEPTIDE MODIFIED ALGINATE FOR THE PROPAGATION AND DIFFERENTATION OF HESC 159

BIBLIOGRAPHY 163

LIST OF TABLES

Table 1. E-cadherin mimicking peptides and sequences. 129

LIST OF FIGURES

Figure 1.1 Schematic of Islet of Langerhans anatomy [3]. 2

Figure 1.2. Schematic of alginate structure and immunoisolation. 4

Figure 1.3. Schematic of hESC differentiation [39]. 7

Figure 1.4. Schematic of culture stimuli which can influence hPSC fate [60]. 10

Figure 2.1. Stage-wise differentiation protocol for deriving mature islet-like cell types from hESCs 27

Figure 2.2. Characterization of mature islet-like cells before encapsulation. 28

Figure 2.3. Definitive endoderm characterization prior to encapsulation. 29

Figure 2.4. Schematic showing the process of calcium alginate encapsulation of hESCs 30

Figure 2.5. Characterization of encapsulated predifferentiated hESCs. 32

Figure 2.6. Viability and proliferation of hESCs encapsulated at the undifferentiated stage. 35

Figure 2.7. Characterization of the definitive endoderm and pancreatic progenitor stage for hESCs encapsulated at the undifferentiated stage. 37

Figure 2.8. Characterization of mature islet-like cells, encapsulated as undifferentiated hESCs. 39

Figure 2.9. Pancreatic islet Hormone localization. 40

Figure 2.10. Intracellular protein quantification and glucose sensing. 41

Figure 2.11. Characterization of enhanced differentiation for cells encapsulated as UD hESCs. 44

Figure 3.1. Schematic of AFM microindentation for hydrogel stiffness measurements 57

Figure 3.2. Characterization of Barium alginate capsule. 63

Figure 3.3. Viability and cell growth dynamics of encapsulated hESCs throughout differentiation. 65

Figure 3.4. Alginate Bead Cracking. 66

Figure 3.5. Proliferation and cell death of encapsulated hESCs, in response to substrate stiffness. 68

Figure 3.6. Increased substrate stiffness enhances DE stage differentiation. 70

Figure 3.7. Increased substrate stiffness suppressed PP stage differentiation. 72

Figure 3.8. Effect of substrate stiffness on TGFβ signaling at the DE stage. 76

Figure 3.9. Effect of substrate stiffness on TGFβ signaling at the PP stage. 78

Figure 3.10. The effect of substrate stiffness on Sonic Hedgehog signaling. 80

Figure 4.1. Schematic of 3D alginate array fabrication and characterization. 97

Figure 4.2. Alginate array parameter selection and characterization. 99

Figure 4.3. Schematic of encapsulation in the 3D alginate array when varying barium concentration and culture configuration. 102

Figure 4.4. hESC viability in response to alginate crosslinking and culture configuration. 104

Figure 4.5. Quantification of DNA and cell proliferation as alginate crosslinking and culture configuration is varied. 106

Figure 4.6. Significance of cation concentration in determining proliferation for each culture configuration. 109

Figure 4.7. Analysis of DE and PP stage differentiation as alginate crosslinking and culture configuration is varied. 111

Figure 4.8. Significance of cation concentration in determining differentiation for each culture configuration. 114

Figure 4.9. Influence of configuration and stiffness in determining proliferation and differentiation. 116

Figure 5.1: Schematic of E-cadherin binding between two hESCs. 127

Figure 5.2. Schematic of peptide conjugated alginate hydrogel and characterization. 134

Figure 5.3. Cell attachment to e-cadherin peptide modified alginate. 136

Figure 5.4. Cell viability and morphology after 6 days of propagation for each peptide, conjugated at 0 – 500 μg/ml..... 138

Figure 5.5. Day 6 hPSC expansion potential on recombinant e-cadherin, or alginate conjugated with each peptide. n=3, results were considered significant if *P<0.05, **P<0.01.140

Figure 5.6. hPSC pluripotency after propagation on the peptide modified alginate substrate. .. 142

Figure 5.7. Differentiation potential of hESCs propagated on e-cadherin peptide mimicking substrates. 144

Figure 5.8. Day 1 hPSC attachment to alginate modified with HAV and ADT peptides. 145

Figure 5.9. hPSC pluripotency after propagation on alginate modified with combination of HAV and ADT peptides. 147

PREFACE

First and foremost, I would like to sincerely thank my advisors Dr. Ipsita Banerjee and Dr. Prashant N. Kumta for their dedication to science, collaborative research, and the exceptional mentorship of my dissertation research. Additionally, I would like to thank Dr. Banerjee and Dr. Kumta for fostering an ideal working environment for collaborative research through their ability to work as a team. My dissertation work was highly collaborative, combing the fields of material science, stem cell biology, and chemical engineering. The work herein would not have been possible without the dedicated mentorship of both Dr. Kumta and Dr. Banerjee. I would like thank Dr. Kumta for the support, encouragement, and feedback, especially relating to biomaterials aspect of my work. I would like to thank Dr. Banerjee for the continuous advice, patience, knowledge, and confidence she imparted to me throughout my dissertation work. I would also like to thank both of my advisors for providing me with countless opportunities to grow and learn as a scientist and engineer. Finally, I would also like to thank my dissertation committee members Dr. Sachin Velankar and Dr. Vijay Gorantla for their support and guidance.

I would like to thank my fellow lab members, for their comradery, advice, and expertise provided during my research. Completion of this PhD work would not have been possible without the help and encouragement of my colleagues. Specifically, I would like to thank Dr. Saik Kia Goh, Dr. Keith Task, Dr. Satish Singh, Dr. Maria Jarmillo, Dr. Joe Candiello, and Hikaru Mamiya. Additionally, I would also like to thank the undergraduate researchers who provided significant help to me during my work: Sierra Barner, Kimaya Padgonkar, and Fatimah

Adisa. Without their help, many aspects of this dissertation would have taken a considerably longer time.

I would like to thank my friends, who help instill in me that mediocrity is not enough, and that I should always strive to be better. Specifically, the encouragement of Taylor Webb and Dee and Brian Bleifeld, caused me to challenge myself, and led me directly down the path to where I am today. I would also like to thank Jeff and Tammy Wolfgong for their spiritual and life mentorship during my time in Pittsburgh.

I would like to thank my family for the endless love and support during my PhD work. Your encouragement during the difficult times of scientific research helped me to continue working and push through hardships. The support and encouragement of my Mother, Kimberly Bates, made me the person I am today, and has been integral to my success.

Finally, I would to like to thank my beautiful wife, Samantha Richardson, for her unwavering love, support, patience, and encouragement. You have been my rock during the continuously challenging years of my PhD work. Without your overwhelming support and love, I would be surely lost. Completion of this dissertation work would not have been possible without you. I would also to like to thank my daughter, Addie Mae, for providing me with continuous laughter and happiness.

1.0 INTRODUCTION

1.1 TYPE 1 DIABETES

Type 1 diabetes (T1D) is an autoimmune disease which constitutes approximately 5-10% of all diabetes cases, wherein the immune system destroys the insulin producing β-cells in the islets of Langerhans in the pancreas [1]. This leaves the individual dependent on a regular insulin supply, and blood glucose levels can no longer be properly controlled without exogenous intervention. Decreased, or complete loss of insulin production, results in high blood glucose levels. This can lead to nerve, kidney, eye, or even foot damage. Current treatment options include exogenous insulin injection, whole organ pancreas transplantation, or pancreatic islet transplantation. Exogenous insulin injections require regular patient compliance and are inconvenient. An alternate option is transplantation of donor pancreata, which offers a more permanent solution. However, this requires a complicated surgical procedure often performed in conjunction with kidney transplantation. Encouragingly, in 2000, Shapiro et al. showed that T1D patients could be returned to normoglycemia after islet transplantation while on regular immunosuppression, known as the Edmonton Protocol, establishing islet transplantation as a promising diabetes therapy [2].

Pancreatic islets of Langerhans consist of 3D cluster of five different endocrine hormone producing cell types (Figure 1.1). The insulin producing beta cells are most predominant, followed by glucagon producing alpha cells. .

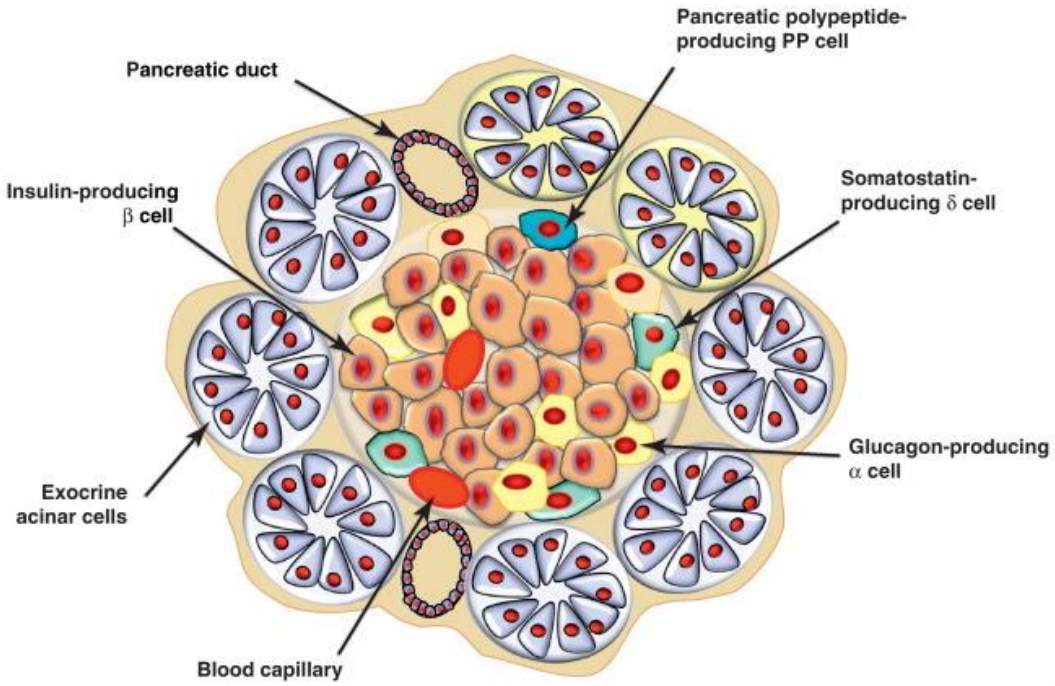

Figure 1.1 Schematic of Islet of Langerhans anatomy [3].

In addition islets consist of a small population of somatostatin producing delta cells, and pancreatic polypeptide producing cells. Each of these endocrine cells work in concert to regulate blood glucose levels through hormone production and regulation.

However, as with any other organ transplantation, patients with islet transplantations were still required to be on regular immunosuppression treatments. Additionally, immunosuppression is also required to combat the abnormal patient autoimmune response to the

new insulin producing cells. This leaves the patient immune deficient and thus, at a high risk for infection. While the Edmonton protocol has shown success in restoring normoglycemia, regular immunosuppression leaves the patient unable to fight infection. As an alternative strategy, isolation of islets from the patient's immune system has been proposed to overcome the need for the use of immunosuppressants. A well-studied approach to immunoisolate implanted primary islets for T1D treatment is to encapsulate the donor islets within a material which acts as a semipermeable membrane. This allows for the diffusion of nutrients and waste, but isolates and protects the cells from the larger immune cells [4-7].

1.2 ALGINATE ENCAPSULATION

Many materials have the capacity to form a semi-permeable hydrogel for encapsulation and immunoisolation of islets, including alginate, polysulphone, poly(ethylene glycol), dimethylaminoethyl methacrylate-methyl methacrylate copolymer, and poly(vinyl alcohol) [8]. However, alginate has been the most widely used naturally derived material as it is non-toxic, chemically inert, non-degradable, easily forms a hydrogel under mild conditions, and cells can be encapsulated with high viability, while still having excellent biocompatibility. Alginate is a naturally derived copolymer composed of guluronic (G) and mannuronic (M) acid, which forms a 3D network when divalent cations bind with the G residues of two adjacent polymer chains (Figure 1.2A), resulting in a cross-linked polymer network [9].

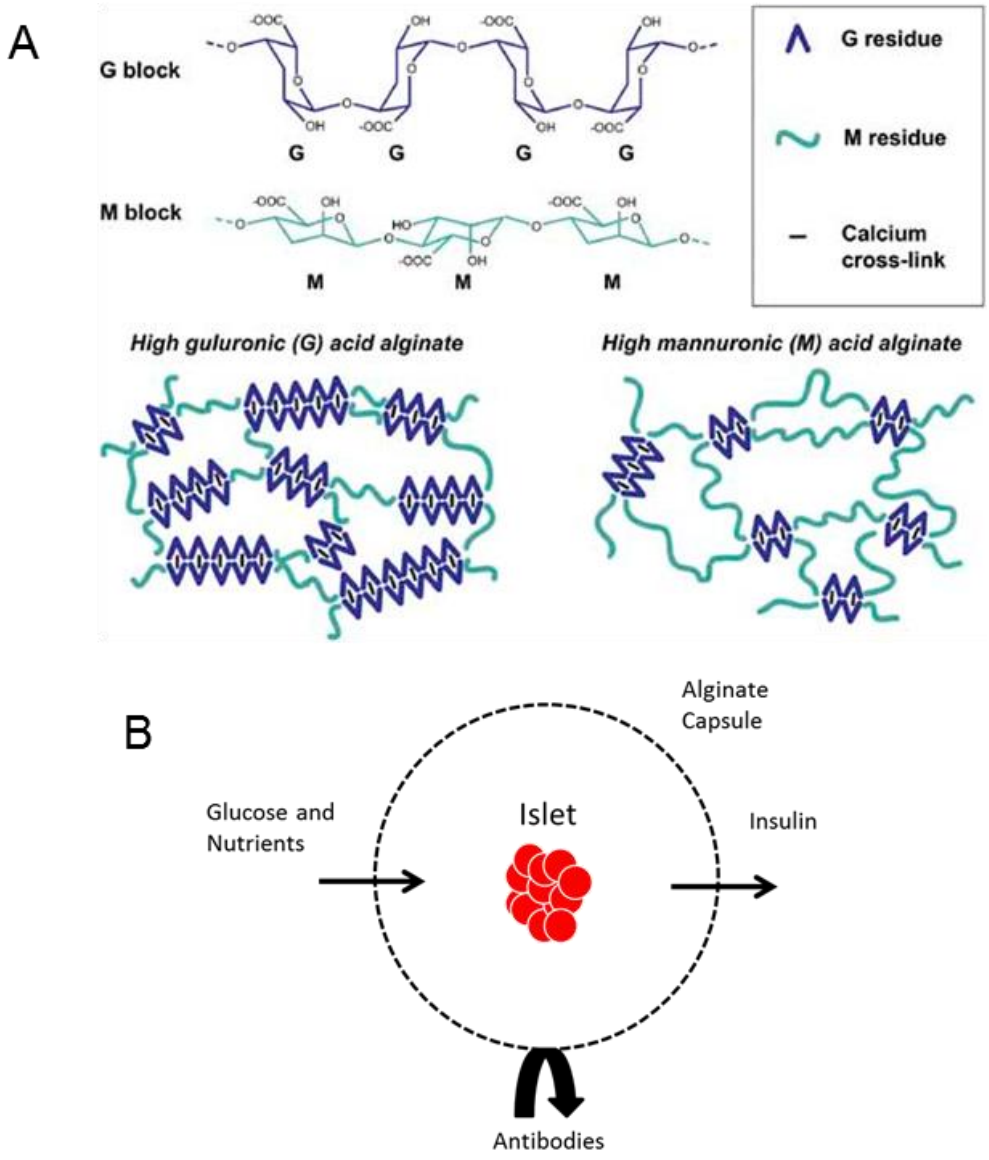

Figure 1.2. Schematic of alginate structure and immunoisolation.

(A) Alginate chemical structure and schematic representation of hydrogel formation when exposed to a cation such as calcium [10]. (B) Schematic of islet immunoisolation using the semi-permeable alginate hydrogel [11].

This material is a chemically inert non-degradable polymer, but most importantly, it has the capability to immunoisolate encapsulated cells (Figure 1.2B) [9]. These characteristics make it

an ideal encapsulation system for islet transplantation, and thus, it has been utilized extensively for this purpose [5, 12-23]. The seminal study by Lim and Sun in 1980 was the first to utilize alginate encapsulation of islets, for the treatment of streptozotocin-induced diabetes in rats [6]. Since then, alginate has been used for cell encapsulation extensively, as well as for drug/protein delivery [24-27], and wound dressing [28, 29]. The physical properties of alginate capsules can be modulated by changing the synthesis parameters during capsule formation [30]. This is done primarily by altering the alginate and cation cross linker types and the ensuing concentration of each. Alginates are available in varying ratios of G/M content, as well as molecular weights. The G/M ratios can vary widely, but is typically classified as either low G (~25-35%) or high G (~65-75%) content [9]. For cell encapsulation, alginate concentrations used are typically between 1-3% [31-35]. Alginate type and concentration can affect capsule properties and thus can influence cellular response. Additionally, cross linker type and concentration can also be used to further modulate the physical properties of the alginate capsules [36]. The most common cation cross linker is calcium, but larger divalent cations such as barium and strontium are also used. Increasing the cation concentration will increase the stiffness of the resulting capsule because the G residues are more highly cross linked, and this is further enhanced by cations such as barium which have higher binding affinity [36, 37].

1.3 HUMAN PLURIPOTENT STEM CELLS

1.3.1 General Background and pancreatic differentiation

Although islet encapsulation can protect the cells from the host immune response, this treatment option is limited in its wide spread applicability due to the shortage of donor organs. In addition to the shortage of donor organs, due to the loss of islet viability after harvesting and transplantation, it takes approximately 2-3 pancreata worth of islets to return a diabetic patient to normoglycemia [38]. However, human pluripotent stem cells (hPSCs), either human embryonic stem cells (hESCs) or induced pluripotent stem cells (iPSCs), have the potential to alleviate this problem. hPSCs have two unique characteristics which make them highly valuable for tissue engineering and cell therapy applications: (1) they can self-renew indefinitely and (2) have the ability to differentiate into any cell type in the body, known as pluripotency. hPSC differentiation is achieved by mimicking the stages of in vivo development in the laboratory setting. Cells are first committed to one of the three germs layers, definitive endoderm (DE), mesoderm, or ectoderm, by modulation of key cell signaling pathways (Figure 1.3).

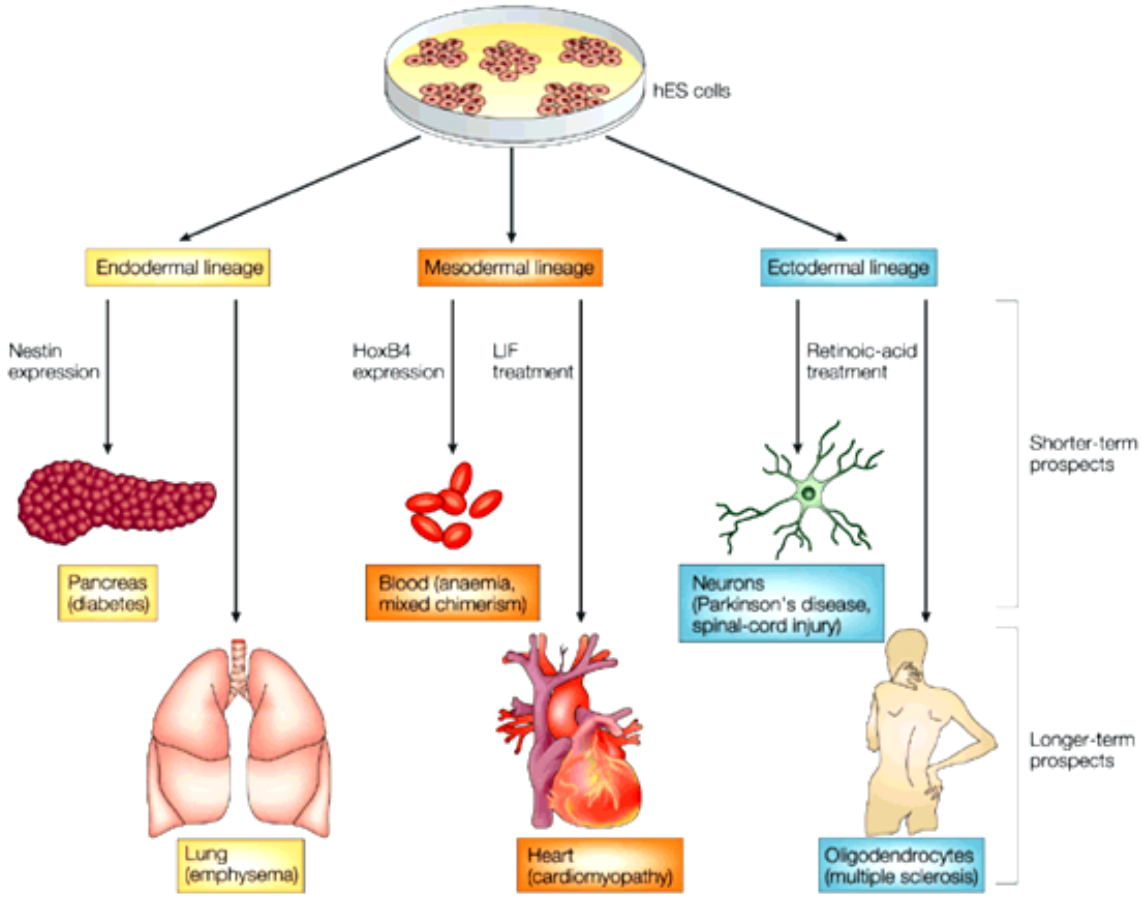

Figure 1.3. Schematic of hESC differentiation [39].

Generation of the desired functional cell type is then accomplished by subsequent stage wise differentiation through necessary progenitor stages. Current strategies have revealed the feasibility of deriving functional islet-like cells from hPSCs, thereby enabling the feasibility of replacing donor islets by hPSC-derived islets for the treatment of T1D.

Our laboratory, as well as others, have developed stage-wise pancreatic differentiation protocols which mimic major stages of pancreatic development. Undifferentiated hESC are first differentiated to the definitive endoderm (DE) germ layer, followed by further induction to a pancreatic progenitor (PP) stage, and finally to mature insulin producing cells (MAT). Previous

studies have focused on the induction of islet-like cells from hESCs primarily on tissue culture plastic (TCP), a two-dimensional monolayer (2D) platform, by the stage-wise addition of soluble chemical factors in the culture medium [40-45]. However, more recently the benefits of 3D culture configurations are gaining appreciation in tissue engineering in general and stem cell differentiation in particular. Specifically for pancreatic differentiation, the Melton group and the Kieffer group have reported significant breakthroughs in generating glucose responsive insulin producing β-cells from hPSCs in vitro, using 3D cell aggregate configurations [46, 47]. While this will overcome the cell source restriction, the next step towards successful clinical translation of hPSC-derived β cells for T1D therapy will require protection of the cells from the host immune system [48]. Additionally, while these studies have been successful in deriving insulin producing cells from hPSCs, they are not directly translatable for type 1 diabetes treatment.

1.3.2 Alginate Encapsulation for the culture and differentiation of hPSCs

Encapsulation of ESCs has been an active area of research over the last decade. We hypothesize that the implementation of this culture strategy is supportive of scalable culture, as well as fulfills the requirement of immunoisolation, necessary for type 1 diabetes therapy. The majority of the efforts, however, have been restricted to mouse embryonic stem cells (mESCs) and its differentiation to various cell types [49-51]. Since platforms established for mESCs cannot be directly translated to hPSCs; targeted platforms need to be developed to handle issues associated with hPSC encapsulation. Alginate encapsulation has previously been shown to support long term hESC propagation [52], as well as prevent teratoma formation in mice [53]. Additionally, alginate encapsulation has also been shown to support differentiation to the endoderm germ layer [54], midbrain neurons [55], and retinal cells [56]. These studies clearly establish the potential

benefits in encapsulating hESCs and demonstrate the feasibility of inducing early differentiation in these encapsulated hESCs.

Alginate encapsulation provides an environment during differentiation which is drastically different from conventional adherent culture on TCP. Cells cultured on TCP experience a stiff and noncompliant environment, while cells encapsulated in alginate experience a more compliant environment. The cellular response is further influenced by the alginate capsule physical properties. The seminal 2006 study by Engler et al. showed that mesenchymal stem cell (MSC) lineage specificity could be controlled by substrate stiffness [57]. Cells cultured on soft substrates mimicking the brain committed to neurogenic phenotype, while cells cultured on stiffer substrates mimicking muscle or bone, committed to myogenic and osteogenic phenotypes, respectively. It has become clearly evident that hPSC differentiation is controlled by both soluble factors, as well as insoluble factors, such as substrates stiffness, interactions with extracellular matrix proteins, and cell-cell interactions (Figure 1.4) [58, 59].

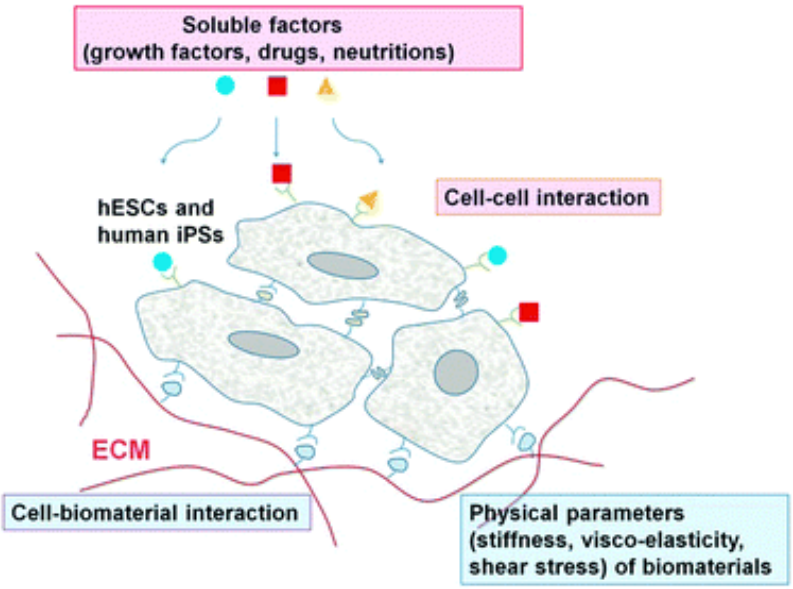

Figure 1.4. Schematic of culture stimuli which can influence hPSC fate [60].

As mentioned previously, the properties of alginate capsules can be easily modulated by alginate and cation type and concentration, and thus can be utilized to influence cell response. Wilson et al. showed that encapsulation of preformed mESC aggregates in either high G or high M content alginate resulted in delayed differentiation of cells encapsulated with high G content alginate [31]. Lee et al. have shown that encapsulation of preosteoblast cells differentiated more efficiently when alginate concentration increased from 1% to 2%, but cell proliferation decreased [61]. Banerjee et al. have shown that decreasing calcium concentration while maintaining constant alginate concentration resulted in a decrease in elastic moduli and an increase in proliferation and differentiation of encapsulated neural stem cells [62]. Previous studies for islet encapsulation have shown that alginate capsule composition has a significant effect on the materials capacity to immunoisolate [63]. On the other hand, as discussed above, such capsule composition can modify the differentiation of the encapsulated cells.

1.4 HUMAN PLURIPOTENT STEM CELL BIOMANUCFACTURING AND LARGE SCALE CULTURE

hPSCs have the capacity to differentiate into all mature cell types, making them attractive candidates for cell therapy based regenerative medicine [64]. Current success in deriving various functional cell types from hPSCs, including beta cells [46, 47], neurons [65], cardiac cells [66], and retinal epithelial cells [67], have moved the field closer to realizing its clinical potential. To date, 11 clinical trials involving hPSC-based therapies have been registered with the NIH, including trials for treatment of diabetes, Parkinson's disease, heart failure, and macular degeneration, among other therapeutic targets. While current clinical trials are primarily using laboratory scale culture and propagation methods of hPSCs, such methods will be restrictive for large scale clinical translation of hPSCs. Hence, the first step towards biomanufacturing of therapeutic hPSCs will be to ensure controlled, scalable propagation of hPSCs with reduced variability and retained pluripotency.

Laboratory scale productions of hPSCs utilizes adherent culture, and has been traditionally conducted on TCP coated with Matrigel, an ECM extract from mouse sarcoma cells. Since Matrigel is a poorly defined animal product, there has been extensive recent effort to replace it with xeno-free, chemically defined recombinant protein based substrates, which are compatible with downstream cell-therapy applications [68, 69]. However, recombinant proteins are difficult to produce and highly expensive, making them major a bottleneck for large scale hPSC biomanufacturing.

1.4.1 Current approaches for large scale hPSC biomanufacturing

Current approaches towards scalable culture of hPSCs include planar culture on adherent surfaces and suspension cultures [70]. Planar cultures offer precise control of the cell microenvironment but are limited in their throughput, and require enormous surface area to produce clinically relevant cell numbers [71, 72]. On the other hand, suspension 3D culture systems have the potential for large scale non-linear hPSC expansion. Current suspension cultures use either microcarriers for adherent cells or culture hPSC aggregates in suspension [73, 74]. Microcarrier culture consists primarily of hPSCs attached to protein coated polymer spheres; however, controlling microcarrier agglomeration and harvesting of cells from the carrier is a limitation of this technology. Suspension cultures are highly scalable; but controlling aggregate size and preventing multi-aggregate coalescence is difficult. Further, in both of these platforms, cells are exposed to hydrodynamic shear stress when cultured in a bioreactor, which can result in uncontrolled spontaneous differentiation, increased variability and also enhanced cell death [75-77]. Hence, in current 3D culture methods it is difficult to ensure controlled hPSC propagation with reduced variability.

Finally, use of single cell hPSCs, to date, results in high cell death, thereby compromising its potential for clonal expansion. Single cell hPSCs trigger the apoptotic pathway upon losing cell-cell contact. A critical requirement for hPSC survival and proliferation is the tight cell-cell contact, the absence of which results in ROCK pathway activation, actomyosin hyperactivation, and ultimately dissociation induced apoptosis. This effect can be somewhat overcome through chemical inhibition of the ROCK pathway, which still results in over 50% cell death upon dissociation [78]. The Rho/ROCK signaling cascade is initiated by dissociation of the transmembrane glycoprotein E-cadherin, a primary homophilic adhesion molecule responsible

for hPSC survival [79]. Thus current culture strategies often require hPSC colonies as the starting population to retain high viability, while compromising its scalability.

1.5 SPECIFIC AIMS

The use of hPSCs has the potential to provide an unlimited supply of any cell type in the body, and thus, can be used to alleviate donor organ shortages. hPSCs can be differentiated to any cell type in response to chemical stimuli, physical stimuli, or a combination of both. The overall goal of this work is to understand how encapsulation affects the growth and pancreatic differentiation of hPSCs, as encapsulation is a requirement for transplantation-based T1D therapy. Over the last decade there has been significant progress in deriving functional cells from hPSCs. The next stage of clinical translation will require overcoming the challenge of immune rejection and scalable culture. We hypothesize that encapsulation will allow us to meet both challenges using the same platform. Encapsulation will allow 3D culture of cells in aggregates, which is increasingly being seen as preferable to 2D adherent culture. However, interaction of the cells with the substrate will also make the cell fate susceptible to substrate properties. Hence, in the first two aims of this dissertation we will test the feasibility of achieving pancreatic differentiation under encapsulation, and subsequently, investigate how substrate properties affect cell fate. Then in the 3rd aim, we will develop a biomimetic hydrogel which can support single cell hPSC growth and propagation for large scale hPSC culture. Accordingly, three specific aims have been formulated as detailed below.

1.5.1 Specific Aim 1: To evaluate the feasibility of obtaining hPSC derived pancreatic cell types under encapsulation.

The objective of this aim is to use alginate encapsulation as a platform for islet-like differentiation of hPSCs to offer a potentially directly transplantable treatment option for T1D. In Chapter 2, we have investigated the specific stage of pancreatic differentiation most amenable to encapsulation and differentiation. hPSCs were encapsulated at various stages of the directed differentiation protocol, and analyzed for cell phenotype and viability upon encapsulation. These results demonstrated that hESCs can be efficiently differentiated to the pancreatic lineage under alginate encapsulation, which could be used as a directly translatable treatment option for T1D.

1.5.2 Specific Aim 2: To determine the effect of cell physical microenvironment on the pancreatic differentiation of hPSCs.

The objective of this aim is to investigate the effect of physical stimuli on the pancreatic differentiation of hPSCs. This aim is spread across 2 chapters: Chapter 3 and Chapter 4. In Chapter 3, we determined the effect of varying alginate capsule composition by varying cation concentration on the pancreatic differentiation of hESCs. The results of this chapter elucidate the role that capsule stiffness plays on pancreatic differentiation of hESCs. In the second part of this aim, in Chapter 4, we developed a high throughput 3D alginate array platform to expose the cells to multivariate perturbations. Analysis of cell response with a statistical model helped to identify the sensitivity of cell fate to individual perturbations. Using this approach, we dissected the role of capsule substrate properties and culture configuration on pancreatic islet cell fate of hPSCs.

1.5.3 Specific Aim 3: To develop a synthetic biomimetic substrate for supporting single cell viability and biomanufacturing of hPSCs.

The objective of this aim is to develop an alginate based substrate that can support single hPSC viability for the improved expansion potential of hPSCs for large scale culture applications. The dissociation of hPSCs into single cells results in the loss of cell-cell contact through the transmembrane protein, E-cadherin, and results in dissociation induced apoptosis. Considering this limitation of hPSC culture, in Chapter 5, we incorporated peptides into the alginate substrate which mimic the bioactive domains of E-cadherin. E-cadherin mimicking peptides were conjugated onto alginate, and subsequent hPSC attachment, viability, pluripotency, and the differentiation potential were evaluated to determine peptide efficacy. This aim was thus intended to transition the alginate differentiation platforms developed in Aims 1 and 2, into one that can support efficient large scale hPSC culture for cell therapy applications.

2.0 ALGINATE ENCAPSULATION OF HUMAN EMBRYONIC STEM CELLS TO ENHANCE DIRECTED DIFFERENTIATION TO PANCREATIC ISLET-LIKE CELLS

The content of this chapter is taken from Richardson Thomas, Kumta Prashant N., and Banerjee Ipsita. Alginate Encapsulation of Human Embryonic Stem Cells to Enhance Directed Differentiation to Pancreatic Islet-Like Cells. Tissue Engineering Part A July 2014, 20 (23-24)

2.1 INTRODUCTION

It is well known that type 1 diabetes constitutes approximately 5-10% of all diabetes cases, wherein the immune system destroys the insulin producing β-cells of the pancreas [1]. Success of the Edmonton protocol has established islet transplantation as a promising diabetes therapy [2]. However, as with any other organ transplantation, with islet transplantations, patients were still required to be on regular immunosuppression treatments. As an alternative strategy, encapsulation of islets has been proposed to overcome the need for immunosuppressants. The encapsulation systems utilize materials that are permeable enough to allow the diffusion of glucose and other nutrients to the islets, and the diffusion of waste and insulin away from the islets; while masking the islets from the host immune response [80-83]. Alginate is a chemically inert non-degradable polymer, and most importantly it has the capability to immunoisolate encapsulated cells [9]. A simple and commonly used method to ensure alginate encapsulation

provides sufficient immunoisolation for many cells types is the application of a polycationic coating, followed by an alginate coating [84-86]. These characteristics make it an ideal encapsulation system for islet transplantation, and thus it has been utilized for this purpose for decades [5, 12-19]. Although these methods of transplantation isolate the islets from the host immune response, this treatment option is plagued by shortage of donor islets. Specifically, approximately 2-3 pancreata worth of islets are necessary to return a diabetic patient to normoglycemia [38].

A promising alternative to the whole organ or islet transplantation is the use of human embryonic stem cells (hESCs). Pluripotent stem cells have the potential to differentiate to any cell type in the body and are also in virtually unlimited supply, rendering hESC-derived islet-like cells a promising alternative to islets. The focus of our study, thus, is to establish the feasibility of obtaining encapsulated hESC derived islet like cells, which can be directly transplanted for diabetes therapy. While immunoisolation is the primary advantage of islet encapsulation, it offers the additional advantage of scalability for hESC derived islets. The high throughput of encapsulation systems will allow the capability of producing the enormous number of pseudo-islets needed for tissue engineering applications.

Encapsulation of embryonic stem cells has been an active area of research over the last decade. The majority of the efforts, however, had been restricted to mouse embryonic stem cells (mESCs) and its differentiation to various cell types [49-51]. Since platforms established for mESCs cannot be directly translated to hESCs; targeted platforms need to be developed to handle issues associated with hESC encapsulation. Siti-Ismail et al. [52] have recently shown the feasibility of propagating hESCs encapsulated in calcium alginate for up to a period of 260 days. The encapsulated hESCs were reported to retain their characteristic pluripotency, and could be

further induced to each specific germ layer. In another report, Chayosumrit et al. [54] have shown the feasibility of inducing definitive endoderm in encapsulated hESCs. Dean et al. [53] have shown that encapsulation of hESCs could prevent teratoma formation for up to four weeks after implantation into mice. Finally, Kim et al. [55] have used alginate encapsulation for differentiation of hESC to midbrain dopamine producing neurons. Finally, most recently Hunt et al. have shown that hESC-derived embryoid bodies (EBs) maintained in RGD-modified alginate showed an increased percentage of EBs with pigmented retinal pigmented epithelium (RPE) foci, optic vessels, and pigmented RPE [56]. These initial studies cleary establish the potential benefits in encapsulating hESCs and demonstrate the feasibility of inducing early differentiation in these encapsulated hESCs. There have been no reports to date however, to the best of our knowledge on exploiting encapsulation strategies for achieving late stage differentiation of hESCs to the pancreatic lineage. The objective of this chapter is thus to demonstrate for the first time the feasibility of generating hESC derived islet-like cells under alginate encapsulation, which can be readily transplanted for diabetes therapy.

In our previous studies we have reported directed differentiation of hESCs to pancreatic islet cell types in adherent 2D culture consisting of the following stages: definitive endoderm (DE), pancreatic progenitor (PP), and maturation (MAT) [87]. Translation of this protocol into a 3D encapsulation configuration first requires determination of the specific stage of differentiation when the hESCs can be encapsulated. First we evaluated the possibility of encapsulating fully or partially differentiated hESCs. Encapsulation of hESC-derived mature cells resulted in both low viability and reduction of the maturation markers upon culture. Encapsulation of hESC-derived DE cells resulted in high maturation upon further differentiation; however the viability of the cells was low. Finally, we showed that encapsulation of

undifferentiated hESCs followed by the stage-wise differentiation, successfully results in islet specific maturation and high viability. Furthermore, the maturation obtained under encapsulation was significantly stronger than parallel differentiation conducted in the conventional adherent 2D configuration. Hence these results show that the stage of encapsulation greatly affects the translation of this protocol. We have further investigated the mechanisms mediating this enhanced maturation under encapsulation and determined that extracellular matrix molecules or adhesive molecules may not be mediating the process. On the other hand, investigation of the involved signaling pathways revealed that while the magnitude of key protein expression was low under encapsulation, the ratio of pSMAD/pAKT was significantly higher than the corresponding 2D cultures, indicating the encapsulation strategy as being an efficient approach enhancing differentiation.

2.2 MATERIALS AND METHODS

2.2.1 Cell Culture

Undifferentiated H1 hESCs were maintained on hESC-qualified Matrigel (BD Biosciences) coated tissue culture plate for 5-7 days in mTeSR1 (StemCell Technologies) at 37°C and 5% CO_2 before passaging. Experiments were performed with p55-p70 hESCs.

2.2.2 hESC Encapsulation

Single cell suspension of undifferentiated or predifferentiated hESCs was encapsulated according to previous studies [54, 88]. hESCs were incubated with 10μM Y-27632 (Millipore) for two hours prior to passaging. Cells were incubated with Accutase (Life Technologies) for 5-7 min at 37°C to detach cells, and pipetted to obtain single cell. Cells ($1x10^6$ cells/ml) were suspended in filtered 1.1% (w/v) low viscosity alginate (Sigma-Aldrich) with 0.2% (v/v) gelatin (Sigma-Aldrich) and added drop wise to a solution of 100 mM $CaCl_2$ (Sigma-Aldrich) with 10 mM HEPES (Sigma-Aldrich) using a 22 gauge needle. The resulting capsules were 1.98 ± 0.14 mm in diameter. The alginate used for encapsulation consisted of 39:61 guluronic to manuronic acid residues and an endotoxin content of approximately 88 EU/g [89]. Alginate capsules were incubated for 6-8 min in the $CaCl_2$ solution. Capsules were washed three times with PBS and suspended in appropriate medium with 10 μM Y-27632 for 4 day prior to differentiation.

2.2.3 Differentiation of Encapsulated hESCs

The stage-wise induction protocol for mature islet-like differentiation of hESCs was adopted from our previous study [87]. First, definitive endoderm was induced using 100 ng/ml ActivinA (R&D Systems, Minneapolis, MIN) with 25 ng/ml Wnt3A (R&D Systems) for 4 days. Afterwards, pancreatic progenitor was induced with 0.2 μM KAAD-cyclopamine (Millipore) for 2 days and 0.2 μM KAAD-cyclopamine with 2 μM retinoic acid (Sigma-Aldrich) for 2 days. Finally, maturation was induced by 10 μM nicotinamide (Sigma-Aldrich) for 2 days and 10 μM nicotinamide with 30 μM DAPT (Santa Cruz, CA, USA) for 7 days. All differentiation media

was made using DMEM/F12 (Life Technologies), supplemented with 0.2% BSA (Sigma-Aldrich) and 1xB27® (Life Technologies).

2.2.4 Viability

LIVE/DEAD (Life Technologies) viability assay was performed according to manufacturer's instructions. Briefly, encapsulated cells were incubated with 2 µM ethidium homodimer-1 and 1 µM calcein-AM in DMEM/F12 for 25 min at room temperature. Capsules were washed three times with DMEM/F12 before fluorescent imaging.

2.2.5 Proliferation

Cell proliferation was measured using AlamarBlue (Life Technologies) assay according to manufacturer's instructions. Briefly, encapsulated cells were incubated with medium containing 10% (v/v) AlamarBlue for 4 hours. Fluorescence intensity of the supernatant was measured using a Synergy 2 multi-mode Microplate Reader (BioTek, Winooski, VT, USA).

2.2.6 Quantitative reverse transcription polymerase chain reaction

Cells were decapsulated with 100 mM EDTA (Sigma) and washed twice with PBS before lysis. mRNA was isolated using the NucleoSpin RNA II kit (Macherey-Nagel, Bethlehem, PA). cDNA was obtained using the ImpromII Reverse Transcription System (Promega, Madison, WI). Each PCR reaction contained 5 µl SYBR Green Master Mix (Agilent, Santa Clara, CA), 2 µl nuclease free H2O, 2 µl primer, and 1 µl cDNA. Samples were normalized to the house keeping gene

GAPDH and analyzed relative to undifferentiated hESC using the ΔΔCt method. For the RT^2Profiler™ PCR array analysis, cDNA was obtained using the RT^2 First Strand kit according to manufactures instruction (SA Biosciences, Valencia, CA). Each qRT-PCR reaction for the Extracellular matrix and Adhesion molecule array (human) contained 12.5 µl RT^2 qRT-PCR Master Mix, 0.94 µl cDNA, and 11.56 µl RNase-free water and was distributed (25 µl) into each well of the PCR 96-well array. Encapsulated samples were normalized to the house keeping gene GAPDH and analyzed relative to hESC differentiated on TCP using the ΔΔCt method. Gene expression was measured with quantitative polymerase chain reaction (qRT-PCR) using an MX3005P system (Agilent).

2.2.7 MagPix

Intracellular expression of the proteins c-peptide and glucagon was measured by MagPix analysis using the BioPlex Pro Human Diabetes kit (Bio-Rad) according to the manufacturer's instructions. Briefly, samples and standards were incubated with 1x c-peptide and glucagon labeled magnetic beads at room temperature for 1 hour. All incubation steps were done on at plate shaker for at 300 RPM. After incubation, the beads were washed and incubated with a 1x biotinylated detection antibody solution at room temperature for 30 minutes. Next, the beads were washed and incubated with 1x steptavidinePE for 15 minutes at room temperature. The TGFβ pathway was analyzed using the MILLIPLEX MAP TGFβ Signaling Pathway Magnetic Bead 6-Plex (Millipore) for pSMAD2, pSMAD3, pERK1/2, and pAKT as well as total TGFβII and SMAD4 according to manufactures instruction. Briefly, 25 µl of each control and sample was incubated with 25 µl of a 1x beads solution over night at 4°C. After incubation, the beads were washed twice and incubated with 1x detection antibody for 1 hour in the dark, followed by

1x streptavidin-PE for 15 min. Fluorescence intensity was measured using the xMAP (Luminex, Austin, TX) machine. The total protein was measured using a BCA total protein kit (Thermo Scientific), according to manufactures instruction.

2.2.8 Glucose Stimulated Hormone Release

After mature differentiation of UD encapsulated hESC, cells were incubated overnight in low glucose (2.8 mM) differentiation media containing 10 µM nicotinamide. Next the cells were included for 1 hour in Krebs-Ringer buffer at 37°C followed by a 1hour or 3 hour stimulation with high glucose (16.7 mM) differentiation media containing 100 µM tolbutamide and 30 µM KCl. Levels of secreted glucagon and c-peptide in the supernatant were measured at basal conditions (low glucose) and after stimulation using MagPix analysis as previously described. Secreted hormones were normalized to the total protein of the stimulated cells.

2.2.9 Western Blot

Cell lysis was carried out in Cell Extraction Buffer (Invitrogen) by incubation with cells on ice for 30 minutes, followed by centrifugation for 30 minutes at 3220xg at 4°C. Proteins (30 µg per sample) were separated using 4-20% SDS-PAGE at 100 V, and were transferred to nitrocellulose membrane at 4°C overnight. The membrane was blocked with Odyssey blocking buffer (LI-COR Biosciences, Lincoln, NB) for 2 hours at room temperature. Primary antibodies against β-Catenin (Cell Signaling, 1:1000), and GAPDH (Cell Signaling, 1:5000) were diluted in Odyssey blocking buffer with 0.1% tween (Sigma-Aldrich) and were added to the membrane and incubated overnight at 4°C. The membrane was washed three times for 5 minutes each and incubated with

IR conjugated anti-rabbit secondary antibody (LI-COR, 1:20,000) for 1 hour at room temperature. The membrane was washed three times for 5 minutes each before analysis using the Odyssey CLx (LI-COR) machine. Samples were normalized with GAPDH values.

2.2.10 Flow Cytometry

Cells were harvested after Accutase treatment to obtain a single cell suspension, and were fixed with 4% formaldehyde (Thermo Scientific) in PBS for 30 minutes. Cells were permeabilized with 0.1% Saponin (Sigma-Aldrich) with 0.5% BSA in PBS for 30 minutes. Blocking for non-specific binding was done by incubating cells with 3% BSA with 0.25% dimethyl sulfoxide (DMSO) and 0.1% Saponin in PBS for 30 minutes. Samples were incubated in blocking buffer with rabbit anti-c-peptide (1:500, Abcam, Cambridge, MA) primary antibody for 30 min at room temperature. Next, cells were incubated with donkey anti-rabbit Alexafluor 555 (Life Technologies) for 30 min at room temperature. Secondary antibody only without primary antibody was used as the negative control. Samples were washed and suspended in PBS before transferring to flow cytometry tubes. Accuri C6 © Flow Cytometer was used to quantify the protein expression. The gate was set beyond cells positive for secondary antibody only to eliminate false positives.

2.2.11 Immunostaining

Encapsulated cells were fixed with 4% formaldehyde for 30 min. Cells were dehydrated with increasing concentrations of ethanol and paraffin embedded for sectioning. Antigen retrieval was done using citrate buffer. Slides were permeabilized with 0.1% Triton-X (Sigma) in PBS for 5

min. A blocking step with 10% donkey serum in PBS was done for 1 hour. For primary antibodies, we used goat anti-SOX17 (1:200 dilution, Santa Cruz Biotechnology, Santa Cruz, CA), rabbit anti-FOXA2 (1:200 dilution, Santa Cruz), goat anit-PDX1 (1:50 dilution, R&D Systems), rabbit anti-c-peptide (1:500 dilution), goat anti-glucagon (1:200 dilution, Santa Cruz), rabbit anti-MAFA (1:500 dilution, Bethyl Laboratories, Montgomery, TX), and mouse anti-somatostatin (1:200, Beta Cell Biology Consortium, Nashville, TN). The incubation time for primary antibodies were overnight at 4°C. The slides were incubated with the secondary antibody for 45 min at room temperature. Secondary antibodies used were: donkey anti-rabbit Alexafluor 555 (1:500 dilution), anti-goat Alexafluor 555 (1:500 dilution), and anti-mouse Alexafluor 488 (1:500 dilution). The slides were washed three times with PBS (5-10 min) before covering with hardening mounting medium containing DAPI (Vectashield, Vector laboratory).

2.2.12 Statistical Analysis

Data were presented as mean ± SD. Statistical significance between groups was determined using the two tailed Student T-test for two group comparisons. Probability values at $P < 0.05$ (*) and $P < 0.01$ (**) indicated statistical significance.

2.3 RESULTS

2.3.1 Pancreatic differentiation and characterization of hESCs

We have previously reported a stage-wise directed differentiation protocol for induction of human embryonic stem cells (hESC) to mature islet-like cell types [87] on conventional 2D monolayer (2D) tissue culture plastic. Figure 2.1 shows our protocol for islet-like differentiation of hESCs, which consists of the following stages: definitive endoderm (DE), pancreatic progenitor (PP), and maturation (MAT).

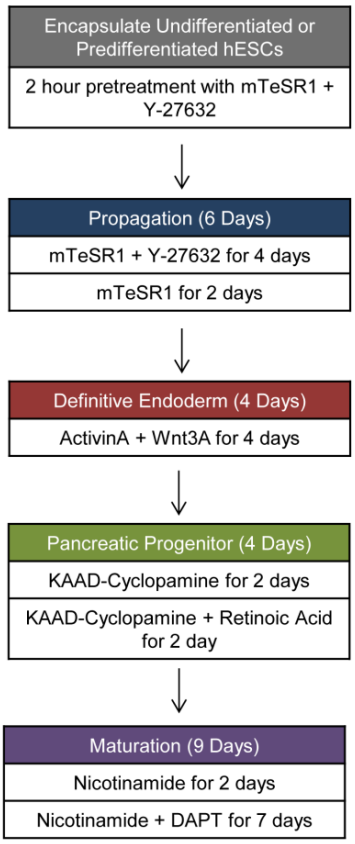

Figure 2.1. Stage-wise differentiation protocol for deriving mature islet-like cell types from hESCs.

Our first objective was to investigate the possibility of calcium alginate encapsulation of predifferentiated hESCs either after full maturation or upon DE induction, and test the viability and functionality upon encapsulation. UD hESCs were first induced to mature or DE cells on Matrigel-coated tissue culture plastic using the previously described differentiation protocol, and encapsulated in alginate. The mature stage was characterized by upregulation of insulin (~$9.5x10^5$, Figure 2.2A) by qRT-PCR, as well as flow cytometry and immunostaining for c-peptide (Figure 2.2B, C). Our differentiation protocol yielded approximately 24% of the population positive for c-peptide by flow cytometry.

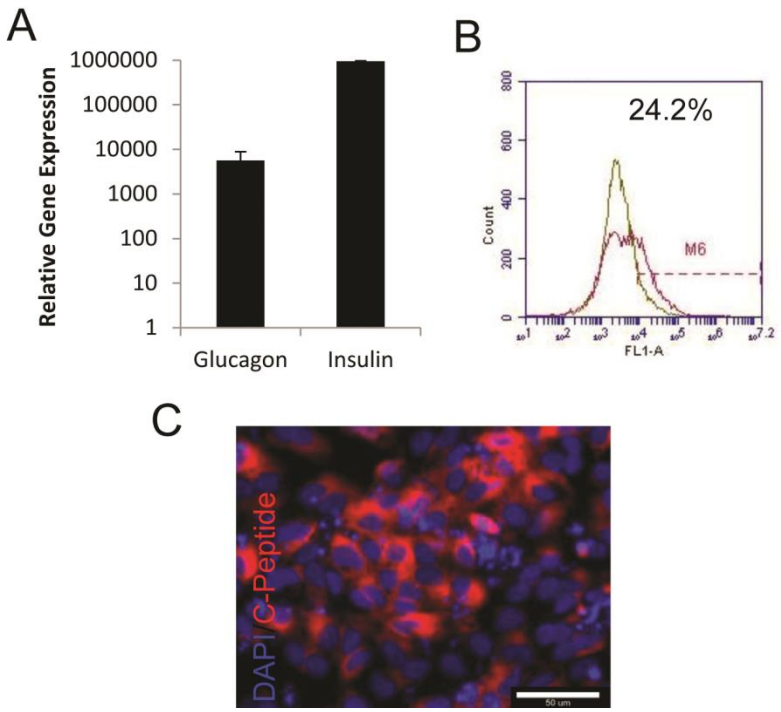

Figure 2.2. Characterization of mature islet-like cells before encapsulation.

A) Gene expression by qRT-PCR at the mature stage on tissue culture plastic (TCP) for glucagon and insulin, compared to undifferentiated hESCs (n = 3). B) Flowcytometry analysis for c-peptide on hESC-derived mature cells on TCP. Secondary antibody only was used as negative control. C) Immunostaining analysis for c-peptide on hESC-derived mature cells on TCP.

Before encapsulation of DE cells, differentiation in 2D was confirmed by analysis of DE markers by qRT-PCR (Figure 2.3A), flow cytometry (Figure 2.3B) and immunohistochemistry (Figure 2.3C). Encapsulated mature cells were maintained for 7 days in basal maturation media (B27, BSA and nicotinamide), while encapsulated DE cells were further differentiated according to Figure 2.1A.

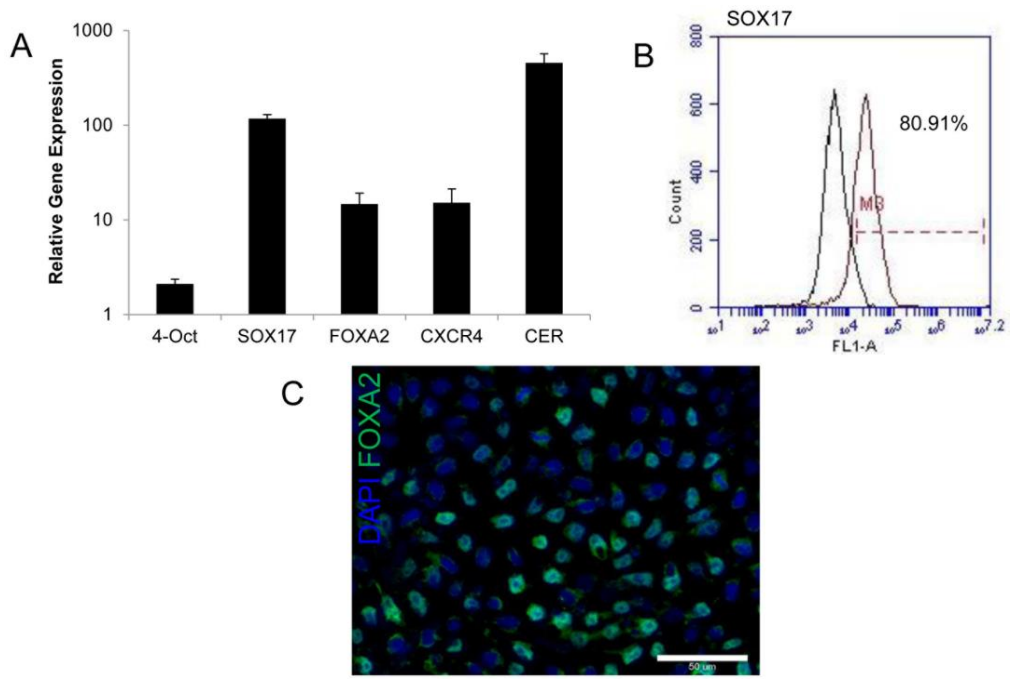

Figure 2.3. Definitive endoderm characterization prior to encapsulation.

A) Gene expression by qRT-PCR at the definitive endoderm stage on tissue culture plastic for SOX17, FOXA2, CXCR4 and CER compared to undifferentiated hESCs (n = 3). B) Flow cytometry analysis at the definitive endoderm stage for SOX17. Secondary antibody only was used as negative control. C) Immunostaining at the definitive endoderm stage for FOXA2. Scale bar is 50 µm. Primary AB - 1:200 goat anti-human SOX17 (Santa Cruz Biotechnology, Santa Cruz, CA, USA). Secondary AB - 1:2000 donkey anti-goat Alexafluor 488 (Life Technologies).

2.3.2 Encapsulation of predifferentiated hESC results in low yield of viable cells

2.3.2.1 Viability and Proliferation.

In order to encapsulate the hESC-derived cells, undifferentiated (UD) or pre-differentiated hESCs at each stage of differentiation were harvested and dispersed as single cells in 1.1% alginate with 0.2% gelatin and added drop-wise to a bath of $CaCl_2$ (Figure 2.4). This resulted in uniform capsules with encapsulated cells, which were washed and further continued in culture in relevant media depending on the stage of encapsulation.

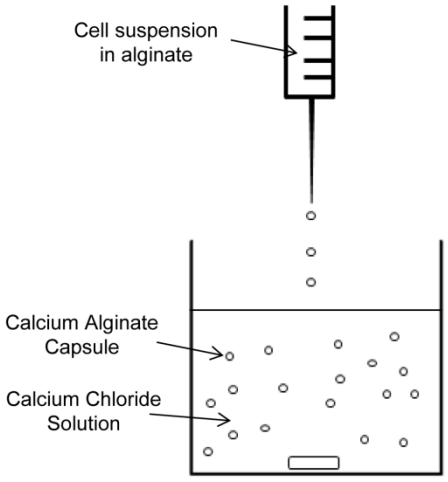

Figure 2.4. Schematic showing the process of calcium alginate encapsulation of hESCs

The viability of encapsulated MAT cells was analyzed on days 1, 3 and 7 post-encapsulation, using the LIVE/DEAD assay. Figure 2.5A show images from days 1 and 7. Viable cells fluoresce green by metabolically converting calcein-AM to calcien, while the dead cells fluoresce red by diffusion of ethedium-homodimer-1 into the cell due to the permeability of

apoptotic cells. Day 1 bright field and fluorescent images confirm the presence of live cells in the alginate capsule, indicating successful encapsulation of the hESC derived islet-like cells. Apoptotic single cells were also observed in the alginate capsules, which are expected due to the increased stress on the cells during harvesting and encapsulation. The hESC derived mature cells are, however, not strongly proliferative. Hence the number of viable cells in the alginate capsules remains unchanged throughout the 7 days of culture. Consequently, colony formation was not observed and the yield of the viable encapsulated cells was low.

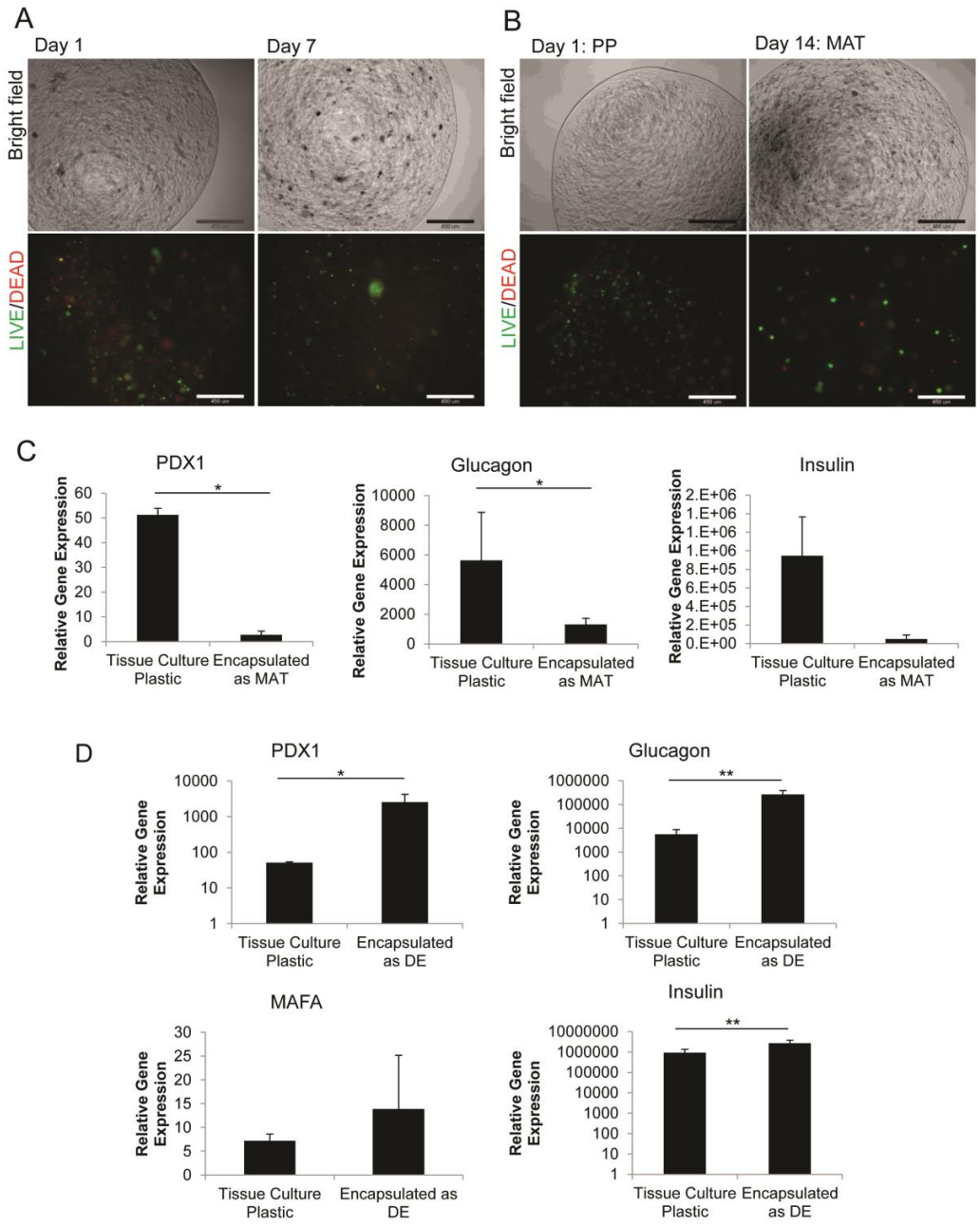

Figure 2.5. Characterization of encapsulated predifferentiated hESCs.

A) LIVE/DEAD assay on days 1 and 7 after encapsulation of hESCs after MAT on TCP. B) LIVE/DEAD assay on days 1 and 14 after encapsulation of hESC-derived DE cells. C) Gene expression on islet-like cells, 7 days post encapsulation, for PDX1, glucagon, and insulin, compared to UD hESCs (n = 3). D) Gene expression by qRT-PCR at the mature stage on cells encapsulated at the DE stage, for PDX1, Glucagon, MAFA, and Insulin. The results were considered significant if $^{*}P<0.05$, $^{**}P<0.01$ (n = 3). Scale bar is 450 µm.

Next, DE cells were harvested and encapsulated as mentioned previously, and the subsequent PP and MAT differentiation stages were followed under encapsulation. Viability of encapsulated DE cells was analyzed at the end of each stage of the differentiation, after encapsulation. Figure 2.5B shows that although beyond day 7, cellular aggregation into small colonies was observed; the size of these colonies did not increase appreciably by the end of maturation as show by the LIVE/DEAD images on day 14. Although the yield of the viable cells is higher compared to encapsulating mature cells, the overall yield of viable cells is still low.

2.3.2.2 Effect of Encapsulation on hESC Maturation

The encapsulated MAT cells were further analyzed for mature pancreatic markers after 7 days of culture to verify if the encapsulated cells maintained their differentiated phenotype. Differentiated cells analyzed at the point of encapsulation showed strong upregulation of PDX1 (51), glucagon (5635), and insulin ($9.5x10^5$). This condition was used as a positive control. Upon culture under encapsulation the cells still retained their maturation markers: PDX1 (~3), MAFA (~19), glucagon (~1309), and insulin (~$4.8x10^5$) (Figure 2.5C). However, the strength of upregulation was reduced with culture: expression of PDX1, glucagon, and insulin showed respectively 18.6, 4.3, and 19.6 fold lower upregulation after 7 days under encapsulation. This indicates that, while it is feasible to encapsulate hESC derived islet-like cells, the cells tended to lose their mature phenotype upon encapsulation.

Analysis of the encapsulated DE cells after pancreatic induction showed strong upregulation of PDX1 gene expression, a crucial transcription factor in pancreatic development. The encapsulated hESC-derived DE cells were further matured into islet-like cells, and analyzed for the gene expression of more mature pancreatic islet markers. As illustrated in Figure 2.5D, maturation of encapsulated cells resulted in strong upregulation of many of the mature markers:

PDX1 (~2500 fold), glucagon (~$2.5x10^5$ fold), MAFA (~14 fold), and insulin (~$2.5x10^6$ fold) compared to UD hESCs. PDX1 and insulin expression were respectively 50 and 2.8 fold higher upon encapsulation, compared to 2D tissue culture plastic controls. These results indicate the enhanced pancreatic potential of the hESC-derived DE cells upon encapsulation. However, although encouraging as a differentiation platform, the above configuration is restrictive for cellular yield.

2.3.3 Encapsulation of undifferentiated hESCs results in high viability and strong islet-specific maturation

The above analysis indicated the difficulty in encapsulating pre-differentiated hESCs, but it established the positive attribute of encapsulation on differentiation. Hence in the next step we evaluated the feasibility of encapsulating undifferentiated (UD) hESCs and conducting all the stages of differentiation under encapsulation. UD hESCs were pretreated with Y-27632 for two hours, harvested, and encapsulated in alginate. Upon encapsulation, the cells were further propagated for 4 days in mTesR1 with Y-27632, followed by 2 days in only mTeSR1, to allow colony formation. After propagation, the encapsulated cells were induced towards differentiation according to the previously described protocol (Figure 2.1A).

2.3.3.1 Viability and Proliferation

Viability and proliferation of UD encapsulated cells were assessed by LIVE/DEAD and AlamarBlue assays throughout the differentiation protocol. Some apoptotic single-cells were observed immediately after encapsulation (Figure 2.6A), but the apoptotic cell population did not increase even after 23 days of encapsulation. Unlike previous encapsulation configurations,

small cell colonies were visible after the propagation stage, which continued to grow into large viable colonies by the end of maturation. The vast majority of the cells in the individual colonies remained viable after maturation, although some apoptotic cells were observed on the periphery of colonies towards the end of maturation. Figure 2.6B shows proliferation of encapsulated hESCs, represented as fluorescence intensity per capsule. Proliferation of encapsulated cells progressively increased up to the end of pancreatic progenitor stage, and decreased slightly after maturation. These results clearly indicate a significant increase in the cellular viability and overall yield of mature cells by encapsulating UD hESC rather than pre-differentiated hESCs.

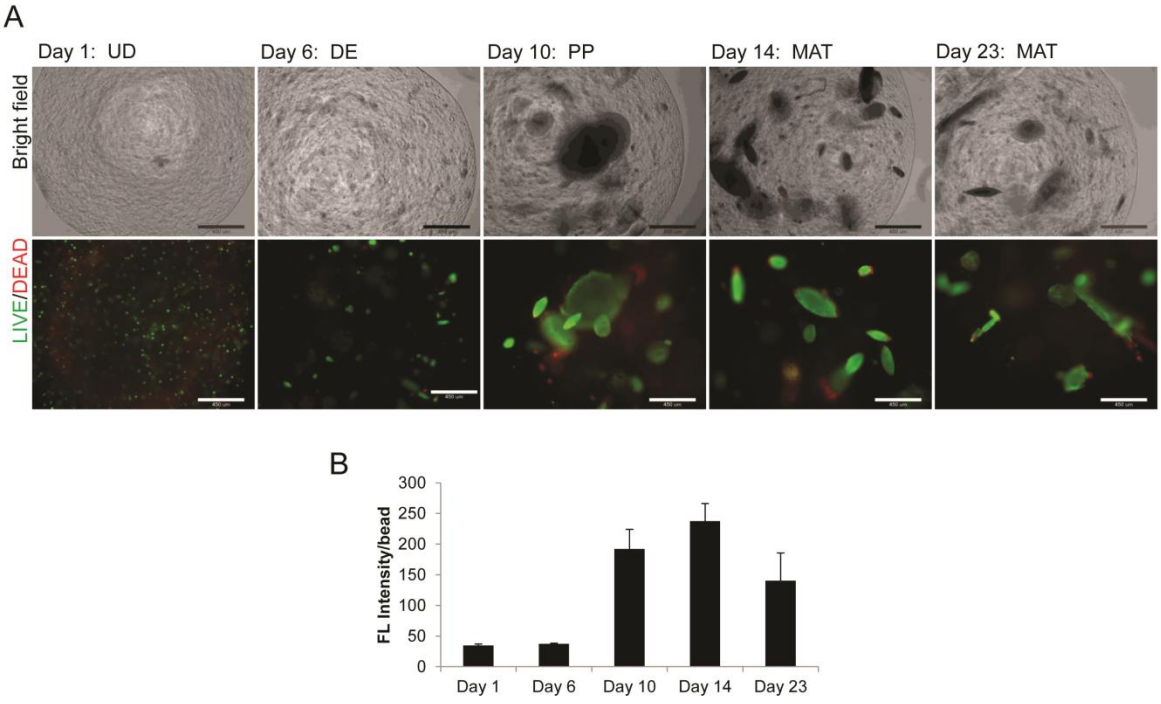

Figure 2.6. Viability and proliferation of hESCs encapsulated at the undifferentiated stage.

A) LIVE/DEAD viability assay on the first and last day of differentiation, for each stage after encapsulation. B) AlamarBlue proliferation assay on the first and last day of differentiation, for each stage after encapsulation (n = 3). Scale bar is 450 µm.

2.3.3.2 Differentiation under Encapsulation

Having confirmed high viability of the encapsulated hESCs, the next question is the differentiation potential of the encapsulated cells. Cellular differentiation was analyzed in detail after each stage of the induction protocol by using stage-specific markers. Gene expression analysis after DE induction of the encapsulated hESCs showed strong upregulation of the DE markers SOX17 (~400 fold), FOXA2 (~90 fold), CXCR4 (~72 fold), CER (~175 fold) compared to UD hESCs (Figure 2.7A). All these DE markers were found to be upregulated under encapsulation, although the levels were not significant different from parallel 2D controls. Analysis of protein expression using immunostaining confirmed SOX17 and FOXA2 positive cells in the encapsulated cells (Figure 2.7B). These findings indicate successful induction of encapsulated hESCs to the DE stage.

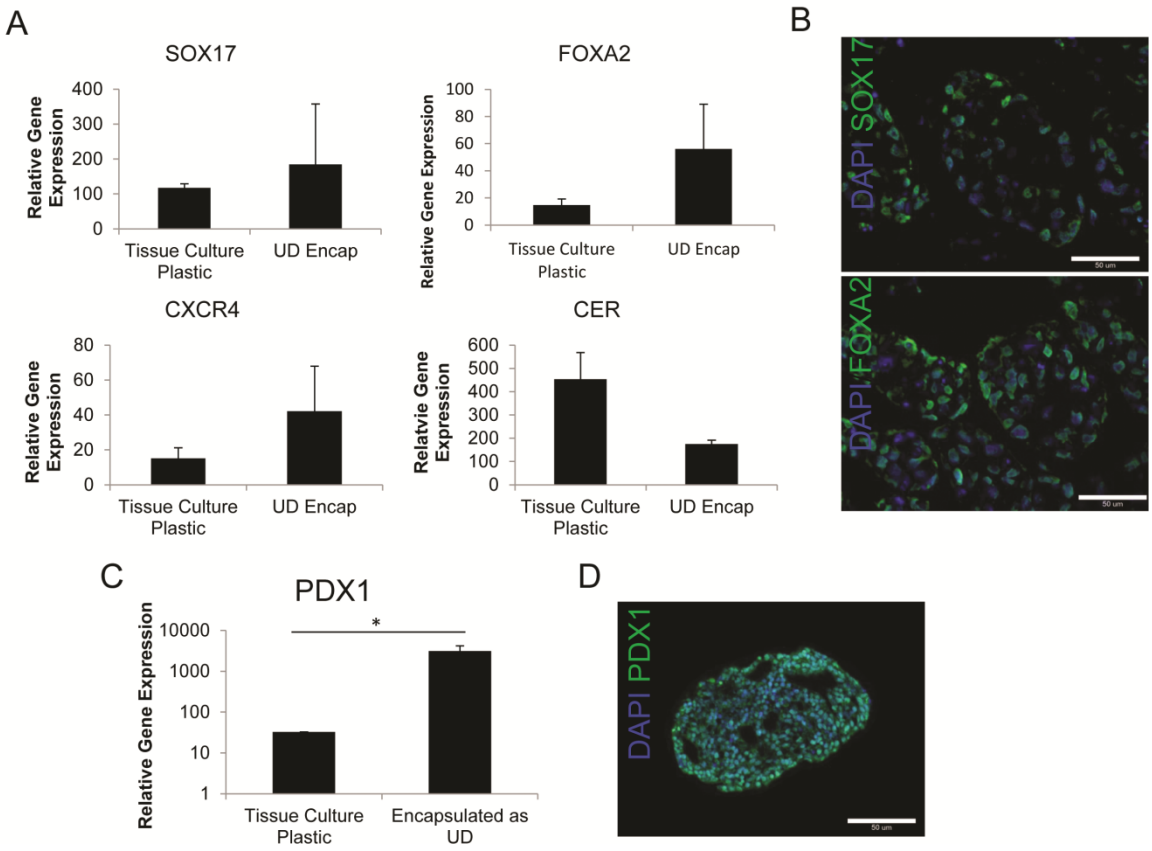

Figure 2.7. Characterization of the definitive endoderm and pancreatic progenitor stage for hESCs encapsulated at the undifferentiated stage.

A) Gene expression by qRT-PCR at the definitive endoderm stage for SOX17, FOXA2, CXCR4, and CER, compared to undifferentiated hESCs (n = 3). B) Immunostaining at the definitive endoderm stage for SOX17 and FOXA2. C) Gene expression at the pancreatic progenitor for PDX1 stage after encapsulation, compared to undifferentiated hESCs (n = 3). D) Immunohistochemistry at the pancreatic stage for PDX1. Scale bar is 50 μm. The results were considered significant if $^{*}P<0.05$.

The next step was analysis of the pancreatic progenitor stage. Similar to DE, the PP stage also showed strong upregulation of PDX1 when encapsulated, showing approximately 3000 fold increase compared to UD hESCs (Figure 2.7C) which was folds higher than parallel 2D controls.

Immunofluorescence analysis showed colonies of encapsulated cells strongly positive for the PDX1 protein (Figure 2.7D), confirming differentiation to the PP stage.

The encapsulated cells were further induced towards islet maturation as detailed in Figure 2.1A. Maturation was achieved by notch inhibition by addition of DAPT for 7 days. At the end of the entire protocol the encapsulated cells were analyzed for mature pancreatic islet-specific markers. Gene expression analysis at the mature stage showed strong upregulation of the beta cells markers insulin (~$8x10^5$ fold) and MAFA (14 fold), as well as the alpha cell marker glucagon (~$3x10^4$ fold), compared to UD hESCs (Figure 2.8A). Unlike the previous stages, the strength of the mature markers under encapsulation was comparable to that of the control in conventional 2D cultures. The exception to this is PDX1 (800 fold), which was several folds stronger than parallel TCP controls, although this difference was not significant. Detailed immunostaining characterization of the encapsulated cells revealed cell colonies positive for PDX1, as well as MAFA, which has been implicated in the mechanism of glucose responsive insulin secretion (Figure 2.8B). Additionally, cells were positive for glucagon and somatostatin, as well as a considerable number of cells positive for c-peptide, all of which are hormones secreted by islets (Figure 2.8B).

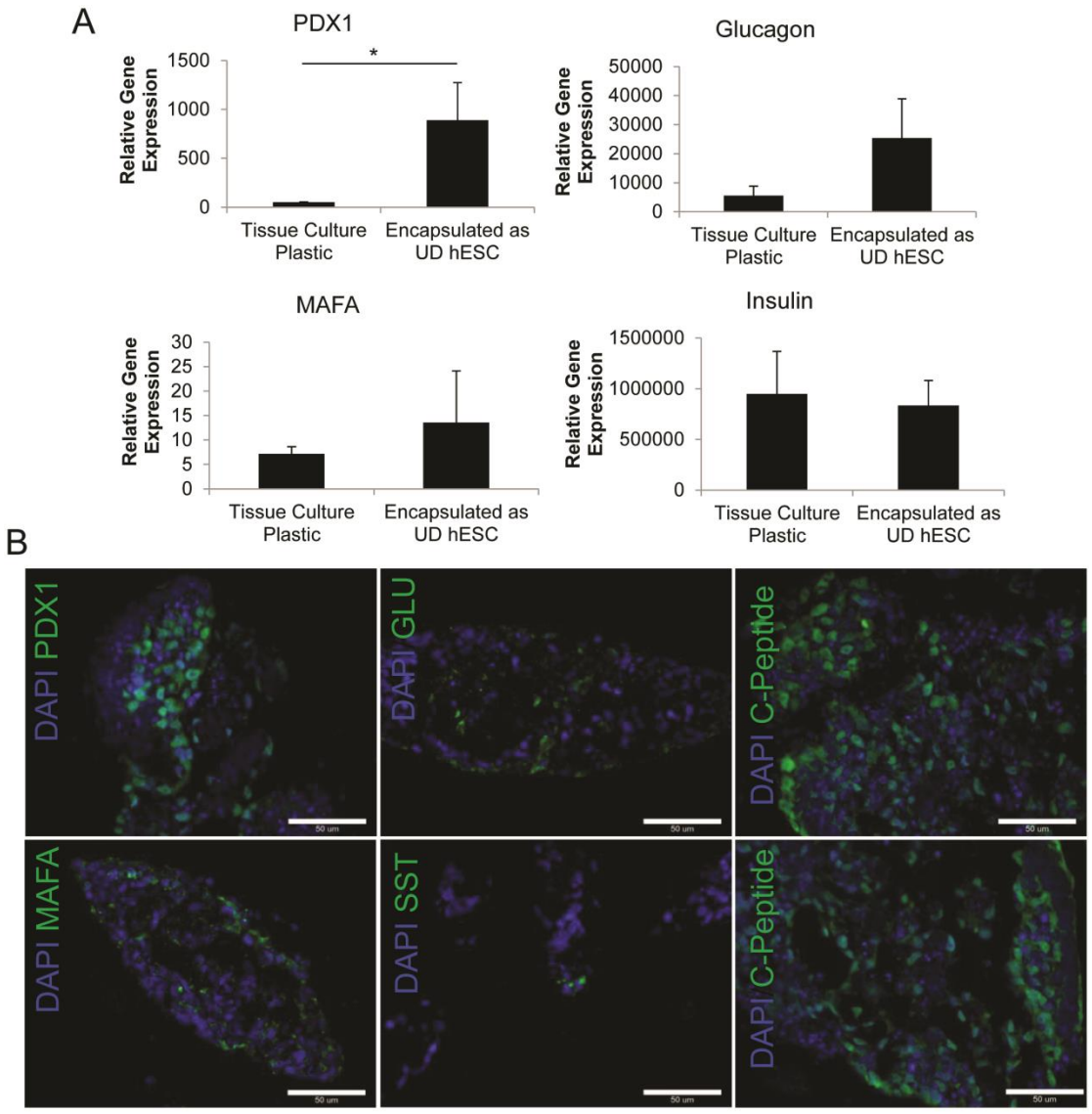

Figure 2.8. Characterization of mature islet-like cells, encapsulated as undifferentiated hESCs.

A) Gene expression of the mature markers PDX1, glucagon, MAFA, and insulin, compared to undifferentiated hESCs (n = 3). B) Immunohistochemistry at the mature stage for PDX1, Glucagon (GLU), MAFA, Somatostatin (SST), and C-Peptide. Scale bar is 50 µm.

While some of the cells were polyhormonal, expressing both c-peptide and glucagon as shown in Figure 2.9A, there were distinct populations of cells expressing single hormones

(Figure 2.9B). Thus differentiation of encapsulated UD cells shows a high cellular yield as well as efficient differentiation to mature pancreatic phenotype, as indicated by gene and protein expression of mature pancreatic islet markers.

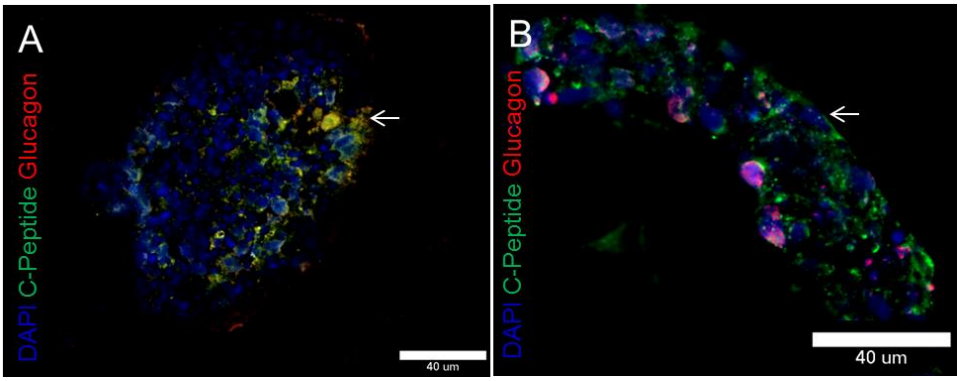

Figure 2.9. Pancreatic islet Hormone localization.

A) Co-staining of UD encapsulated hESCs at the mature stage for c-peptide and glucagon. The white arrow shows a cell which is polyhormonal. B) Co-staining of UD encapsulated hESCs at the mature stage for c-peptide and glucagon showing single hormone positive cells. The white arrow is directed at a cell which is positive for the single hormone c-peptide.

2.3.3.3 Intracellular C-peptide and Glucagon content and release

As a final analysis of the maturation of hESC derived islet-like cells, we measured the intracellular protein content and protein secretion of the islet-specific hormones c-peptide and glucagon, shown in Figure 2.10. Mature insulin is produced by post translational cleavage of proinsulin into insulin and c-peptide. Thus, intracellular c-peptide content is analogous to intracellular insulin, and is a measure of avoiding any artifacts arising from insulin in the culture media. Quantification of the intracellular c-peptide and glucagon protein content was performed

using Luminex based Magpix assay. The encapsulated UD hESCs were found to contain 0.39 pg c-peptide/µg total-protein, which was 20 fold higher than the 2D controls, containing 0.019 pg c-peptide/µg total-protein. Similarly, the encapsulated UD hESC showed 0.085 pg glucagon/µg total-protein, while 2D showed 0.006 pg glucagon/µg total protein (Figure 2.10A).

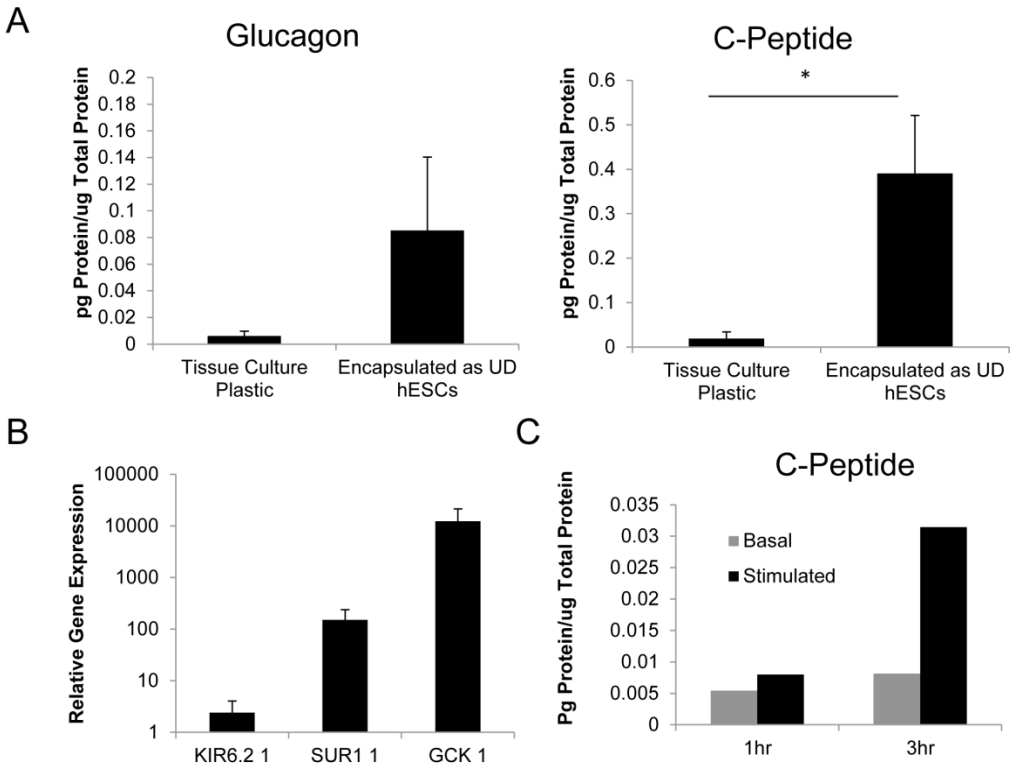

Figure 2.10. Intracellular protein quantification and glucose sensing.

A) Intracellular c-peptide and glucagon content at the mature stage for UD encapsulated hESCs, measured by MagPix analysis. B) Gene expression analysis of the glucose sensing molecules KIR6.2 and SUR1 (subunits of K_{ATP} channel) and glucokinase (GCK) at the mature stage for UD encapsulated hESCs. C) Released c-peptide in response to basal conditions (low glucose) and after stimulation with high glucose (16.7 mM), 100 mM tolbutamide, and 30 mM KCl for 1 and 3 hours respectively, measured by MagPix analysis. The results were considered significant if $^{*}P<0.05$ (n = 2).

After confirming the ability of hESC-derived cells to synthesize islet-specific hormones, we wanted to evaluate the mature functionality of the cells in sensing and responding to extracellular glucose with enhanced insulin/c-peptide release. The presence of potassium channel K_{ATP} required for c-peptide release was confirmed by the upregulation of the K_{ATP} subunits genes KIR6.2 and SUR1 (Figure 2.10B). Glucokinase, a key molecule involved in sensing glucose levels, also showed an upregulation in gene expression (Figure 2.10B). Finally, we analyzed the release of c-peptide in response to stimulation for 1 and 3 hours with physiologically relevant high glucose concentration (16.7), tolbutamide, and KCl. Upon stimulation for 1 and 3 hours, the mature islet-like cells released 0.008 and 0.031 pg c-peptide/µg total-protein into the media, respectively (Figure 2.10C). Stimulation resulted in approximately 1.5 fold and 3.9 fold higher c-peptide release over the basal conditions for 1 and 3 hour stimulation, respectively. Thus it can be construed that hESC differentiation under alginate encapsulation promotes both hormone synthesis and release in response to stimulation.

2.3.3.4 Enhanced differentation is likely due to increased pSmad/pAKT ratio

Since encapsulated differentiation of hESCs enhanced its maturation over the conventional 2D tissue culture plastic control, we further investigated the cause of these enhancements. Our initial hypothesis was the extracellular matrix (ECM) and cell adhesion (CAM) molecules in the encapsulated cell clusters are mediating this process. Hence we first analyzed the global gene expression of ECM and CAM molecules for both the 2D cultures and encapsulated cultures at the DE and PP stage using the Extracellular matrix and Adhesion molecule array. This array profiles genes important for cell-cell adhesion, cell-matrix adhesion, and various ECM molecules. Figure 2.11A shows the results for this gene array represented as a heatmap, for CAM, ECM and molecules categorized as both CAM and ECM (BOTH). The heatmap

represents relative gene expression of encapsulated cells at DE and PP stage, compared to the 2D control evaluated at DE and PP stage, respectively. Overall we observed that most of the tested molecules were either unchanged at the DE stage or down regulated, while the PP stage showed a more prominent downregulation of the tested molecules under encapsulation. There were only few molecules which were consistently upregulated under both DE and PP condition, of which MMP7 had the highest upregulation. MMP15 was strongly upregulated in PP stage, but was unchanged at DE. Of the CAM molecules, VCAM1, NCAM1, ITGA8 and ITGA4 were strongly upregulated at the DE stage but were downregulated at PP.

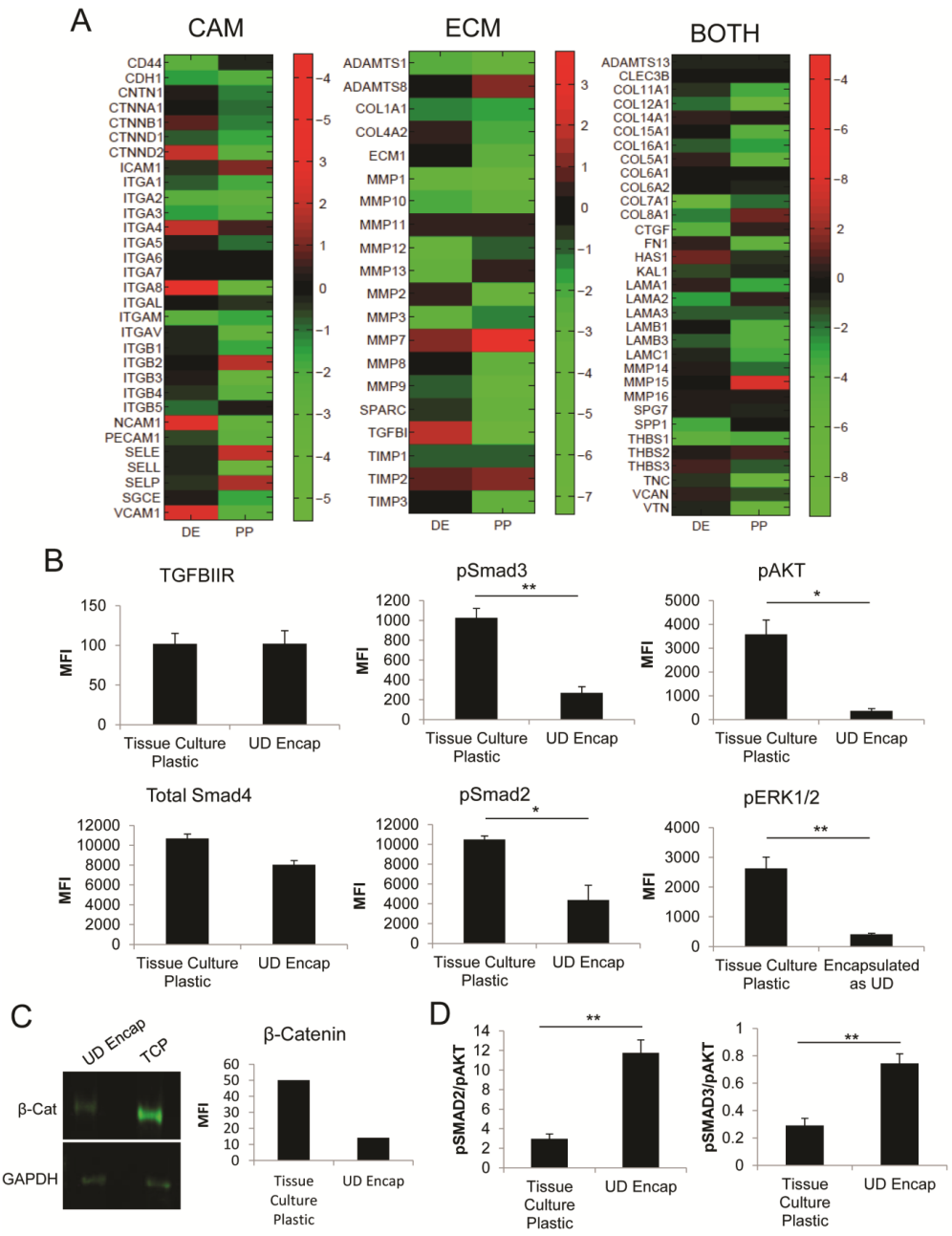

Figure 2.11. Characterization of enhanced differentiation for cells encapsulated as UD hESCs.

A) ECM and adhesion molecule gene array by qRT-PCR at the DE and PP stage, compared to cells differentiated on TCP. B) Protein expression of key molecules in the TGFβ pathway, and molecules which with this pathway by MagPix analysis after DE stage (n = 3). C) Western blot analysis for β-catenin after DE differentiation. MFI is normalized to GAPDH. D) pSMAD3/pAKT and pSMAD2/pAKT after DE differentiation. The results were considered significant is $^{*}P<0.05$, $^{**}P<0.01$.

Next we wanted to evaluate the primary signaling pathways mediating the process of differentiation. We concentrated on the DE stage since DE differentiation is critical in achieving successful maturation of the hESCs into functional cell types. Since DE induction was achieved through the activation of TGFβ and WNT pathway we measured the expression of the primary effectors of these pathways. For TGFβ pathway we focused primarily on expression of key SMAD molecules by Luminex-based MagPix assay, and for WNT pathway we measured expression of β-catenin by western blot analysis. Quite interestingly, we found the expression level of the key effectors of the pathways; pSMAD2, pSMAD3 (Figure 2.11B) and β-catenin (Figure 2.11C) were lower under encapsulation. Consistent with the other molecules, the expression of pAKT and pERK were also found to be lower under encapsulation than in 2D cultures (Figure 2.11B). However, low expression of these crosstalk molecules from parallel pathways will be indicative of less influence of negative feedback. In order to quantify this effect, we evaluated the ratio of pSMAD2 and pSMAD3 with pAKT. It was consistently observed that pSMAD/pAKT ratio was significantly higher under encapsulation compared to TCP cultures (Figure 2.11D). This indicates that the increased differentiation observed under encapsulation could be due to an increased ratio of pSMAD2/3 /pAKT.

2.4 DISCUSSION

In this chapter we are presenting a detailed procedure for obtaining hESC derived encapsulated islet-like cells which can be directly implanted for treatment of the autoimmune disease, type 1 diabetes. The presented study will address the shortage for donor islets by providing a platform for high throughput and directly implantable regenerative cell source. Deriving functional islet-

like cell types from pluripotent stem cells has the potential for creating a major transformative impact in cell therapy. Hence this has been an intensely researched area over the past decade, with multiple studies including our own, investigating pathways for efficient differentiation of hESCs to islet-like cell types on conventional TCP culture configuration [40, 42, 43]. In contrast to those studies, the current report specifically focuses on deriving encapsulated islet-like cells from hESC. The criteria for useful encapsulation will be high insulin per bead which needs (i) adequate maturation of the encapsulated cells and (ii) high yield of viable encapsulated cells.

In our previous study we have reported a stage-wise differentiation protocol for differentiating hESCs to mature islet-like cell types [87]. In the current study, we further extended our 2D protocol to evaluate for the first time the feasibility and configuration for 3D encapsulation of hESC derived cell types. The first logical extension of our 2D protocol to a 3D system was to fully differentiate hESCs to mature islet-like cells in 2D, followed by harvesting and encapsulation of these differentiated mature cells. Our results demonstrated that encapsulated cells were initially viable, but their viability decreased with continuous culture. It is known that the proliferation rate of hESCs progressively reduces with differentiation, and typically the cells are not proliferative after maturation. Hence the cell loss upon encapsulation could not be recovered by the proliferation of the live cells. Furthermore, the encapsulated cells appeared to lose the mature phenotype, as exhibited by the rapid down-regulation of mature gene expression of the encapsulated cells. It is difficult to conclude if the encapsulated cells are going through dedifferentiation, or if the more mature cells are prone to apoptosis, while the surviving cells are a less differentiated sub-population. Alternatively, the disruption of the ECM microenvironment and cell-cell contact formed during the 23 day differentiation protocol during the harvesting step could have led to the low viability of encapsulated cells. Previous studies

have also shown that dissociation of islet clusters leads to loss of cell function and apoptosis[90], possibly indicating that our hESC-derived islet-like cells require cell-cell contact similar to primary islets. Additionally, previous work with islet-like maturation of hESCs by implantation of PPs using the Theracyte device has shown that colony formation is required for development of insulin producing cells, while single cell suspensions failed to develop into insulin secreting cells [91, 92]. Thereby an encapsulation strategy ensuring adequate cell-cell contact and cell-cluster formation will be required to ensure functionality upon complete maturation of hESC.

With the failure to maintain the phenotype of mature cells upon encapsulation, we considered encapsulation of a partially differentiated hESC population which still retains proliferative potential. The hESCs are still proliferative in the DE stage, but proliferation slows down considerably during the induction of the PP stage. Hence we next explored encapsulating pre-differentiated DE cells, followed by further pancreatic induction under encapsulation. When we encapsulated hESC-derived DE cells, we saw moderately better viability immediately after encapsulation compared to encapsulation of mature cells. The cells also grew into small cell colonies upon maturation and proliferation of encapsulated DE cells was highest immediately after encapsulation, but decreased by the end of maturation. This was expected because mature cells are known to show little or very slow proliferation [93]. This, combined with normal apoptosis during differentiation, could explain the decrease in proliferation by the end of maturation. It is unlikely that diffusion limitations from encapsulation was causing any cell death, since the alginate capsule is very porous, and the encapsulated cell aggregates are fairly small in size (~ 350um in diameter). Although DE encapsulated cells show adequate induction to the mature stage, as well as improved viability, the yield of viable cells is still very low. The transplantation of these encapsulated islet-like cells is volume limited. A low yield of

encapsulated viable cells requires an increased volume of capsules to meet insulin requirements. Therefore, it is likely that the number of capsules needed to return to normoglycemia would be too high of a volume for the implantation site. It may be possible to enhance the yield of viable cells by increasing the seeding density. However, compensating for cell death by increasing seeding density may restrict the translational potential of this platform.

In our next configuration we therefore explored the encapsulation of undifferentiated hESC and performing the entire maturation under encapsulation. Our results indeed indicate that when undifferentiated hESCs were encapsulated and differentiated to mature islet-like cell types, the yield of viable cells was greatly improved. Distinct viable colonies were visible at the end of maturation, a result which was never achieved by encapsulating predifferentiated cells. This could be attributed to the propagation of the encapsulated cells before induction of differentiation, which could have been permissive to colony formation and establishment of cell-cell contact prior to differentiation. Similar to encapsulation of DE cells, we saw a peek in proliferation when encapsulating UD hESCs at the end of the PP stage and proliferation decreased by the end of the maturation stage. This decrease in proliferation can be attributed to slower proliferation of maturing cells and cells undergoing apoptosis during the differentiation process. Additionally, encapsulated UD hESCs at the mature stage show upregulation of the gene PDX1, as well as the mature markers glucagon, MAFA, and insulin, confirmed by immunostaining. These results therefore unequivocally demonstrate that alginate encapsulation and differentiation of UD hESC results in adequate islet-like differentiation, as well as a higher yield of viable cells. While encapsulation of hESC-derived PP cells have been previously proposed as a strategy for implantation [94], our results indicate the difficulty of encapsulating partially differentiated cells. Thus from a purely differentiation stand-point it is advantageous to

perform the entire differentiation under encapsulation. However, from the standpoint of implantation, it will be advantageous to minimize the period of in-vitro culture under encapsulation, prior to implantation. This is to minimize the presence of contaminating antigens from encapsulated dead cells during culture and differentiation. Hence we propose the strategy of decapsulating the differentiated hESCs after maturation, followed by its re-encapsulation in ultrapure, endotoxin free alginate. These alginate capsules will be further modified with a polycation coating, followed by an alginate coating [18, 84] and implanted immediately.

Since encapsulation and differentiation of UD hESCs appear to meet the requirements of adequate mature differentiation and high yield of viable cells, we conducted further characterization of these cells by analysis of intracellular c-peptide levels to seek further insight into possible mechanisms. C-peptide was measured to avoid any artifacts arising from insulin in the media. Protein quantification using MagPix showed that the encapsulated UD hESCs expressed intracellular c-peptide (0.39 pg/µg total-protein) and glucagon (0.019 pg/µg total-protein). Although a previous study with primary mouse islets showed a c-peptide content of 9.93 ng/µg total protein [95], considering the present results are obtained with hESCs, this is indeed an encouraging step towards functional islet-like cell types from hESCs in 3D culture. Gene expression analysis showed that the required machinery necessary for glucose stimulated insulin release was present by upregulation of the K_{ATP} subunits SUR1 and KIR6.2 as well as glucokinase. Additionally, the cells were stimulated for 1 hour and 3 hours to determine c-peptide secretion. Upon stimulation, encapsulated UD hESCs at the mature stage secreted 1.5 fold and 3.9 fold higher c-peptide over the basal conditions for 1 and 3 hour stimulation, respectively. It is worth noting that, although gene expression for insulin was similar between 2D controls and encapsulated cells, intracellular c-peptide protein was much higher in encapsulated

cells after maturation. However, it is unclear if differentiation under encapsulation is recruiting more islet-like cells or if the differentiated cells are eliciting higher levels of gene and protein. This enhancement could be attributed to the 3D environment provided by the alginate encapsulation forcing cell-cell contact, and is thus more closely mimicking the native environment cells would experience in vivo [96]. To investigate this further, we analyzed the gene expression levels of ECM and CAM molecules using a PCR array previously used to analyze the dynamics of embryoid body differentiation [97]. We expected to observe higher levels of CAM expression when comparing traditional 2D culture with our 3D alginate system, since the alginate hydrogel confines the differentiating hESCs. However, the gene array revealed that a large majority of the genes profiled were downregulated with respect to the 2D configuration for both ECM and CAM molecules at both the DE and PP stage. While most of the genes were downregulated, ITGA4, ITGA8, were upregulated at the DE stage, and MMP7 as well as MMP15 were however upregulated at the PP stage. ITGA4 is one of the integrins which encode the subunits of heterodimeric integrin's receptors that bind fibronectin and vitronectin, which are important matrix proteins during DE differentiation [98]. MMP15 has been shown to be highly expressed in the mature pancreas and MMP7 to a lesser extent [99]. Next we evaluated the expression pSMAD3 and β-catenin, key molecules which directly influence DE differentiation in the TGFβ and WNT pathways respectively. Surprisingly, the expression of both β-catenin and pSMAD3 was lower in encapsulated cells than in cells on 2D, even though the resultant differentiation initiated by these signaling pathways was significantly higher in encapsulated cells. Hence we analyzed the parallel signaling pathways since the effect of crosstalk has been recently shown to be dominant in differentiating hESCs [100]. pAKT is known to be a strong negative regulator of SMAD3 [101, 102] hence we analyzed the levels of

pAKT which was seen to be weaker under encapsulation. It is thus likely that even though the levels of pSMAD2/3 are higher in 2D cultures, the available proteins for nuclear translocation and hence gene transcription is lower from negative interaction with pAKT. For a more quantitative evaluation we next evaluated the ratio of pSMAD2/pAKT and pSMAD3/pAKT both of which were significantly higher under encapsulation compared to 2D cultures. Hence we hypothesize that even though the expression levels of key protein molecules is lower under encapsulation, the signaling cascade is more effective because of reduced negative interactions, as judged by the high levels of pSMAD3/pAKT and pSMAD2/pAKT ratio. This indicates that under encapsulation more SMAD complex is available for translocation to the nucleus which helps influence the differentiation. While pSMAD/pAKT ratio has been implicated to be critical in TGFβ-induced apoptosis in various different cells types [101], we report its importance in determining the differentiation potential of hESCs towards the DE cell type.

2.5 CONCLUSIONS

This research clearly shows that the configurations (stage) in which cells are encapsulated affects their viability/differentiation, and therefore their transplantation potential. We have shown that encapsulation of mature islet-like cells or hESC-derived DE cells resulted in a low yield of viable cells after maturation. Although encapsulation of hESC-derived DE cells showed adequate cellular maturation, encapsulation of UD hESCs was the preferred configuration since it distinctly showed adequate differentiation along with a high yield of viable cells. In fact, we have shown that differentiation of encapsulated UD hESCs resulted in a stronger expression of primary maturation markers and enhanced hormone synthesis compared to parallel 2D cultures.

This suggests that encapsulation and mature differentiation of UD hESC has the highest transplantation potential for treatment of type 1 diabetes. Furthermore, our analysis indicated that the high levels of pSMAD/pAKT ratio obtained upon encapsulation appear to be the primary mediator for differentiation further validating the promising therapeutic benefits of encapsulation of hESCs in alginate.

3.0 CAPSULE STIFFNESS REGULATES THE EFFICIENCY OF PANCREATIC DIFFERENTIATION OF HUMAN EMBRYONIC STEM CELLS

The content of this chapter is taken from Richardson Thomas, Barner Sierra, Candiello Joseph, Kumta Prashant N., and Banerjee Ipsita. Capsule Stiffness Regulates the Efficiency of Pancreatic Differentiation of Human Embryonic Stem Cells. Acta Biomaterialia. Volume 35, 15 April 2016, Pages 153-165

3.1 INTRODUCTION

In chapter 2 of this work, we showed the successful derivation of insulin producing β-cells from hPSCs encapsulated in calcium alginate capsules, towards a directly transplantable T1D treatment option [103]. Interestingly, we even observed significant enhancement in pancreatic maturation of hPSCs when differentiated under encapsulation, which renders calcium alginate capsules as an attractive platform for differentiation, in addition to immune protection. While calcium alginate has been extensively used in hPSC literature, it is limited in its in-vivo applications because calcium ions can be easily displaced by monovalent cations, such as sodium, resulting in weakening of the capsules over time [104, 105]. Alginate is composed of mannuronic (M) and guluronic (G) acid, which forms a 3D network when divalent cations bind

with the G residues of two adjacent polymer chains [9]. While calcium is commonly used for cell encapsulation, other divalent cations such as strontium and barium can also be used. In comparison to calcium, barium binds to alginate with a much higher affinity, resulting in more robust capsules [10, 36]. Thus barium alginate (BAlg) capsules have been extensively used for encapsulation of islets for T1D treatment [15, 19, 106-108]. However, BAlg has been less explored for pluripotent stem cell encapsulation, with few reported studies in adult stem cells [109-112]. The only successful study with hESCs is by Dean et al., who showed that hESCs encapsulated in BAlg could survive and differentiate when transplanted in mice for a period of four weeks [113]. Thus, the favorable mechanical properties of BAlg capsules warrant investigation of its potential for hESC encapsulation and differentiation.

The effect of insoluble physical cues, such as substrate stiffness or extracellular matrix (ECM) molecules, on stem cell differentiation is well-established [57, 114-116]. In the context of endoderm specific differentiation, our group has demonstrated the feasibility of driving early germ layer differentiation of mESCs by modifying the properties of alginate and fibrin substrates, in the absence of chemical inducers [117-120]. Hence even though pancreatic differentiation of encapsulated hESCs will be directed by chemical cues, it is likely that capsule properties will affect the fate of encapsulated cells. However, information on the effect of physical cues on stem cell differentiation is largely lacking in the context of pancreatic differentiation. The physical properties of alginate capsules can be modulated by changing the alginate (M/G ratio) and/or cation (Ca, Ba, Sr) type and concentration [30, 36]. As a general rule of thumb, increasing cation concentration will increase the stiffness of the resulting capsule by higher crosslinking of G residues; these effects are further enhanced by cations such as barium which have higher binding affinity [36, 37]. All of these can affect the fate and response of

encapsulated cells [61, 62, 121]. Hence, while engineering an encapsulation system for hPSCs, it is necessary to evaluate the effect of substrate properties on the fate of encapsulated cells.

The objective of this chapter was to investigate, for the first time, the use of BAlg encapsulation for pancreatic differentiation of hESCs, and determine how BAlg properties influence growth and subsequent differentiation of encapsulated hESCs. Overall it was observed that the efficiency of chemical induction was largely dependent on the properties of encapsulating substrate, even though diffusion was never restrictive within the capsules. Cell growth was observed to be favorable under the low stiffness regime, and was highly suppressed under high stiffness conditions. Interestingly, the effect of differentiation was more complex and differed based on stage of differentiation, possibly due to the complexity of the interaction of physical cues with non-linear signaling pathways. Increased alginate capsule stiffness appeared to promote TGFβ signaling during the definitive endoderm (DE) stage, which enhanced DE differentiation. However, increased substrate stiffness also promoted sonic hedgehog signaling at the pancreatic progenitor (PP) stage, which suppressed PP differentiation. Overall, cell growth and hESC-PP differentiation was found to be favorable in the stiffness range of approximately 4-7 kPa.

3.2 MATERIALS AND METHODS

3.2.1 Human embryonic stem cell culture

Undifferentiated (UD) H1 hESCs (WiCell) were maintained on hESC-qualified Matrigel (BD Biosciences) coated tissue culture plastic for 5-7 days in mTeSR1 (StemCell Technologies) at 37°C and 5% CO_2 before passaging. Experiments were performed with p55-p85 hESCs.

3.2.2 Barium alginate encapsulation of hESCs

A single cell suspension of UD hESCs was encapsulated by modifying our previous encapsulation protocol with the use of $BaCl_2$ [103]. hESCs were incubated with 10 µM Y-27632 (Millipore) for two hours and harvested with Accutase (Life Technologies) to obtain single cells. Cells ($1x10^6$ cells/ml) were suspended in filtered 1.1% (w/v) low viscosity alginate (Sigma-Aldrich) with 0.2% (v/v) gelatin (Sigma-Aldrich) and added drop wise to a solution of $BaCl_2$ (Sigma-Aldrich) with 10 mM HEPES (Sigma-Aldrich) using a 22 gauge needle. The alginate used for encapsulation consisted of 39:61 guluronic to manuronic acid residues and an endotoxin content of approximately 88 EU/g [89]. hESCs were encapsulated using 10, 15, 20, 50 or 100 mM $BaCl_2$. Alginate capsules were incubated for 6-8 min in the $BaCl_2$ solution. Capsules were washed three times with DMEM/F12 and suspended in mTeSR1 with 10 µM Y-27632 for 4 day, followed by 2 days in mTeSR1 alone to allow for colony formation, prior to differentiation.

3.2.3 Barium alginate capsule characterization

Alginate disks were formed using a 1.7 cm diameter mold, and crosslinked with 10, 15, 20, 50, and 100 mM $BaCl_2$. AFM force indentation measurements were performed using the MFP-3D Atomic Force Microscope (AFM, Asylum Research, CA, USA). The generated force measurements were analyzed using the MFP3D software (Asylum Research) built on IgorPro 6 (Wavemetrics) based on previously described models [122]. For all measurements a 100 micron silicon nitride cantilever (Veeco Systems) with a spring constant of ~0.6 N/m was functionalized with a glass silica sphere (radius 3.5 microns) at the apex. Figure 3.1 shows a schematic of AFM micro indentation using a spherical tip.

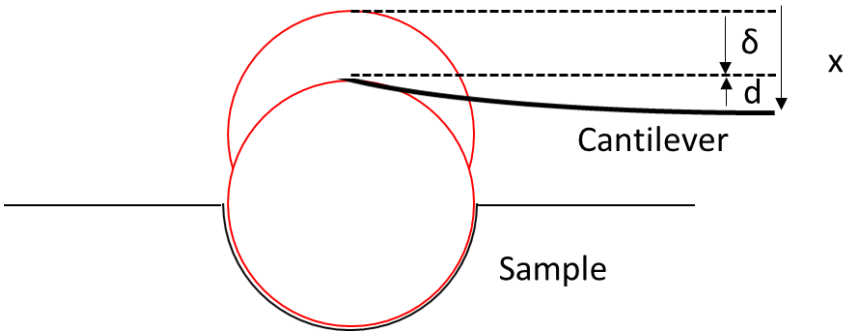

Figure 3.1. Schematic of AFM microindentation for hydrogel stiffness measurements

Young's modulus is proportional to is proportional the hydrogel displacement, δ, determined by the equation $\delta = x - d$. Where x is cantilever position, and d is the cantilever deflection. The hydrogels were maintained in saline after formation to ensure their hydrated state. The stiffness

of each alginate gel was measured at n = 3 random locations and approximately 16 force curves were taken over a 4x4 grid at each location on each sample.

Diffusivity was examined by first forming alginate capsules using 10, 20, and 100 mM $BaCl_2$ without cells. 1 ml of alginate was used to form capsules for each $BaCl_2$ concentrations, and was loaded with 2 mg of bovine serum albumin (BSA, (Sigma-Aldrich)). The capsules were suspended in 2 ml of 0.9% saline, and the supernatant was sampled for released BSA over 24 hours. BSA was measured using the BCA total protein assay (Thermo Scientific) according to manufacturer's instruction, and analyzed using a Synergy 2 multi-mode Microplate Reader (BioTek, Winooski, VT, USA).

3.2.4 Differentiation of encapsulated hESCs

The stage-wise induction protocol for the pancreatic differentiation of hESCs was identical to our previous study, ending at the pancreatic progenitor stage instead of the maturation stage [44]. First, DE was induced using 100 ng/ml ActivinA (R&D Systems, Minneapolis, MIN) with 25 ng/ml Wnt3A (R&D Systems) for 4 days. Afterwards, PP was induced with 0.2 µM KAAD-cyclopamine (CYC) (Millipore) for 2 days and 0.2 µM CYC with 2 µM retinoic acid (Sigma-Aldrich) for 2 days. All differentiation media was made using DMEM/F12 (Life Technologies), supplemented with 0.2% BSA and 1xB27® (Life Technologies).

3.2.5 Cell viability

LIVE/DEAD (Life Technologies) viability assay was performed according to manufacturer's instructions. Encapsulated cells were incubated with 2 µM ethidium homodimer-1 and 1 µM

calcein-AM in DMEM/F12 for 25 min at room temperature. Capsules were washed three times with DMEM/F12 before fluorescent imaging. Viable cells fluoresce green by metabolically converting calcein-AM to calcein and apoptotic cells fluoresce red by diffusion of ethidium-homodimer1 into the cell because of the permeable membrane of apoptotic cells.

3.2.6 Image analysis

The stock LIVE images from LIVE/DEAD analysis were processed using Metamorph. Briefly, the processing steps included thresholding to eliminate background, after which the image was binarized to create a black and white mask; filtered to detect the edges of the individual colonies, forming a mask or outline. From the mask, using Integrated Morphometry Analysis, data was generated for each colony within each image, measuring the area of the colony. This image processing was done on images taken on 5 capsules, each day for each condition.

3.2.7 hESC proliferation and death

Cell proliferation was measured using AlamarBlue (Life Technologies) assay according to manufacturer's instructions. Cells were incubated in the Alamarblue solution for 4 hours (1:10 v:v dilution). Cell death was measured by analysis of released lactate dehydrogenase (LDH), using the CytoTox 96® Non-Radioactive Cytotoxicity assay according to manufactures instruction. LDH released from dead/dying cells in the supernatant was analyzed every other days. Absorbance was measured using a Synergy 2 multi-mode Microplate Reader. To quantify cell death, dilutions of lysed cells were prepared to quantify LDH signal per cell, to create a

standard curve. Cell death measurements were presented as number of dead cells. Fluorescence intensity of the supernatant was measured using a Synergy 2 multi-mode Microplate Reader.

3.2.8 qRT-PCR for gene expression analysis

Cells were decapsulated with 100 mM EDTA (Sigma) and washed twice with PBS before lysis. mRNA was isolated using the NucleoSpin RNA II kit (Macherey-Nagel, Bethlehem, PA). cDNA was obtained using ImpromII Reverse Transcription (Promega, Madison, WI). Each PCR reaction contained 5 µl SYBR Green Master Mix (Agilent, Santa Clara, CA), 2 µl nuclease free H_2O, 2 µl primer, and 1µl cDNA. Samples were normalized to the house keeping gene GAPDH and analyzed relative to UD hESCs using the ΔΔCt method. Gene expression was measured with quantitative polymerase chain reaction (qRT-PCR) using an MX3005P system (Agilent).

3.2.9 MagPix for TGFβ pathway signaling analysis

The TGFβ pathway was analyzed using the MILLIPLEX MAP TGFβ Signaling Pathway Magnetic Bead 6-Plex (Millipore) for pSMAD2, pSMAD3, pERK1/2, and pAKT as well as total TGFβII and SMAD4 according to manufactures instruction. Briefly, 25 µl of each control and sample was incubated with 25 µl of a 1x beads solution over night at 4°C. After incubation, the beads were washed twice and incubated with 1x detection antibody for 1 hour in the dark, followed by 1x streptavidin-PE for 15 min. Fluorescence intensity was measured using the xMAP (Luminex, Austin, TX) machine. The total protein was measured using a BCA total protein kit, according to manufactures instruction.

3.2.10 Immunostaining

Encapsulated cells were fixed with 4% formaldehyde for 20 min and cryopreserved with 30% sucrose for 24 hours before embedding in OCT for cryo-sectioning. H&E staining was done to determine the gross morphology of the colonies for each encapsulation condition. For immunostaining, blocking was done with 10% donkey serum in PBS for 1 hour. Primary antibody staining was done overnight at 4°C, followed by addition of the secondary antibody for 45 minutes at room temperature. For primary antibodies, we used goat anti-SOX17 (1:200 dilution, Santa Cruz Biotechnology, Santa Cruz, CA), rabbit anti-FOXA2 (1:200 dilution, Santa Cruz), and goat anit-PDX1 (1:50 dilution, R&D Systems). Secondary antibodies used were: donkey anti-rabbit Alexafluor 555 (1:500 dilution), anti-goat Alexafluor 555 (1:500 dilution). Finally, slides were covered with hardening mounting medium containing DAPI (Vectashield, Vector laboratory). Slides were washed three times with PBS in between each step of the staining protocol. Primary and secondary antibodies and dilution details are located in the SI methods.

3.2.11 Statistical analysis

Data were presented as mean ± SD. Statistical significance between two groups was determined using the two tailed Student T-test for two group comparisons. Statistical significance comparing multiple groups was determined using one-way ANOVA, with Tukeys or Games-Howell post hoc testing for homogeneous or inhomogeneous variance, respectively. Probability values at $P < 0.05$(*) and $P < 0.01$ (**) indicated statistical significance.

3.3 RESULTS

3.3.1 Barium alginate stiffness, and not diffusion, affects encapsulated hESCs

The mechanical properties, namely stiffness, of organs can vary in a wide range: 1 – 10 kPa in soft tissue like brain or muscle, while hard tissue such as collagenous bone is on the order of 100 kPa [57]. Hence we first identified the range of cation concentrations which produces capsules in the range of 1 – 100 kPa, by varying barium concentrations (5 – 200 mM BaCl2). Alginate capsules were formed by drop-wise addition of alginate into the cation solution, resulting in capsules of 2.07±0.1 mm in diameter. Barium alginate capsules of this size have recently been shown to strongly resist fibrosis compared to traditionally used capsules of smaller diameter for up 175 days in immune competent mice, while supporting islet function and viability [108]. Resulting capsule stiffness was measured using atomic force microscopy (AFM) micro-indentation to determine the Young's Modulus. Capsules created with less than 10 mM $BaCl_2$ did not form homogenous capsules (data not shown), while those created with greater than 100 mM $BaCl_2$ were outside the desired stiffness range noted above. The Young's modulus of the BAlg capsules progressively increased from 3.9±1.3 kPA in the lowest $BaCl_2$ concentration (10 mM), to 73.3±22.4 kPA in the highest $BaCl_2$ concentration (100 mM, Figure 3.2A).

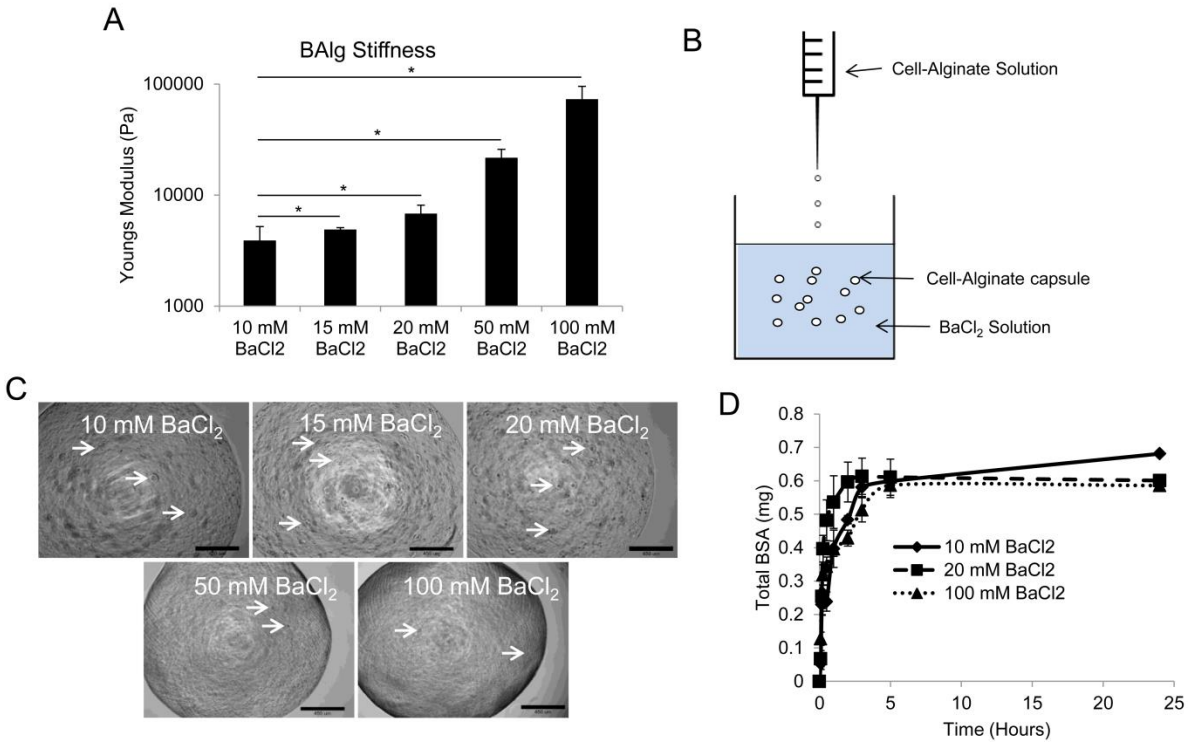

Figure 3.2. Characterization of Barium alginate capsule.

A) Alginate hydrogel elastic moduli (Pa) as measured by AFM nano-indentation of alginate crosslinked with 10, 15, 20, 50, and 100 mM $BaCl_2$. B) Schematic of alginate encapsulation of hESCs with the desired $BaCl_2$ concentration. C) Brightfield images of hESCs encapsulated in alginate crosslinked with 10, 15, 20, 50, and 100 mM $BaCl_2$ after propagation of undifferentiated hESCs for 6 days to allow colony formation. White arrows indicate colonies, which were minimal in the 50 and 100 mM barium alginate conditions. Scale Bar is 450 μm. D) BSA released from alginate capsules crosslinked with 10, 20, and 100 mM BaCl2 over 24 hours. The results were considered significant if *P<0.05.

The chosen range of capsule stiffness was next explored for encapsulating undifferentiated (UD) hESCs. Cells were suspended in 1.1% alginate with 0.2% gelatin and added to a solution of the desired $BaCl_2$ concentration for crosslinking (Schematic in Figure 3.2B). After 6 days of propagation, colony formation was minimal in the 50 and 100 mM BAlg

capsules, as compared to cells encapsulated in 10 – 20 mM BAlg capsules (colonies indicated with white arrows, Figure 3.2C). Since the density of crosslinking could also possibly modulate the diffusivity of the capsule to nutrients, growth factors, or small molecules in the media, we measured BSA diffusivity with changing alginate crosslinking. BSA was chosen for this study for its high molecular weight of 66.5 kDA, in comparison to key differentiation inducers: ActivinA (26 kDA), Wnt3A (40 kDA), CYC (0.4 kDA), and Retinoic Acid (0.3 kDA). Figure 3.2D shows that there was insignificant difference in the release profiles of the BSA loaded BAlg capsules of different crosslinking densities after 24 hours. This indicates that for the range of BAlg used in this study, the encapsulated cells are unlikely to experience any difference in media exposure from diffusion limitations. On the other hand, the effect of crosslinking on the resultant capsule stiffness was significant.

3.3.2 Capsule stiffness suppresses the growth dynamics of encapsulated hESCs

We next quantified the effect of varying $BaCl_2$ concentration, and thereby BAlg capsule stiffness, on the viability and proliferation of encapsulated hESCs throughout differentiation. UD hESCs were encapsulated using 10, 15, 20, 50, and 100 mM $BaCl_2$, propagated for 6 days, at which stage they form visible colonies. Following this, encapsulated cells were induced to differentiate to DE and subsequently to PP, following the protocol detailed in Figure 3.3A [44, 45, 103]. Cell viability was evaluated on days 1, 6, 10, and 14 after encapsulation using the LIVE/DEAD assay. As illustrated in Figure 2B, all the gel conditions show similar viable cells (green fluorescence) on Day 1 after BAlg encapsulation. However, by Day 6 after encapsulation, visible differences were apparent in the number of viable cells across each substrate condition. Softer capsules with lower $BaCl_2$ concentration exhibited larger viable cell colonies and less apoptotic single cells

(red fluorescence). In contrast, stiffer BAlg capsules synthesized with higher $BaCl_2$ concentration showed visibly fewer viable cell colonies and more apoptotic single cells. This effect was more dramatic by the end of the PP stage on day 14, where capsules of 50 mM and 100 mM $BaCl_2$ conditions resulted in very small cell colonies. However, in some of the capsules under these conditions, the colonies grew rapidly in size with unusual morphology as early as day 10 of differentiation (indicated by white arrows, Figure 3.3B).

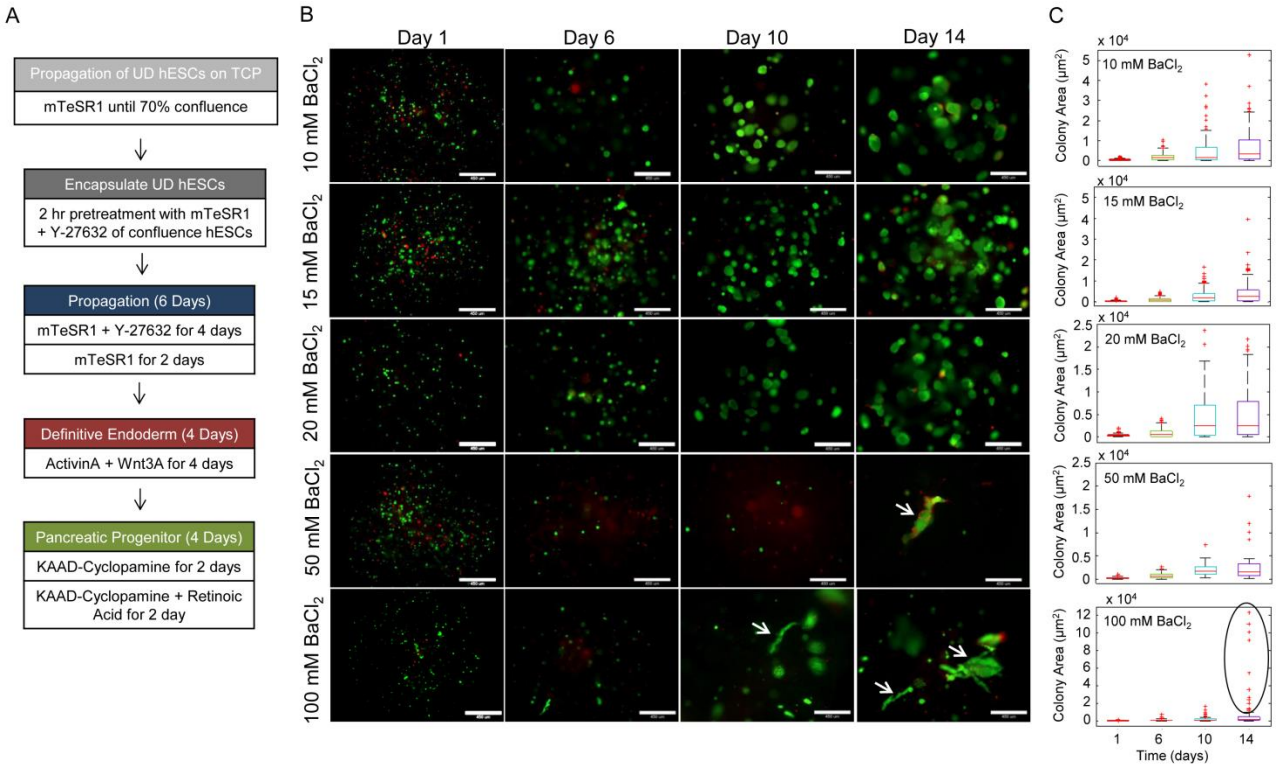

Figure 3.3. Viability and cell growth dynamics of encapsulated hESCs throughout differentiation.

A) Differentiation protocol for inductions of hESCs to PP cells. B) LIVE/DEAD assay of hESCs in response to barium alginate capsule stiffness. Scale bar is 450 μm. C) The LIVE images were processed using Metamorph for each encapsulation condition. Using Integrated Morphometry Analysis, data was generated for each colony within each image, measuring the area of the colony.

Visible cracks were observed on the surface of these capsules, likely due to the non-compliance of the stiffer capsules, which results in cracking as the capsule swells (Figure 3.4). It is thus likely, that cracks also formed within the BAlg capsule, allowing for uninhibited growth.

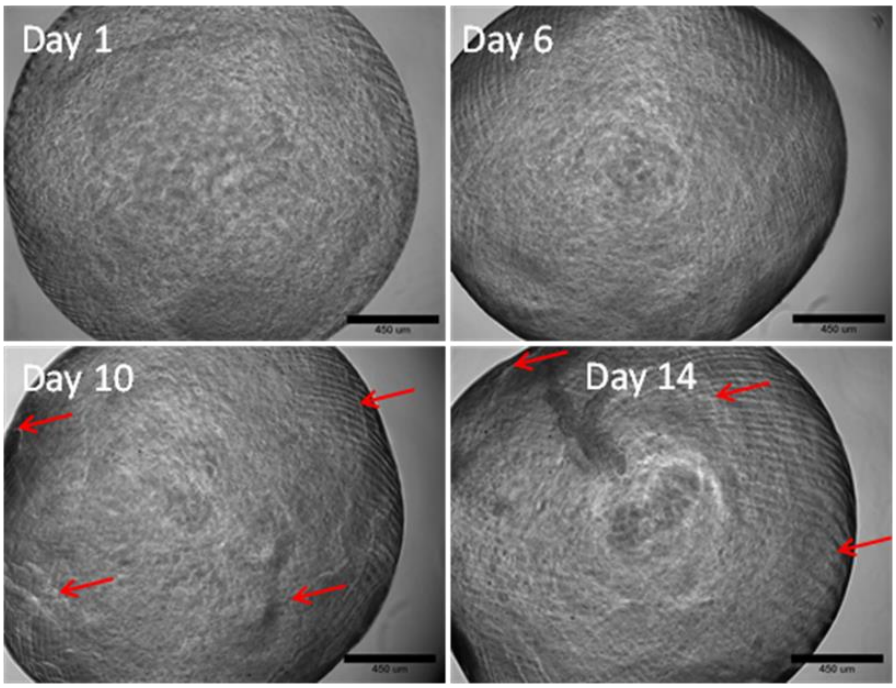

Figure 3.4. Alginate Bead Cracking.

Brightfield images for hESC encapsulated in 100 mM BaCl2 on day 1, 6, 10, and 14 after encapsulation. Scale bar is 450. Cracks indicated with red arrows.

To further characterize the dynamics of cell growth, the images from the LIVE/DEAD assay were quantified using Metamorph image analysis software. The colony area (μm^2) of each live colony was measured, and the dynamics of average colony area for each capsule configuration was quantified (Figure 3.3C). In general, for all crosslinking conditions, the cell

colony size increased initially with propagation. The extent of the growth was, however, strongly dependent on the capsule property. For example, by day 6, cells encapsulated using 10 mM $BaCl_2$ had a larger area as compared to the other conditions. Overall, increased $BaCl_2$ concentration resulted in a progressive decrease in cell colony size. This trend was apparent at the end of propagation stage and continued through the rest of the differentiation stages, with later stages showing an enhanced effect of substrate composition on colony size. An exception to this was the 100 mM BAlg condition, which had minimal growth in cell colonies all through the propagation and differentiation stages. As noted before, the 50 and 100 mM BAlg conditions showed some uninhibited growth, potentially from gel cracking, which are depicted as outliers (circled in black) in Figure 2C. These results clearly show that growth of encapsulated hPSCs is strongly determined by properties of encapsulating gel, with increased gel stiffness suppressing growth.

Consistent with colony sizes, quantification of cell proliferation by the AlamarBlue assay also showed a strong dependence on substrate stiffness. As shown in Figure 3.5A cells encapsulated in softer capsules (10-20 mM $BaCl_2$) are highly proliferative, and resulted in distinct colonies within the capsule. However, stiffer substrates (50, 100 mM $BaCl_2$) were less supportive of proliferation and hence failed to give rise to cell colonies. Along with proliferation, cell death was measured using the LDH assay, to verify if changing capsule properties are having any toxic effect on the cells. As shown in Figure 3.5B, cell death was most predominant in Day 1, immediately after encapsulation. Beyond that, cell death is somewhat suppressed for most of the conditions, while the cells remain highly proliferative as judged by AlamarBlue assay. It is important to note that cell seeding for all conditions was $1x10^6$ cells/ml, and the peak death observed was less than $2.5x10^5$ on day 1 for the 10 mM $BaCl_2$ condition. While this trend is

consistent across the softer gels, cells encapsulated in the stiffer gels remain somewhat static. They are neither proliferative, nor show significant cell death. Overall, the above results clearly show that BAlg capsules in the range of 10 – 20 mM BaCl2 (~4-7 kPa) are supportive of hESC proliferation and colony formation. While the stiffer gels were not necessarily toxic, they did not support sufficient colony growth to be a feasible option for encapsulation.

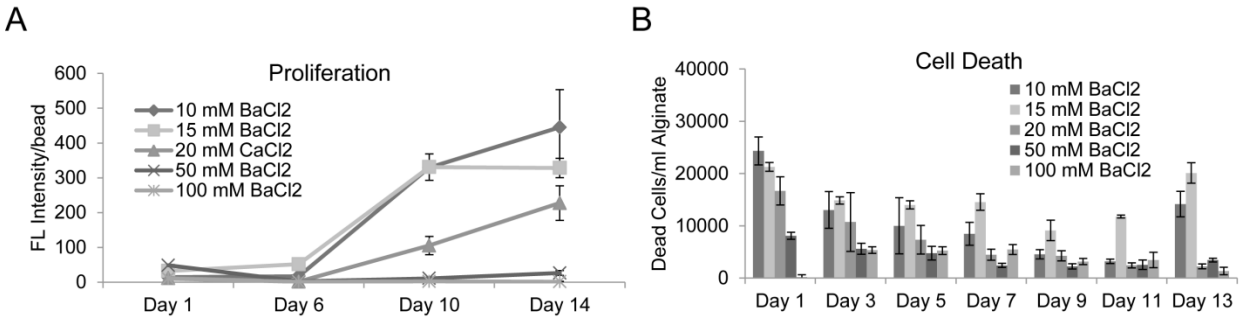

Figure 3.5. Proliferation and cell death of encapsulated hESCs, in response to substrate stiffness.

A) Cell proliferation measured by AlamarBlue assay, of encapsulated hESCs under each barium alginate condition during pancreatic differentiation. B) Cell death measured by the LDH assay, of encapsulated hESCs under each barium alginate condition during pancreatic differentiation.

3.3.3 Increasing capsule stiffness supports DE differentiation, while suppressing PP differentiation

Having confirmed cell viability and colony formation in BAlg capsules, we next evaluated the feasibility of differentiating the cells after encapsulation and growth. Encapsulated hESCs under each BAlg conditions were induced to DE and subsequent PP stage of differentiation following the protocol detailed in Figure 3.3A. Differentiation efficiency was analyzed by gene and protein

expression for both DE and subsequent pancreatic commitment. Figure 3.6A, B compares the efficiency of germ layer commitment across varying capsule stiffness, which shows a distinct biphasic response. Mesendodermal markers EOMES and CER both showed an initial increase in expression with increased capsule stiffness (Figure 3.6A), reaching a peak upregulation of ~3800-fold at 50 mM $BaCl_2$ for EOMES and ~6900-fold at 20 mM $BaCl_2$ for CER. Further increase in substrate stiffness, however, resulted in a reduction in gene expression. A similar biphasic trend was also observed for the DE markers SOX17 and FOXA2, with peak upregulation of ~8400-fold at 50 mM $BaCl_2$ for SOX17 and ~29500-fold at 20 mM $BaCl_2$ for FOXA2 (Figure 3.6B). Hence BAlg capsules crosslinked with 20–50 mM $BaCl_2$ (~7–22 kPa) exhibited the most significant upregulation of mesendoderm and DE markers. However it is worth noting that even the lowest observed gene expression at 10mM $BaCl_2$ is still substantial differentiation as judged by the strong upregulation of relevant genes. Further analysis of SOX17 and FOXA2 protein expression by immunostaining confirmed the strong presence of cell colonies with significant expression of these proteins in 10, 15, and 20 mM $BaCl_2$ (Figure 3.6C).

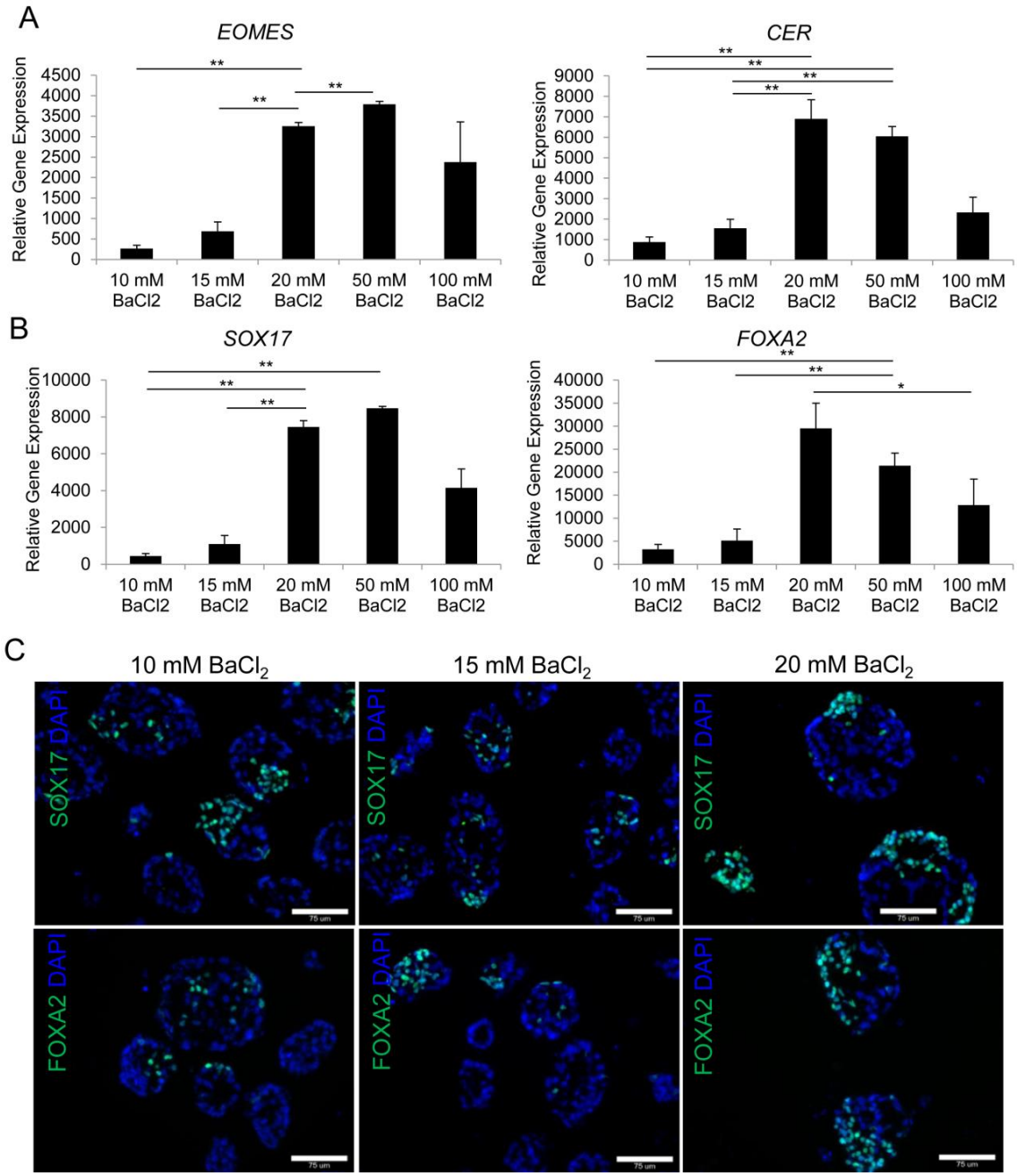

Figure 3.6. Increased substrate stiffness enhances DE stage differentiation.

A) Relative gene expression of the mesendodermal genes EOMES and CER for each barium alginate condition at the DE stage, relative to UD hESC. B) Relative gene expression of the DE genes SOX17 and FOXA2 for each barium alginate condition at the DE stage, relative to UD hESCs. C) Immunostaining of hESCs encapsulated with 10, 15, and 20 mM $BaCl_2$ at the DE stage, for SOX17 and FOXA2. Scale bar is 75 μm. The results were considered significant if *P<0.05, **P<0.01.

Having confirmed germ layer commitment, the next step was to analyze the effect of substrate stiffness on pancreatic commitment. We first looked at HNF4α, which is a marker of the primitive gut tube, and is expressed in pancreatic development between the DE and PP stages. Interestingly, consistent with the DE makers, gene expression of HNF4α increased as BAlg capsule stiffness increased (Figure 3.7A), but lacked the biphasic nature and was highest under the stiffest condition tested: ~510-fold increase over UD hESCs at 100 mM $BaCl_2$. Figure 3.7B shows gene expression of PTF1A, a precursor to PDX1, which showed a similar increasing trend with BAlg capsule stiffness, from ~3-fold to ~3300-fold upregulation over UD hESCs. A crucial transcription factor for endocrine pancreatic development is PDX1, which is also necessary for β cell maturation. In contrast with the previous analysis, PDX1 gene expression showed strong inverse relationship with BAlg capsule stiffness (Figure 3.7C). The highest PDX1 expression was obtained at 10 mM $BaCl_2$ which resulted in ~3800-fold increase over UD hESCs. All of the other gel conditions tested had a significantly lower PDX1 gene expression (~370 – 580 fold increase over UD hESCs).

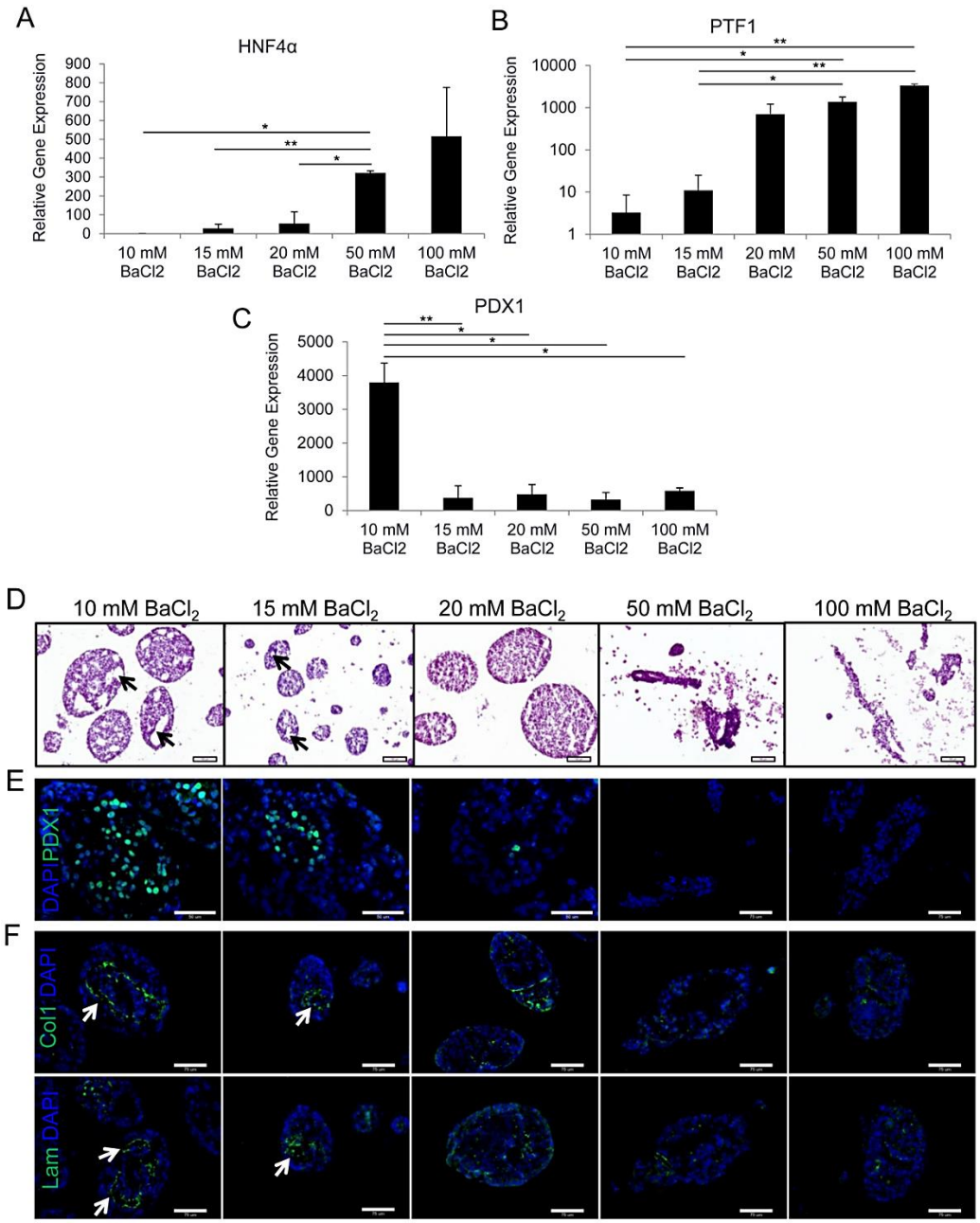

Figure 3.7. Increased substrate stiffness suppressed PP stage differentiation.

Relative gene expression of A) HNF4α, B) PTF1A, and C) PDX1 for each BAlg condition, at the PP stage. Gene expression was normalized to UD hESCs. The results were considered significant if *P<0.05, **P<0.01. D) H&E staining of hESC colonies encapsulated using each cation concentration, after the PP stage. Scale bar is 100 μm. Immunostaining for PDX1 E) and collagen 1 and laminin F) for hESCs encapsulated with 10, 15, 20, 50, and 100 mM $BaCl_2$. Scale bar is 50 and 75 μm, respectively.

We subsequently compared the morphology of PP colonies across the gel conditions. At the end of PP induction, the BAlg capsules were dissolved and the collected cell colonies were sectioned and stained with H&E to visualize the colony morphology for each BAlg condition (Figure 3.7D). Cells differentiated in the 10 and 15 mM BAlg capsules resulted in colonies which were visibly less dense in higher $BaCl_2$ concentrations. The cell colonies within 10 and 15 mM BAlg were found to have distinct cavities (indicated with black arrows) within the colonies, which was significantly reduced at 20 mM condition and completely absent in 50 and 100 mM BAlg capsules. As indicated earlier, 50 and 100 mM BAlg capsules resulted in either small restricted colonies or in some cases, large elongated colonies.

Pancreatic differentiation was next confirmed by immunostaining of colony sections for PDX1. Consistent with the gene expression analysis, cells encapsulated in the 10 mM $BaCl_2$ gel were strongly positive for the protein PDX1 (Figure 3.7E). While PDX1 protein expression was also detected in 15 mM and 20 mM conditions, the number of PDX1 positive cells decreased significantly with increasing gel stiffness. In the stiffest gels formed with 50 or 100 mM $BaCl_2$, no detectable cells were positive for the protein PDX1. Hence, while higher stiffness was conducive for mesendoderm and DE differentiation, the lower stiffness BAlg capsule was more supportive of endocrine pancreatic differentiation, as shown by high PDX1 gene and protein expression.

Since ECM can play a significant role in modulating cell fate, we further analyzed the PP colonies across gel conditions for relevant ECM proteins. In particular, laminin and collagen 1 are known to be important basement membrane and structural proteins in the pancreas, respectively [123-125] and were analyzed by immunostaining. Consistent with the differentiation data, the presence of ECM was more evident in lower stiffness gels (Figure 3.7F). Interestingly,

the ECM deposition appeared to be localized primarily around the cavities within the colony (indicated with white arrows).

3.3.4 Capsule Properties impact signaling at both the DE and PP stage

Our results showed that in spite of identical chemical induction, the differentiation potential of the encapsulated cells was significantly modified by the properties of the encapsulating substrate. Further, the effect of the substrate was specific to the stage of differentiation and not consistent throughout. Since signaling pathways are also known to have similar stage specific effect on differentiation, we hypothesized that substrate properties are modulating the efficacy of relevant signaling molecules. The TGFβ pathway is known to play a critical role in the process of endoderm and pancreatic differentiation. High activation is necessary for endoderm induction, while it is detrimental to pancreatic differentiation. Hence to analyze how substrate properties are affecting differentiation, we chose to measure the SMAD molecules, which are key effectors of the TGFβ pathway. However, the complex interactions between parallel pathways make it difficult to understand pathway behavior by analyzing molecules and pathways in isolation [126]. Hence we also measured pERK and pAKT which are known to have significant interaction with the TGFβ pathway. Using a Luminex-based MagPix assay, we measured the expression of relevant signaling molecules after the DE and PP stage in 10 and 20 mM $BaCl_2$ condition (Figure 3.8 and Figure 3.9). These conditions were chosen because they had the most contrasting effect between the DE and PP stage differentiation. We first focused on how gel stiffness influenced signaling at the DE stage (Figure 3.8A). Total TGFβRII levels were significantly lower in the 20 mM BAlg, while t-SMAD4 levels were insensitive to changes in response to capsule stiffness. Interestingly, the primary effectors of the TGFβ pathway,

pSMAD2/3, showed an opposite trend. While pSMAD2 was significantly lower in the 20 mM BAlg compared to 10 mM BAlg, pSMAD3 was significantly higher. The cross talk molecule pERK1/2 also showed significantly higher expression in the 20 mM BAlg, while pAKT, a negative regulator of the TGFβ pathway, showed significantly lower expression in this condition compared to 10 mM BAlg. To evaluate the level of negative regulation, we analyzed the ratio of pSMAD2/3/pAKT to estimate the level of available pSMAD2/3 which can influence differentiation (Figure 3.8B). While the ratio of pSMAD2/pAKT was not significantly different between the gel conditions, pSMAD3/pAKT was significantly higher in 20 mM BAlg. Both higher levels of pSMAD3 and higher pSMAD3/pAKT ratio in 20 mM BAlg condition, as compared to the 10 mM BAlg condition, indicates a larger pool of active pSMAD3 molecules are available to direct mesendoderm gene transcription.

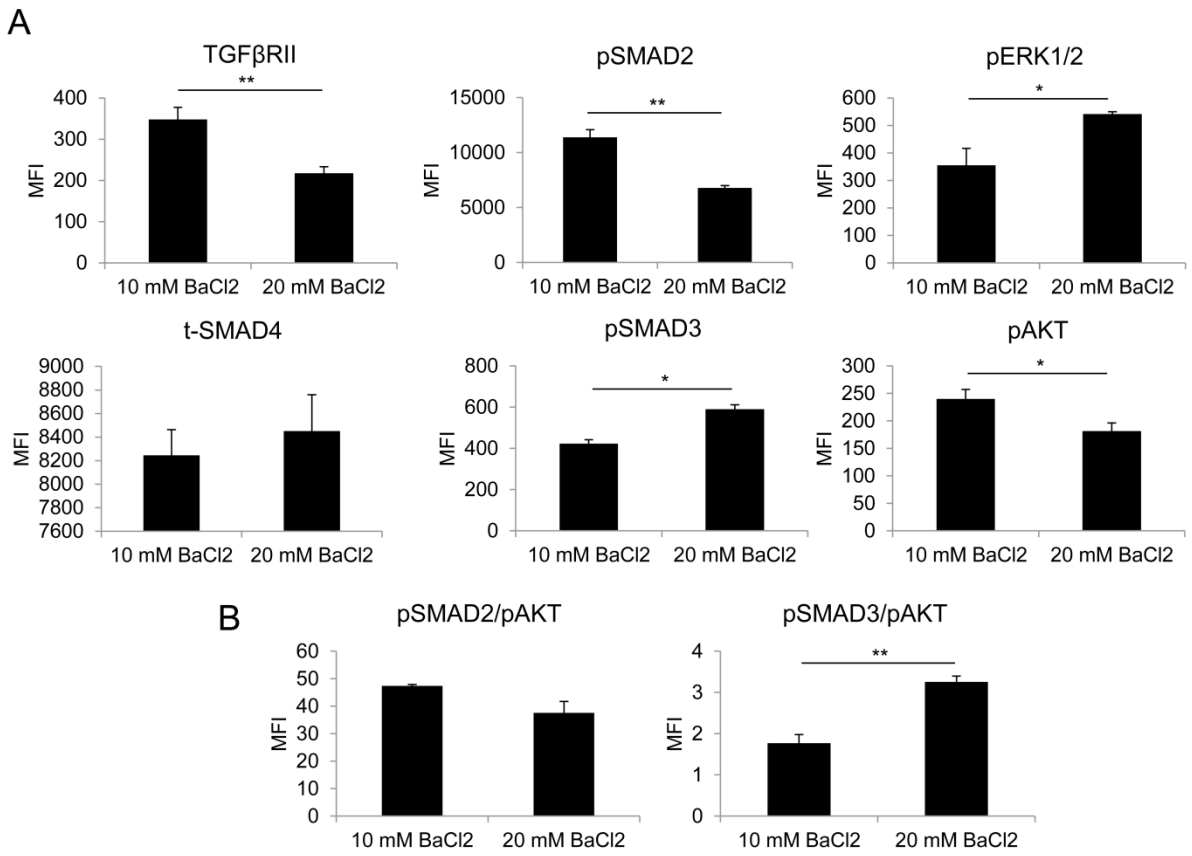

Figure 3.8. Effect of substrate stiffness on TGFβ signaling at the DE stage.

A) Expression of key signaling proteins of the TGFβ pathway, and key cross talk pathway molecules by Magpix analysis, after DE stage differentiation for hESCs encapsulated using 10 or 20 mM $BaCl_2$. B) The ratios of pSMAD2/pAKT and pSMAD3/pAKT, which indicated the level of available pSMAD2/3. The results were considered significant if *P<0.05, **P<0.01.

High TGFβ signaling activation is of paramount importance for DE induction; however, following DE specification, activation of this pathway is detrimental to pancreatic commitment [127]. In our experimental set-up, beyond the DE stage there was no exogenous activation of the TGFβ pathway. Even then we observed significant dynamics of the pathway molecules, the nature of which depended on the substrate properties (Figure 3.9A). Both 10 and 20 mM BAlg

conditions showed a significant increase in the receptor level and t-SMAD4 levels from DE to PP. However for 20 mM BAlg, the key signaling molecules pSMAD2/3 remained similar between DE and PP. This was surprising since the DE differentiation is conducted under high TGFβ stimulation and the PP stage is devoid of it. Even more surprising was the response of the 10 mM BAlg condition. While pSMAD2 was significantly reduced from the DE to PP stage, as expected from the removal of ActivinA, pSMAD3 was significantly enhanced from DE to PP under the 10 mM BAlg condition. Furthermore, this increase in pSMAD3 is in disagreement with the enhancement of the PP stage differentiation we observe under the 10 mM condition, since SMAD molecules are known to interfere with PP induction [128]. pSMAD3 levels under 10 mM BAlg at the PP stage is not only increasing from the corresponding DE stage, it is also higher than the 20 mM BAlg at the PP stage. However, as mentioned earlier, it is difficult to conclude on the state of signaling by evaluating signaling pathways in isolation. Hence we also evaluated pAKT and pERK levels to characterize the signaling events in more detail (Figure 7A). We observed that both pERK and pAKT increased significantly from the DE to PP stage under both gel conditions. However, the difference was insignificant for both signaling molecules between the two conditions at the PP stage. These pathways alone do not explain the observed difference in differentiation. Hence, we analyzed the ratio between the key signaling molecules, in order to quantify the interaction. We observed that the pSMAD2/3/pAKT ratio was significantly suppressed when the cells were differentiated from DE to PP, in both the gel conditions with the exception of pSMAD2/pAKT for 20 mM BAlg (Figure 3.9B). This indicates that the availability of active pSMAD levels lower upon withdrawal of ActivinA, while moving from DE to PP. While this analysis explains the feasibility of PP differentiation, it does not explain the superior performance of the 10mM BAlg condition.

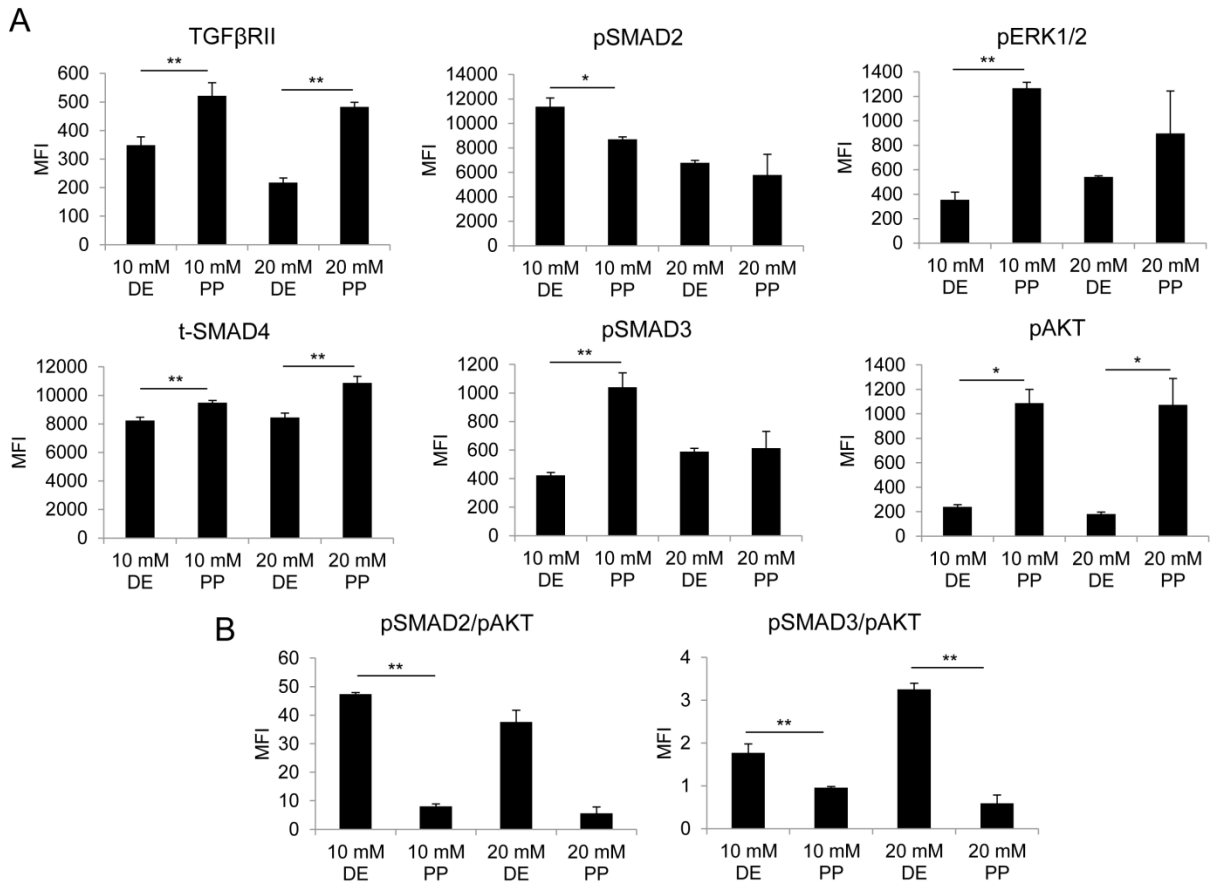

Figure 3.9. Effect of substrate stiffness on TGFβ signaling at the PP stage.

A) Expression of key signaling proteins of the TGFβ pathway, and key cross talk pathway molecules by Magpix analysis, after PP stage differentiation for hESCs encapsulated using 10 or 20 mM $BaCl_2$. B) The ratios of pSMAD2/pAKT and pSMAD3/pAKT, which indicated the level of available pSMAD2/3. The results were considered significant if *P<0.05, **P<0.01.

We next specifically analyzed pathways which are being directly modulated for pancreatic induction. This includes inhibition of the sonic hedgehog (SHH) signaling pathway, the presence of which promotes liver bud formation [127]. Hence, we examined the substrate-specific effect of SHH inhibition by measuring the gene expression levels of the SHH ligand and

GLI1, a transcription factor downstream of and activated by SHH. Comparing the two gel conditions at the PP stage, we observed that cells encapsulated in 10 mM BAlg capsules had lower expression of SHH and significantly lower expression of GLI1, compared to the 20 mM BAlg condition (Figure 3.10A). However, for both of these conditions, the gene expression of GLI1, was significantly higher at the PP stage than the corresponding DE stage, even when the signaling was suppressed with the inhibitor CYC (Figure 3.10A). A previous report has shown that the TGFβ pathway can activate SHH signaling through pSMAD3, independent of the SHH receptor smoothened [129]. Since we observed an increase in TGFβ signaling activation at the DE stage in the stiffer 20 mM BAlg conditions, we next wanted to examine if increased stiffness is activating SHH through the TGFβ pathway. We inhibited TGFβ signaling with the addition of Alk5i during the PP stage for the 20 mM BAlg condition. However, Figure 3.10B shows that in the presence of the TGFβ inhibitor, PDX1 expression decreased, while SHH and GLI1 expression increased slightly. This indicates that the stiffer substrates are more strongly activating SHH pathway independent of TGFβ, and thus is detrimental to PP induction, even though these same conditions favored DE differentiation.

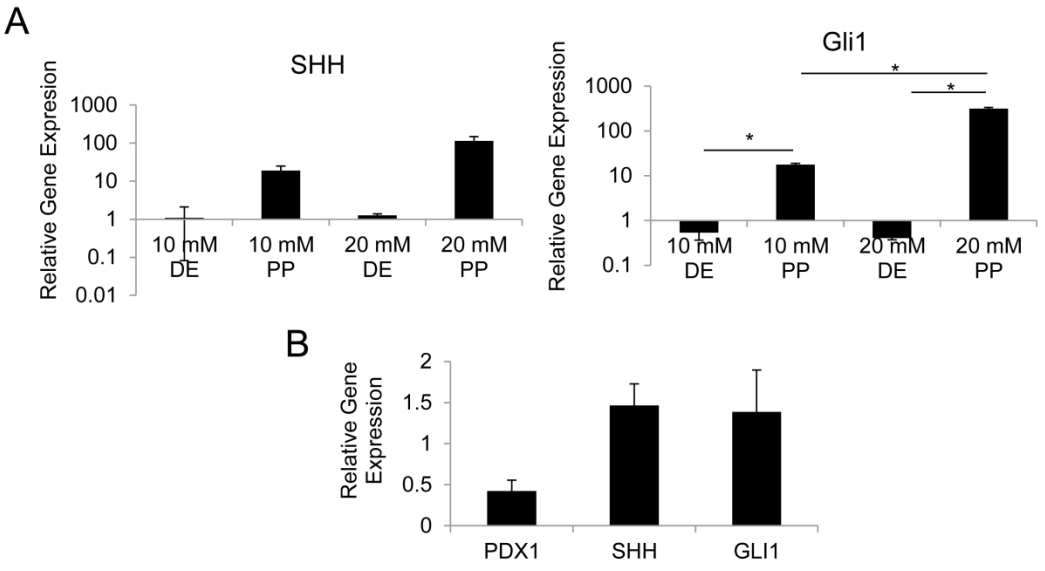

Figure 3.10. The effect of substrate stiffness on Sonic Hedgehog signaling.

A) Gene expression of SHH ligand, and its downstream target GLI1 at the DE and PP stage for hESCs encapsulated with 10 or 20 mM $BaCl_2$. Gene expression was normalized to undifferentiated hESCs. B) Gene express of PDX1, SHH, GLI1, at the PP stage for hESCs encapsulated using 20 mM $BaCl_2$, with the PP stage media supplemented with the TGFβ receptor inhibitor Alk5i. Gene expression was normalized to hESCs encapsulated with 20 mM $BaCl_2$ at the PP stage, which where differentiated without the Akl5 inhibitor. The results were considered significant if *P<0.05.

3.4 DISCUSSION

The objective of this study was to evaluate the feasibility of using BAlg encapsulation for pancreatic differentiation of hESCs, and how capsule properties regulate growth and differentiation. These capsules can then be subsequently used for implantation for T1D treatment, where BAlg is expected to immunoisolate the cells within. For hPSC-derived β-cell therapy for T1D to reach fruition, high capacity biomanufacturing techniques are required to

generate the necessary cell numbers (~10^9/patient). Hence, essential features to consider while engineering a platform for regenerative cell therapy for T1D are (i) supportive of cell growth (ii) supporting/promoting differentiation and (iii) amenable to immune protection, which has not yet been demonstrated. We observed that DE differentiation was enhanced as capsule stiffness increased; however, high capsule stiffness was not supportive of cell growth and proliferation. Low stiffness capsules were supportive of both cell growth, and pancreatic differentiation. Signaling pathways analysis showed that increasing capsule stiffness activated TGFβ signaling, which supports DE differentiation, and SHH signaling, suppressing PP differentiation. Hence in the current study we report for the first time, specific barium alginate configurations most supportive of growth and pancreatic differentiation of encapsulated hPSCs.

In evaluating the growth and differentiation properties of barium alginate capsules, the parameter we modulated was the crosslinking concentration. Even though the encapsulated cells were continuously induced by specific growth factors and chemical inducers, we hypothesized that the substrate properties play a critical role in modulating cell fate, as has been well known in stem cell literature, [57, 58, 115]. In islet encapsulation studies, 20 mM $BaCl_2$ capsules are the most ubiquitous, which results in a stiffness of 6.8 kPa. This is in a similar range as has been reported in mouse, 1.210±0.77 [117], and adult human pancreata, 1.4±2.1 kPa – 4.4 ±5.1 kPa [130]. Based on this, we selected a wide range of cation concentrations encompassing this range, where capsules made using 10 – 20 mM $BaCl_2$ (~4 – 7 kPa) most closely mimicked the stiffness of the pancreas in vivo. As seen in previous reports, increasing $BaCl_2$ concentration increases the young's modulus, E (kPa), of the resulting alginate capsule [36, 37], which significantly affected both growth and differentiation of the encapsulated hESCs. Most significantly, BAlg capsules using 10-20 mM $BaCl_2$ (first regime) was very supportive of cell proliferation, resulting in large

viable cell colonies by the end of the 14 day differentiation protocol. In contrast 50 - 100 mM $BaCl_2$ (second regime) resulted in marginal proliferation into small colonies. Although gel stiffness increased as $BaCl_2$ concentration increased in the first regime, it was not adverse to cell growth and differentiation. While in the second regime, the resulting stress from the capsule stiffness was too high to sustain healthy cell growth. It was not entirely clear if this poor viability was due to potential effects of barium toxicity [131], or from the high physical stress imparted by the capsule stiffness preventing cell proliferation. However, 1 day after hESC encapsulation, the highest cell death by the LDH assay was found in the lower barium concentration, which still showed 97% viability. Additionally, the high stiffness capsules were found to be cracking on the capsule surface and likely within the capsules, resulting in distinctly large and irregularly shaped cell colonies. This leads us to believe that the capsule was physically restraining the cells, and relieving the stress resulted in rapid cell growth in the cracked regions. The possibility of healthy cell growth in high barium capsule indicates the effects of barium toxicity in this system are minimal. This is further supported by the observation that better viability was observed in 100 mM BAlg, compared to the 50 mM BAlg on day 14 in Figure 2B. Barium concentration was higher in 100 mM BAlg, but cracking of the gel resulted in cell overgrowth, and more viable cells than in 50 mM BAlg, containing less barium. However, barium may still be toxic to the body in future implantation studies. Matching the most supportive capsule stiffness found in this study using a combination of calcium and low barium concentration, as done previously for islet encapsulation [132], may be useful in mitigating potential barium toxicity in the body. Taken together, this indicates that within the stiffness range of approximately 4 – 7 kPa, it is possible to maintain healthy growth and high expansion of hESCs, while beyond this range is not amenable to cell growth.

While the effect of stiffness was clear on cell viability and expansion, the effect of stiffness on pancreatic differentiation was much more complex. We evaluated the most supportive capsule properties to obtain PP cells, since implantation of PP cells have been widely reported to be successful in reinstating glucose homeostasis in diabetic mice upon implantation [133-136]. While the higher stiffness capsules are much stiffer than most soft tissue, it was not obvious how stiffness would influence differentiation in the presence of chemical differentiation factors. Remarkably, during both the DE and PP stage, alginate stiffness significantly influenced differentiation, even though the soluble chemical cues were identical and there were no diffusion limitations. Even minimal change in stiffness (1.7 fold) between 10 and 20 mM $BaCl_2$ significantly affected differentiation. Similarly, Wilson et al. have shown that endoderm differentiation of alginate encapsulated mESC aggregates can be significantly increased by a minimal decrease in capsules stiffness (1.4 – 1.7 fold) [31]. In our study, both DE and early pancreatic differentiation had a positive correlation with BAlg stiffness, showing increased stiffness enhanced differentiation. However, mesendoderm and endoderm differentiation had a slight bi-phasic behavior, with reduced differentiation in the high range, which was not observed in the pancreatic progenitor markers. The effect of stiffness on the key pancreatic endocrine transcription factor PDX1 was in complete contrast to the early markers. Increased gel stiffness strongly suppressed PDX1 expression, with the highest expression being at 10mM $BaCl_2$ (3.9 kPa). While this is completely opposite to the early pancreatic markers tested, an explanation can be that increased higher elastic moduli is suppressing or delaying differentiation and maintaining a progenitor pool. This is supported by the increase in gene expression with increased stiffness of HNF4α, a primitive gut tube marker involved in early pancreatic development, and PTF1A, a precursor to PDX1. Narayanan et al. have shown an approximately 10% increase in insulin and

PDX1 gene expression in hESC after pancreatic differentiation on 2D hyaluronic acid gels of stiffness 2.1 kPA compared to controls [137]. While this study only investigated a narrow stiffness range with only three gel stiffness's (1.3, 2.1, and 3.5 kPa) in 2D, it confirms that a delicate balance must be struck between physical and chemical cues.

The inconsistent effect of capsules stiffness on differentiation at the DE and PP stage is clearly indicative of the complex interactions between biophysical properties and signaling pathways. The mechanism of such interactions is still lacking in the context of stem cell differentiation, while understanding such interactions will significantly enhance the efficiency of engineering substrates for hPSC differentiation. To better understand such interactions, we evaluated the expression of key molecules of the TGFβ pathway, as well as key cross talk molecules. TGFβ is a critical signaling pathway in hPSCs; however, its effects are specific to the stage of differentiation. Low level TGFβ signaling is required for maintenance of pluripotency and self-renewal of hESCs, and high TGFβ signaling induces DE differentiation [126]. While high levels are needed for DE differentiation, as mentioned previously, continued activation of TGFβ is detrimental to further pancreatic differentiation. From our analysis of the effect of capsule stiffness on SMAD molecules, it is possible that the increased substrate stiffness is promoting DE stage differentiation by increased TGFβ signaling activation. Previous work with UD hESCs [138, 139] and chondrocytes [140] have shown changes in substrate mechanical properties can result in TGFβ signaling activation. Thus it is clear that physical stimuli imparted on the encapsulated cells can influence differentiation by modulating the signaling pathways. In analyzing the 10 and 20 mM BAlg conditions we observed a decrease in pSMAD2 levels in 20 mM from 10 mM BAlg, with a corresponding increase in pSMAD3 expression. However, since there is significant cross talk between pathways, parallel signaling pathways must also be

examined. Specifically the PI3K pathway acts as a negative regulator of the TGFβ pathway through sequestration of the R-SMADs by pAKT. Hence we measured the ratio of R-SMADs/pAKT as an estimate of R-SMADs available for gene transcription. While pSMAD2/pAKT was not significantly different, pSMAD3/pAKT was significantly higher in the 20 mM BAlg conditions, indicating higher TGFβ activity by less negative regulation by the PI3K pathway. This trend follows previous reports for prostatic epithelial cells and human embryonic kidney cells, which have shown that pAKT suppresses TGFβ signaling specifically through suppression of SMAD3 phosphorylation, and not SMAD2 [141, 142]. Additionally, we also examined pERK1/2 expression, a primary effector of the MAPK pathway. We observed significantly higher pERK1/2 expression in the 20 mM BAlg conditions. DE stage differentiation is induced by activation of the WNT pathway with Wnt3A, in addition to the TGFβ pathways. Singh et al. have shown that pERK promotes DE stage differentiation by inhibition of the WNT pathway inhibitor, Gsk3β [126]. This indicates that the increase in DE stage differentiation as substrates stiffness increased may be due to higher TGFβ and WNT signaling through a decrease in pAKT and GSK3β, respectively.

While it is clear that increased substrate stiffness supports DE stage differentiation, the effect of stiffness on PP stage is more variable. Previous reports have shown that beyond DE commitment, TGFβ signaling must be suppressed for subsequent pancreatic induction [127, 143, 144]. However analysis of the PP cells for signaling molecules revealed that even after removal of the TGFβ ligand (Activin) and further PP induction, the TGFβ pathway still remained active in a non-intuitive substrate dependent manner. The ratios of both pSMAD2/3/pAKT decreased from the DE to PP stage, indicating reduced levels of active pSMAD2/3 after the removal of ActivinA at the PP stage. However, this does not explain the superior PP stage differentiation at

lower capsule stiffness. Hence, we investigated the direct signaling pathways inducing PP differentiation; namely, retinoid signaling activation and sonic hedgehog (SHH) inhibition. Lopez-Carballo et al. have shown than retinoic acid treatment of human neuroblastoma cells activated PI3K signaling and resulted in increased AKT phosphorylation [145]. Induction of PP stage by addition of retinoic acid may serve to suppress TGFβ signaling by the PI3K pathway, in addition to retinoid signaling activation. Inhibition of SHH signaling is achieved by addition of CYC, which inhibits SHH through the receptor smoothened [146]. Even in the presence of the CYC, we saw an increase in SHH ligand and its downstream transcription factor GLI1, after PP stage differentiation in 20 mM BAlg, as compared to 10 mM BAlg. Dennler et al. showed that even in the presence of CYC, TGFβ induced expression of GLI1 and GLI2 specifically through SMAD3, in multiple human cell types [129]. Importantly, this activation of SHH signaling by TGFβ was independent of the SHH receptor. Our results clearly show an increase in TGFβ signaling in response to increased substrates stiffness at the DE stage. However, upon inhibition of TGFβ at the PP stage with Alk5i in the 20 mM BAlg condition, we did not observe a rescue of PDX1. It is thus unlikely that the increase in SHH in 20 mM BAlg is TGFβ mediated. This indicates the possibility that higher capsule stiffness is strongly increasing SHH signaling to the point where CYC cannot fully inhibit SHH, which has not been previously demonstrated. Abnormal hedgehog (HH) signaling is common in many human cancers, and can involve "non-classical" HH signaling activation independent of the "classical" ligand-smoothened HH activation [147]. As we have seen in our differentiation studies; this results in the ineffectiveness of HH signaling inhibitors like CYC. It is possible that the increase in substrate stiffness is activating "non-classical" SHH signaling, independent of the ligand-receptor binding.

3.5 CONCLUSIONS

In the present study we evaluated the feasibility of adopting BAlg capsules as a unifying platform for hPSC growth, differentiation and implantation. Since BAlg is well studied for islet transplantation, we focused our study on its usefulness for hPSC encapsulation and pancreatic differentiation. Our results clearly indicate the excellent performance of BAlg capsules in supporting growth and pancreatic differentiation of encapsulated hPSCs, highlighting its potential as a single platform for hPSC scale-up, differentiation and final implantation. However, it also highlights the importance of considering capsule synthesis as an important parameter. Cell growth and differentiation were strongly dependent on the stiffness of the substrate. We determined that capsule stiffness of approximately 4 to 7 kPa was most supportive of cell proliferation, while ~3.9 was best for pancreatic differentiation. Analysis of the signaling pathway indicated increased stiffness strengthens TGFβ signaling, driving DE differentiation. However, it also strengthens SHH signaling, which is detrimental to PP differentiation. Future implantation studies will first require investigation of the perm-selectivity of the barium alginate capsules with changing stiffness to determine the exact capsule parameters which support viability, differentiation, and immunoisolation from the patient immune system.

4.0 DECOUPLING THE EFFECT OF MULTIPARAMETRIC PERTUBATIONS ON HUMAN PLURIPOTENT STEM CELLS DURING PANCREATIC DIFFERENTIATION

4.1 INTRODUCTION

Stem cell fate is known to be sensitive to its local microenvironment, both chemical and physical in nature. In the previous chapter we showed that the pancreatic differentiation of hPSC was highly sensitive to alginate capsule stiffness. However, there could be other factors affecting cell fate as well. Given the complexity of stem cell response to environmental parameters, it will be important to evaluate cell response to multiple combinatorial perturbations, in isolation and conjugation. Such combinatorial perturbations are best enabled by high throughput screening platforms, which also minimize the cost of materials, time of experimentation, and physical space. The sensitivity of stem cells to various environmental factors has inspired the development of high throughput platforms. This approach has been used in 2D for screening physical stimuli such as material stiffness [148], topography [149, 150], and ECM protein or peptide composition [151-153] on stem cell attachment, growth and differentiation. However the complexity of stem cell response limits the information gathered from single perturbations and necessitates combinatorial perturbations. For example, Gobba et al. developed a microengineered hydrogel microarray which can vary substrate stiffness while being functionalized with protein combinations, which was used to test MSC differentiation [154]. The advent of 3D culture of

stem cells has initiated the development of array platforms supportive of 3D cell culture. Ranga et al. utilized nanoliter-dispensing technology to synthesize over 1000 unique environments to simultaneously probe the effect of matrix elasticity, degradability, and signaling proteins on mESC self-renewal and proliferation [155]. Yang et al. developed a 3D combinatorial ECM hydrogel platform to identify optimal ECM combinations which support linage specific differentiation of hESCs [156]. Thus, the use of 3D array platforms permits the analysis of the effects of combinatorial stimuli on cells in an environment which can closely mimic in vivo organogenesis. However, many of these high-throughput techniques mentioned above require special robotic setups, which cannot be achieved commonly in the laboratory setting. While these techniques provide a rich multitude of data, our primary interest in this study was to conduct a small number of specific perturbations in a laboratory set-up. The Jonathan Dordick group developed a simple alginate-based array platform, originally for the purpose of toxicological studies in 3D [157], and later utilized to track mESC fate to quantify the expression of key proteins in 3D [158]. While this platform also utilized robotic techniques, the simplicity is particularly attractive. We have adapted this platform for bench-scale screening without the use of robotics, and further modified it to perturb the physical microenvironment. This array platform was originally built for chemical perturbations, while in our work we have modified the system to induce combinatorial physical perturbations, and was achieved using simple laboratory tools.

Encapsulation for 3D culture of hPSCs seems to be a promising avenue to meet both biomanufacturing goals and immune protection in a single platform. However, the signals used to drive differentiation not only include soluble chemical cues, but also include insoluble physical cues. Previous work has clearly indicated that stem cell fate is highly sensitive to its

chemical, as well as physical microenvironment. More specifically for pancreatic differentiation, we have shown in the first part of Aim2 (Chapter 3) that encapsulation will influence stem cell fate. Microenvironment can constitute soluble chemicals/growth factors, interactions with extracellular matrix (ECM) proteins, cell-cell contact, or physical stimuli such as stiffness or tension. In 2006, Engler et. al. showed that culture of mesenchymal stem cells (MSC) on substrates of stiffness matching those of tissues in the body resulted in tissue stiffness specific differentiation of the MSCs [57]. In our earlier work from our lab, we demonstrated the effect of substrate properties using fibrin and alginate on the differentiation of mouse embryonic stem cells (mESCs) [117, 118]. More recently, covered in the preceding chapter of this dissertation, we demonstrated the feasibility of pancreatic differentiation of hESCs within alginate capsules; and as expected, pancreatic maturation within the capsules was sensitive to alginate capsule properties [159]. Cell-cell contact, especially in 3D cellular aggregates, is another important insoluble cue which can influence hPSC differentiation. Lee et al. showed controlling hPSC colony size could control specification to mesoderm (1200 μm in diameter) or endoderm in the presence of soluble differentiation factors, linking cellular organization to hPSC differentiation [160]. Recently, Toyoda et al. have shown that the pancreatic induction of hPSCs was correlated with increasing cell density in 2D, and was further improved in aggregate culture [161]. Thus clinical translation of encapsulated hPSCs will require a thorough evaluation of optimum parameters supporting hPSC growth and differentiation [10, 162, 163]. In this chapter, which constitutes the second part of Aim 2, we evaluated the sensitivity of proliferation and differentiation of encapsulated hPSCs to both cell culture configuration and substrate mechanical properties, through the development and use of a 3D alginate array platform.

Conceptually, the alginate array immobilizes individual alginate beads to the culture surface, enabling convenient imaging and analysis of the same. Our objective here was to investigate the effect of alginate properties and encapsulated culture configurations on the propagation and pancreatic differentiation of hPSCs. This simple alginate array platform allowed for multiparametric perturbations and quantitative imaging. As this alginate array generated a rich complex data set, the use of a simple linear statistical model allowed us to decouple the complex interactions between the stem cells and the effect of their microenvironment. Thus, in combination with statistical modeling, this allowed us to identify the sensitivity of stem cell proliferation and fate to multiparametric modulation.

4.2 METHODS

4.2.1 Human embryonic stem cell culture

Undifferentiated (UD) H1 hESCs (WiCell) were maintained on hESC-qualified Matrigel (BD Biosciences) coated tissue culture plastic for 5–7 days in mTeSR1 (StemCell Technologies) at 37°C and 5% CO_2 before passaging. Experiments were performed with p55-p85 hESCs.

4.2.2 Alginate array formation and hESC encapsulation

Fabrication of the 3D alginate array was done by adopting an approach developed previously by Fernadez et al [158]. The 3D alginate array was created by coating the culture surface with nitrocellulose (Fisher), followed by spotting 0.5 – 5 µl of a $BaCl_2$-poly-(l-lysine) (PLL) mixture in the desired array configuration using a Eppendorf Repeater Plus pipette. The $BaCl_2$-PLL spot was allowed to dry, after which the alginate solution was added directly to the dried spot, resulting in alginate hydrogel crosslinking and attachment to the culture surface. To vary alginate crosslinking, the barium concentration in the $BaCl_2$-PLL mixture was varied from 10 – 500 mM.

For hESC encapsulation, hESCs were treated with 10 µm Y-27632 (R&D Systems, Minneapolis, MIN) for 2 hours prior to harvesting by Accutase (Invitrogen) treatment for 5-7 min at 37°C and 5% CO_2. For encapsulation of single cells, 3 or $5x10^6$ cells/ml were suspended in 1.1% (w/v) low viscosity alginate (Sigma-Aldrich) with 0.2% (v/v) gelatin (Sigma-Aldrich), and was spotted onto the dried $BaCl_2$-PLL spots as described above. hESC aggregates were formed by culturing the Y-27632-treated single cell suspension of hESC in low adherence 30 mm dishes on a plate shaker set at 55 rpm, at 37°C and 5% CO_2. Cells were seeded at $1x10^6$ cells/ml, using 2 ml of media in each 30 mm dish. Aggregate formation was allowed to proceed for 2 day on the plate shaker before collecting and encapsulating the alginate array, as described above. The resulting aggregates from one 30 mm dish were suspended in 1 ml of alginate for encapsulation in the array.

4.2.3 hESC differentiation

The stage-wise induction protocol for the pancreatic differentiation of hESCs was identical to our previous study, ending at the pancreatic progenitor stage instead of the maturation stage [164]. Encapsulated single cells were propagated for 4 days in mTeSR1 with 10 μm Y-27632 followed by 2 days in mTeSR1 alone. Preformed aggregates were allowed to acclimate to the hydrogel for 2 days in mTeSR1 prior to starting differentiation. First, DE was induced using 100 ng/ml ActivinA (R&D Systems) with 25 ng/ml Wnt3A (R&D Systems) for 4 days. Afterwards, PP was induced with 0.2 μM KAAD-cyclopamine (CYC, Millipore) for 2 days and 0.2 μM CYC with 2 μM retinoic acid (Sigma–Aldrich) for 2 days. All differentiation media was made using DMEM/F12 (Life Technologies), supplemented with 0.2% BSA (Sigma) and 1xB27® (Life Technologies).

4.2.4 Atomic Force Microscopy

The alginate array was formed as described previously, crosslinked with 10, 50, 150 200, and 500 mM $BaCl_2$. AFM force indentation measurements were performed using the MFP-3D Atomic Force Microscope (Asylum Research, CA, USA). The hydrogels were maintained in saline after formation to ensure their hydrated state. The stiffness of each alginate gel was measured at n = 3 random locations and approximately 16 force curves were taken over a 4 × 4 grid at each location on each sample.

4.2.5 Viability

LIVE/DEAD (Life Technologies) viability assay was performed according to manufacturer's instructions.

4.2.6 DNA and protein immunostaining and quantification using LICOR

Encapsulated cells in the alginate array were fixed with 4% formaldehyde for 20 min. Cells were permeabilized with 0.1% Triton-X 100 (Sigma-Aldrich) for 5 mins prior to blocking with 10% donkey serum in for 1 hr. For primary antibodies, we used we used goat anti-Ki67 (1:100, Santa Cruz Biotechnology), goat anti-SOX17 (1:400 dilution; R&D Systems), rabbit anti-FOXA2 (1:400 dilution; R&D Systems), goat anit-PDX1 (1:200 dilution; R&D Systems), and rabbit anti-Nkx6.1 (1:400 dilution; R&D Systems). Primary antibody staining was done overnight at 4°C, followed by addition of the anti-goat or anti-rabbit IR-conjugated secondary antibodies (1:800; LI-COR) for 1h at room temperature. DNA was stained by addition of Draq5 (1:5000, Fisher) during the secondary antibody staining step. Encapsulated cells were washed three times with 0.9% saline in between each step of the staining protocol. The entire array was imaged at the same time using Odyssey CLx (LI-COR) machine. Protein and DNA expression were quantified using the LI-COR Odyssey and Image Studio software.

4.2.7 Regression analysis

To relate the expression of markers representing proliferation and pancreatic differentiation to cation concentration and seeding configuration, linear regression analysis was performed [165].

In the first stage, the influence of the cation concentration alone was determined using the relation below:

$$\left[\frac{\text{Marker}}{\text{DNA}}\right] = \text{Intercept} + \beta_C C + \beta_{C^2} C^2 + \beta_{C^3} C^3 \quad \ldots (1.1)$$

Here, C denotes cation concentration. The model parameters, Intercept and $\beta_C{}^i$'s are estimated by applying the training data on the model and performing optimization to minimize the error between the true response and predicted response. The process is repeated for each culture configuration and marker separately. A linear least squares error model was selected. The data used for training the model was obtained from the individual experimental repeats using a bootstrapping approach. The technique generates large datasets from a small number of experimental replicates, using sampling with the replacement technique [166, 167]. Each such surrogate dataset was selected to contain the same number of cation concentration values (total of 5) and configuration types (total of 3). The regression analysis was performed on each individual bootstrap dataset and the model parameters and their p-values were recorded. The final distribution of the p-values and the coefficients was monitored for convergence. Only those models where the R squared values ranged from 0.5 to 0.95 were taken in the final distribution of p-values and coefficients and for the current analysis, 1000 such bootstrap datasets were sufficient to make the final conclusions.

To evaluate relative importance of configuration and cation concentration simultaneously, configuration was added into the equation to get a multiple linear regression model given below:

$$\left[\frac{\text{Marker}}{\text{DNA}}\right] = \text{Intercept} + \sum_{i=1}^{3}\left(\beta_{C^i} C^i\right) + \sum_{i=2}^{3}\left(\beta_{\text{config}_i}\text{Config}_i\right) \quad + \sum_{i=2}^{3}\left(\beta_{C\times\text{config}_i} C \times \text{Config}_i\right) \ldots (1.2)$$

In Equation 1.2, the configuration variables are binary. The variables config 2 and 3 take values of 0/1 or 1/0 or 0/0 simultaneously to represent one configuration at a time. Note that config 1 is chosen as the reference (when config 2 and config 3 are null) and therefore does not explicitly appear as a variable in this equation, but is absorbed by the intercept term. This schema, hence, captures the relative influence of config 2 and config 3 over config 1. Concentration terms occur in two forms: one by itself (third order polynomial) and one as a bi-linear term with configuration. All coefficients are estimated in a similar manner as discussed above for Equation 1.1, except that the bootstrap data is now sampled to include all configurations and cation concentrations together for a chosen marker.

4.3 RESULTS

4.3.1 3D alginate array formation

The alginate array was constructed by first coating the culture surface with nitrocellulose (Figure 4.1A), a negatively charged coating. This was followed by depositing a barium (Ba^{2+}) chloride-PLL mixture in the desired array configuration (Figure 4.1B), where positively charged PLL ionically interacts with negatively charged nitrocellulose. Once this coating has dried, the alginate-cell solution was spotted directly on top of the $BaCl_2$ (Figure 4.1C).

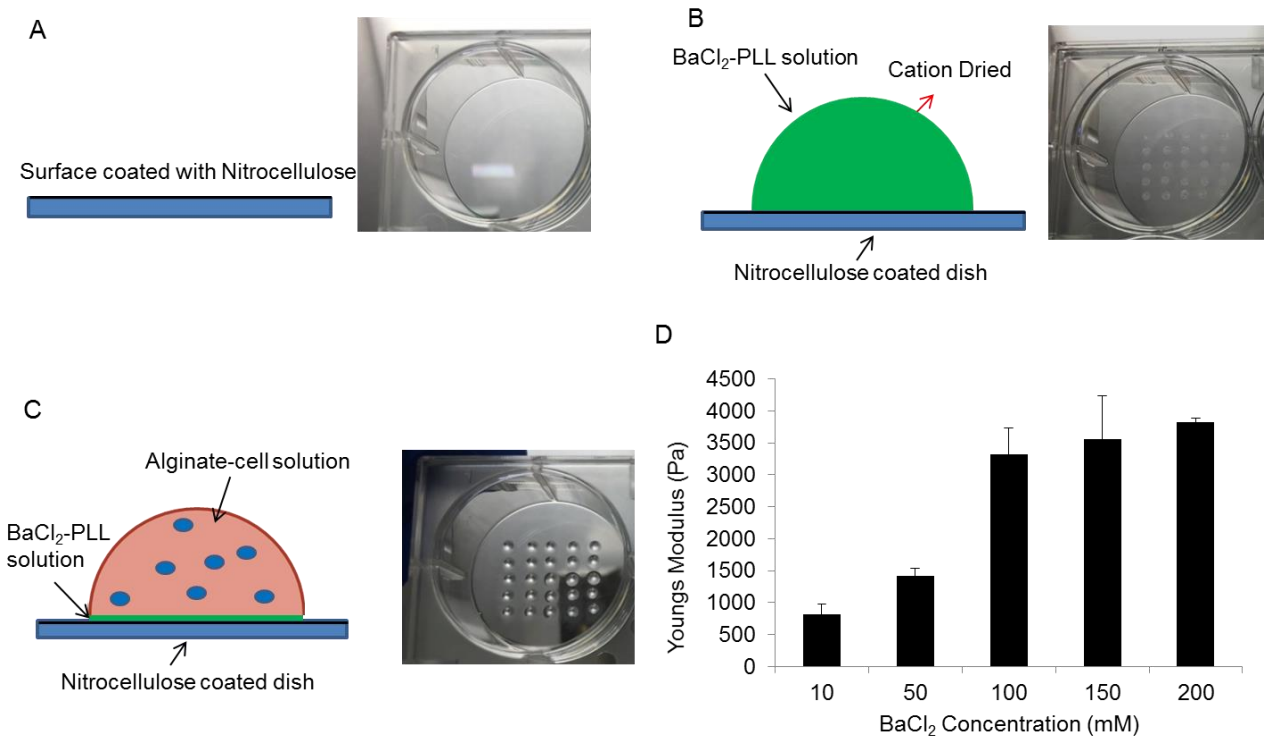

Figure 4.1. Schematic of 3D alginate array fabrication and characterization.

(A) The culture surface is coated with nitrocellulose. An example is shown for fabrication in a well of a 6-well plate. (B) Next, a $BaCl_2$-poly-(L-lysine) (PLL) mixture is spotted onto the nitrocellulose coated surface in the desired array configuration. In this study, a 5x5 array was predominantly used. (C) Finally, the cell-alginate solution is added directly onto the dried $BaCl_2$-PLL spot, resulting in crosslinking of the alginate and attachment to the culture surface by ionic interaction between the alginate, PLL, and nitrocellulose. (D) The alginate array was formed using 10, 50, 100, 150, 200, mM $BaCl_2$ for alginate crosslinking. The resulting alginate hydrogel elastic moduli (Pa) was measured by AFM micro-indentation.

The Ba^{2+} crosslinks the alginate, forming a cell-encapsulating hydrogel, and the PLL serves to ionically adhere the alginate to the nitrocellulose, and thus the culture plate. An example of 5x5 arrays in three wells of a six-well plate can be seen in Figure 4.1 C. We next evaluated the feasibility of modifying the stiffness of the alginate within the array by modulating the $BaCl_2$

(cation) concentration. In Chapter 3 of this work, we identified a stiffness range of approximately 3 – 6 kPa to be ideal for cell growth and pancreatic differentiation [159]. To encompass this stiffness range, we formed the alginate array with varying barium concentrations within the same array, ranging from 20 mM - 500 mM Ba^{2+}. Measurement of the alginate spot stiffness within the alginate array, using atomic force microscopy (AFM) micro-indentation (Figure 4.1D), shows that the Young's Modulus increased from 819 ± 151 Pa for 10 mM Ba^{2+} to 3821 ± 63 Pa for 200 mM Ba^{2+}. As expected, the Young's Modulus of the alginate spots increased with increased cation concentration. Hence, this simple platform allows for synthesis of alginate spots with varying physical properties within the same array. This will enable a convenient procedure to evaluate cell response, both short and long term, to physical stimuli

4.3.2 3D alginate array characterization

A critical component of a high throughput platform for studying cell response is the successful integration of appropriate imaging, analysis, and quantification techniques to measure cell response. Our current objective is the quantitative analysis of viability and phenotype of hESCs encapsulated within the array, primarily using immunostaining. Since this system requires analysis of cell aggregates suspended in an alginate hydrogel, and not adherent cells, the imaging technique requires sufficient penetration into both the hydrogel and cell aggregates. For this purpose, we integrated the LICOR Odyssey scanner, which utilizes a near infrared wave length to detect and quantitatively measure the fluorescence intensity in immunostained samples. The LI-COR near-infrared fluorophores enhance penetration depth, and dramatically reduce autofluorescence. This system is often used for small animal imaging, and is thus well suited for

imaging and analysis of encapsulated cell aggregates [168-170]. Therefore, we first needed to determine the optimal volumes for the array spots to ensure adequate signal intensity, without exceeding the detection limits of the LICOR scanner. hESCs were encapsulated in the array at $1x10^6$ cells/ml using 0.5 - 5 µl of the barium (10 mM)/PLL and alginate solutions (Figure 4.2A).

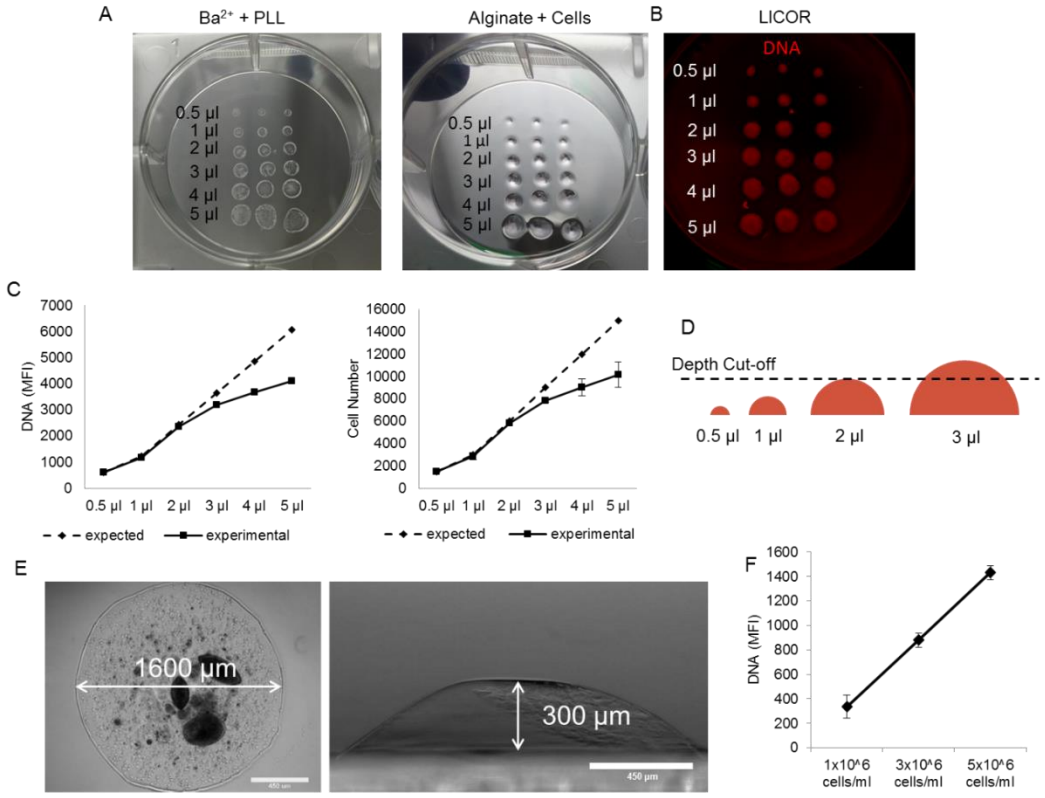

Figure 4.2. Alginate array parameter selection and characterization.

(A) Cells were encapsulated in the array at $1x10^6$ cells/ml using 0.5 - 5 µl of the cation and alginate. (B) DNA was stained with DraQ5, and imaged using the LICOR Odyssey and (C) quantified using the Image studio software. The dashed line represents the expected MFI and the solid line is the experimental DNA MFI. Data was represented as both MFI and cell number/array volume. (D) Schematic of the detection limits of the LICOR Odyssey in the 3D alginate array system. (E) Spot diameter and depth. (F) DNA quantification within the alginate array using the volume of 1 µl, as hESC seeding density is increased.

This resulted in increasingly larger alginate spots, with a corresponding increase in cell number, while retaining the same cell density. Cells within each spot were stained using DRAQ5, which stains cell DNA and is proportional to cell number, and was quantified using the LI-COR Odyssey and Image Studio software (Figure 4.2B). Figure 4.2C shows that an increase in the array volume resulted in an increased fluorescent signal up until an array volume of 2 µl. When we compared the quantified MFI (solid line) with the expected MFI based on cell number (dashed line, Figure 4.2C), there was close correspondence between the two, up until array volume of 2 µl. An increase in array volume above 2 µl resulted in a decrease in the measured MFI from the expected values, indicating these spots were too large for the LICOR scanner to fully penetrate (Figure 4.2D). The LI-COR Odyssey Imager scans over 6 logs of linear dynamic range with no image saturation, it is thus likely that the differences between quantified and expected MFI were from hydrogel penetration. Thus, for the remainder of this work, the array volume was restricted to 1 µl in order to obtain reliable MFI values from the LICOR Odyssey scanner (Figure 4.2C). These volumes resulted in alginate spots with diameter and height of 1600 and 300 µm, respectively (Figure 4.2E).

Next, we wanted to determine the range of cell density over which the LI-COR Odyssey retains accuracy in quantification. (Figure 4.2F). Cell number should not be so high as to saturate the signal, but not so low that the signal is below the detection limit. hESCs were encapsulated at a density of 1, 3, and $5x10^6$ cells/ml, stained with DRAQ5 and quantified using the LI-COR Odyssey and Image Studio software. As expected, the MFI values increased by a factor of 2.8 ± 0.9 and 4.6 ± 1.6, as seeding density was increased by a factor of 3 and 5, respectively. Thus, seeding densities between 1-$5x10^6$ cells/ml were used for the remainder of this study.

4.3.3 hESC growth and viability in the alginate array during pancreatic differentiation

The array platform is specifically developed to quantitatively track the effect of microenvironment on stem cells, in a high throughput manner. In the current application, we chose to evaluate the effects of cell density, cell culture configuration and substrate stiffness on hESC fate. Toyoda et. al. have shown that culture configuration influences the pancreatic induction of human pluripotent stem cells (hPSCs): pancreatic induction increases with cell density in adherent cultures, and the effect was further enhanced in aggregate cultures [161]. In our previous reports we have shown that substrate properties can strongly modulate pancreatic differentiation [117, 118, 159, 171]. Our objective here is to adapt the array platform to enable simultaneous perturbation of both substrate stiffness and culture configurations and evaluate its effect on viability, growth, and proliferation of hESCs during pancreatic differentiation. In this work, culture configuration refers to encapsulating hESCs in the array starting as single cells (SC) or as preformed aggregates (Agg) formed using stirred suspension. Figure 4.3 shows a schematic of the experimental plan.

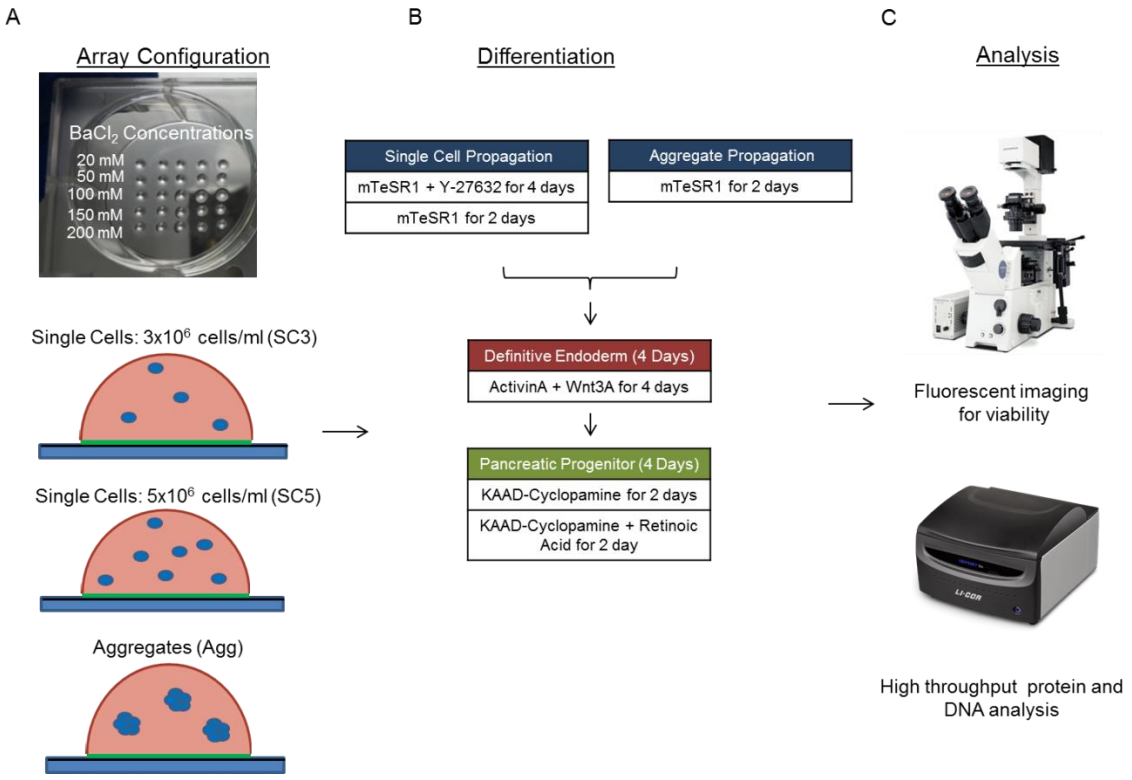

Figure 4.3. Schematic of encapsulation in the 3D alginate array when varying barium concentration and culture configuration.

(A) The array configuration used for cell viability, proliferation and differentiation experiments. hESCs were encapsulated as single cells, at 3 or $5x10^6$ cells/ml, or as preformed aggregates. (B) Propagation and stage-wise differentiation protocol for differentiation of hESCs to pancreatic progenitor cells. (C) Schematic of tools used for analysis in the 3D alginate array for cell viability (fluorescent imaging) and high throughput protein and DNA analysis (LICOR Odyssey scanner).

Undifferentiated (UD) hESCs were encapsulated in the array as single cells (seeding density of 3 (SC3) or $5x10^6$ cells/ml (SC5)) or preformed UD aggregates, using 20 – 500 mM $BaCl_2$ to crosslink the alginate (Figure 4.3A). Encapsulated single cells were propagated for 6 days, at which point they started forming small colonies. The encapsulated aggregates were allowed to

stabilize for 2 days post encapsulation and prior to induction of differentiation, which didn't result in significant changes in aggregate size. Encapsulated hESCs were first differentiated to the definitive endoderm (DE) stage, followed by further differentiation to the pancreatic progenitor (PP) stage (Figure 4.3B). Throughout the differentiation protocol, cell viability and protein expression were analyzed directly on the array (Figure 4.3C). Figure 4.4 illustrates cell viability by LIVE/DEAD staining performed at the end of the DE and PP stages, for each culture configuration, with simultaneous variation in the alginate substrate properties.

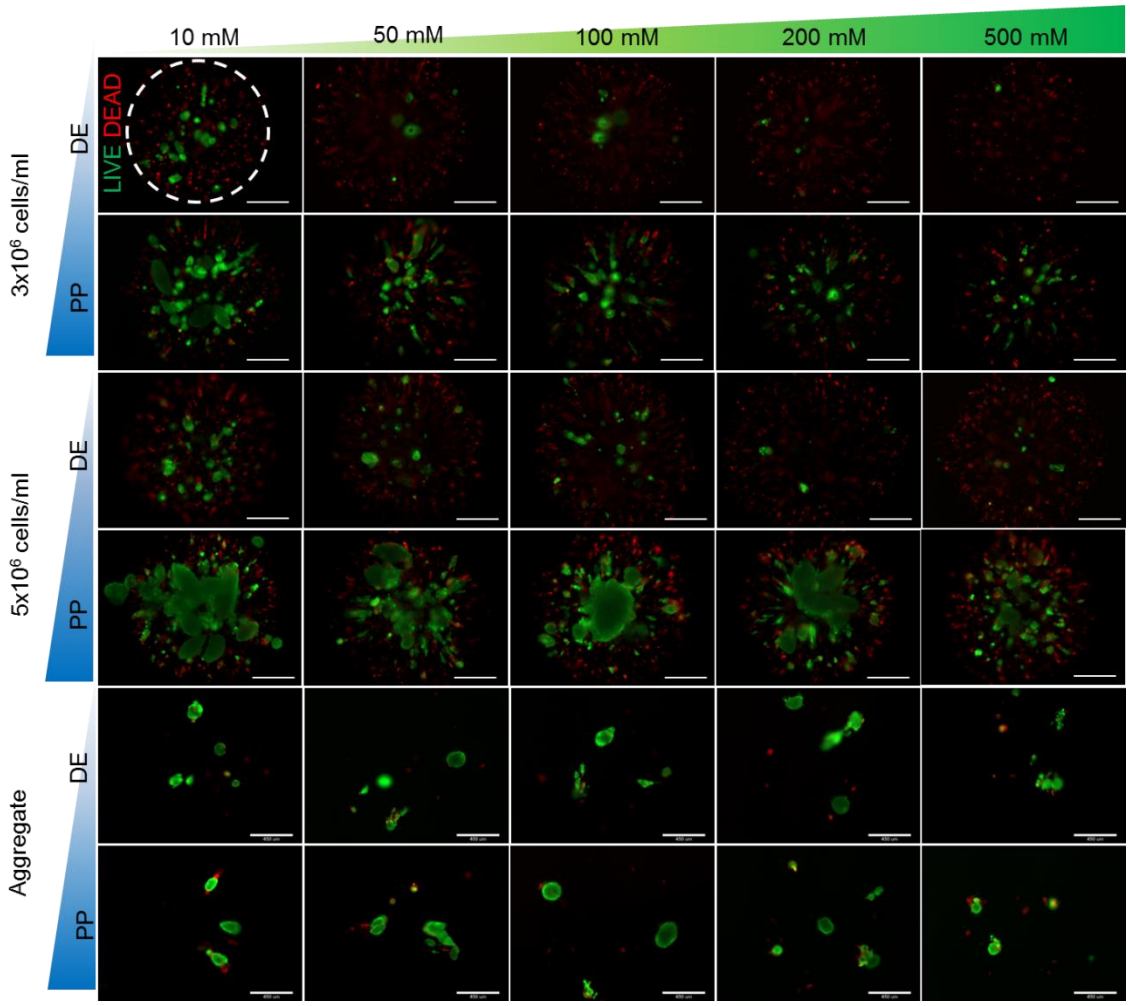

Figure 4.4. hESC viability in response to alginate crosslinking and culture configuration.

LIVE/DEAD assay after the DE and PP stage for encapsulated single cells, at 3 and 5x10^6 cells/ml, and aggregates, indicating cell viability in response to increasing crosslinking. Scale bar is 450 μm.

For each condition, the alginate crosslinking concentration was found to significantly affect hESC viability and its colony forming capability. This effect is most significant with encapsulated single cells. SC3 showed viable cell colonies after DE differentiation when encapsulated in 10 mM BAlg. However, the number and size of viable colonies decreased as alginate crosslinking was increased. This similar trend was observed to continue through PP

stage; with the surviving cell colonies growing larger with subsequent differentiation to the PP stage. Hence, more viable cells were observed at the PP stage (over DE stage) for high crosslinking conditions. SC5 showed a similar trend as observed in the SC3 configuration at the DE and PP stages, with the exception that more cells were observed in each stiffness condition, given that the starting population was approximately 1.7 fold higher.

Encapsulation of preformed aggregates, in contrast to single cells, showed good viability after the DE and PP stage for each BAlg condition. Further, the aggregate size was fairly insensitive to the substrate properties and maintained similar sized colonies throughout. However, the aggregates did not grow appreciably over time, when differentiated from the DE to PP stage, which also contrasts with the behavior of encapsulated single cells. While cell growth was low when encapsulating hESC as aggregates, cell death was also minimal, as judged by the relative absence of red DEAD stains. Single cell encapsulation, on the other hand, resulted in significant cell death, both immediately after encapsulation as well as over propagation and differentiation. Overall these results indicate that while encapsulation of single cells showed higher expansion potential for surviving cells compared to preformed aggregates, they are more prone to cell death under encapsulation.

4.3.4 Quantitative analysis of growth and proliferation in the alginate array during pancreatic differentiation

In order to further confirm this finding, we next quantified cell growth and proliferation by staining for DNA and Ki67 for each of the tested conditions, at both the DE and PP stages. DNA and Ki67 staining was done using LICORs near-infrared fluorophores, and quantified using the LICOR Odyssey scanner. Figure 4.5 compares cell growth, determined by amount of total DNA

present, and cell proliferation by KI67 staining, at the DE and PP stage for each configuration and crosslinking combination.

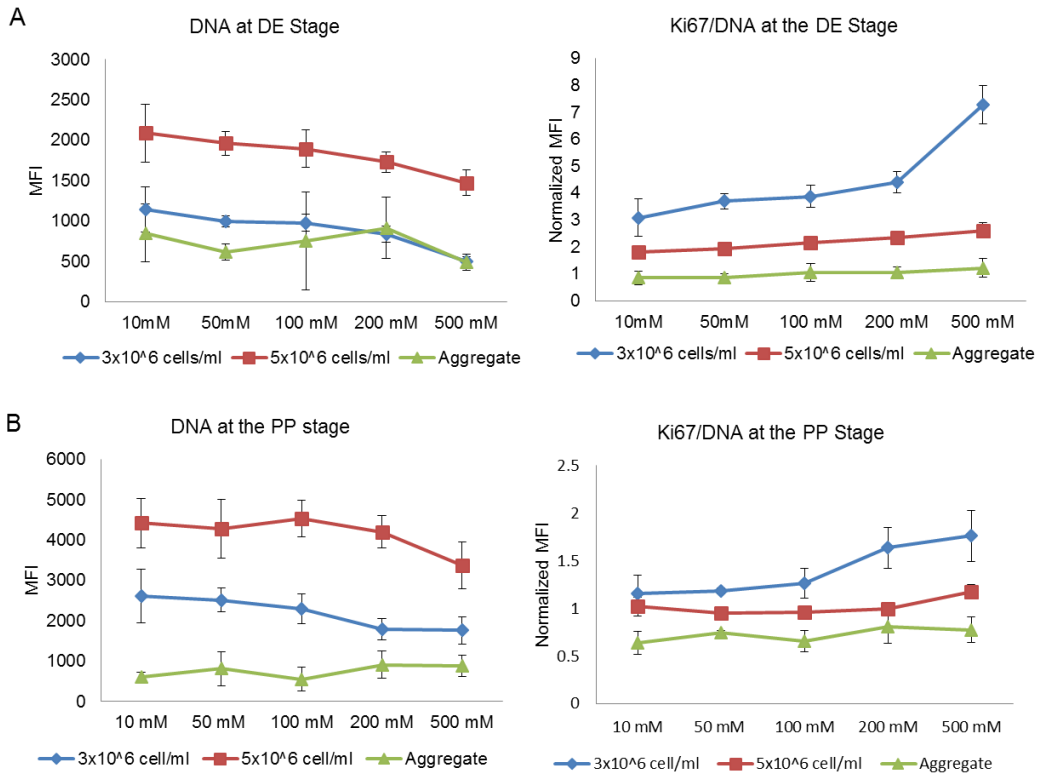

Figure 4.5. Quantification of DNA and cell proliferation as alginate crosslinking and culture configuration is varied.

(A) Quantification of DNA and Ki67 protein expression after DE differentiation for single cells encapsulated at 3 or $5x10^6$ cells/ml and preformed aggregates; encapsulated using 10, 50, 100, 200, and 500 mM $BaCl_2$. (B) Quantification of DNA and Ki67 protein expression after PP stage differentiation for single cells encapsulated at 3 or $5x10^6$ cells/ml and preformed aggregates; encapsulated using 10, 50, 100, 200, and 500 mM $BaCl_2$. Ki67 expression of each array spot was normalized the cellular DNA content within the array spot. Each crosslinking and culture configuration condition represents the average of n=5 array spots.

At the DE stage, DNA staining showed an increase in MFI with an increase in cell seeding density from 3 to $5x10^6$ cells/ml (Figure 4.5A). For both the conditions, though, an increase in crosslinking concentration decreased the overall DNA content. The DNA content of the aggregate configuration was similar to that of the SC3 configuration, and did not change considerably with changes in substrate properties. Analysis of cell proliferation after DE differentiation by Ki67 staining showed that the SC3 configuration possesses higher proliferative potential, compared to SC5, irrespective of substrate condition. At both seeding densities, the Ki67 expression increased slightly as stiffness was increased, with the exception of the SC3 configuration in the 500 mM BAlg spots, which showed a sharp increase in expression. The aggregate configuration showed lower Ki67 expression than both single cell configurations, which did not change appreciably as alginate stiffness increased.

At the PP stage, the trends in DNA content were similar to that observed at the DE stage (Figure 4.5B). As expected, the DNA content was higher at the PP stage for both single cell configurations, since the cells continued to grow in culture. For the aggregate configuration, however, the DNA content remained similar between the DE and PP stage. Ki67 expression at the PP stage for both single cell configurations decreased as compared to the DE stage, indicating that the cells become less proliferative with differentiation. We observed only a slight decrease in Ki67 expression in the aggregate configuration at the PP stage as well, compared to the DE stage. Additionally, at the PP stage the aggregate configuration showed little to no change in Ki67 expression as substrate stiffness increased, similar to what was observed at the DE stage. These results confirm the qualitative trend that was observed in the LIVE/DEAD images seen previously. Additionally, these results indicate that while alginate stiffness did affect proliferation, culture configuration had a larger impact on proliferation.

Next, a regression analysis was performed to quantify the effect of substrate properties on proliferation of hPSCs in the array. The cation concentration was chosen as the independent variable, and the proliferation marker as the response variable. In the regression equation, non-linear dependence on the cation concentration is modeled in the form of higher order polynomial relationships (up to third order), but each such non-linear term is linear in the regression coefficients. Regression coefficients denote the strength of the contribution of the corresponding regression term to the marker level (see Methods section 2.7 for more details). In addition to these regression coefficients, p-values of the F statistic are calculated and these denote the statistical significance of including the particular regression term in the overall equation. Data from Figure 5 was used to train the regression model (see Equation 1.1).

As a first step, regression analysis was performed to find the importance of cation concentration in determining the marker levels for each culture configuration separately. Due to experimental variability, it is necessary to check for robustness of the regression estimates. Therefore, regression analysis was repeated on multiple datasets (chosen from data for the same culture configuration and response marker) obtained by resampling of the original experimental 'repeats' using a bootstrapping with replacement algorithm (see Methods for further details) [172]. At the end of the analysis, the distributions of regression coefficients and p-values of each term in the regression equation (over bootstrapped datasets) were collected and used for comparison. From this analysis, the sensitivity of proliferation to cation concentration was determined at both the DE and PP stage, and evaluated for each culture configuration. Figure 4.6 shows the regression coefficients for the proliferation marker Ki67.

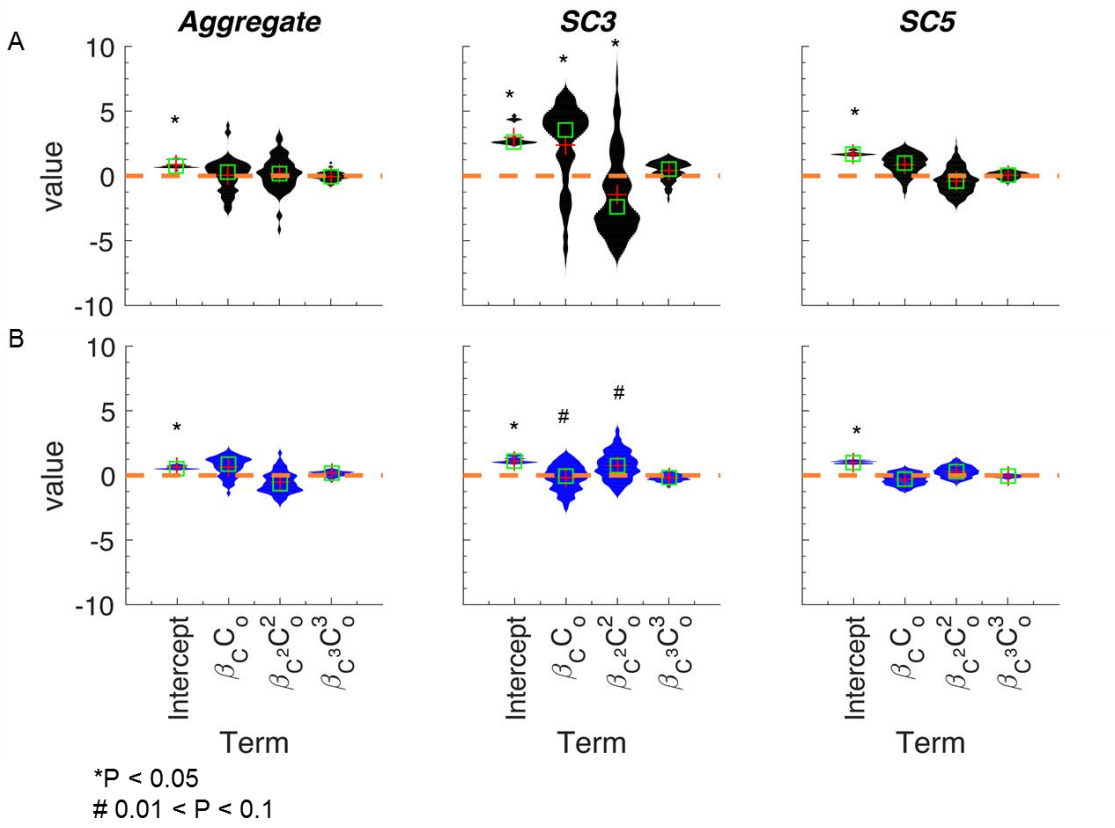

Figure 4.6. Significance of cation concentration in determining proliferation for each culture configuration.

(A) DE stage and (B) PP stage. Shown here are the intercept and regression coefficients, with the coefficients scaled by appropriate order mean concentration (C_o = 172 mM). The mean and median of the distributions in the violin plot are shown as red crosses and green squares. The p-values of the F-statistic are given for the significant terms. *P < 0.05 and # 0.01 < P < 0.1

Only those bootstrap samples for which the R squared values ranged from 0.5 to 0.95 are shown (the number of such samples ranged from 50 to 95% of 1000 bootstrap samples). The x-axis includes the intercept, first order, second order and third order terms for the DE (Figure 4.6A) and PP stage (Figure 4.6B) for each configuration. Note that the terms for each order are

multiplied by an average concentration (C_o = 172 mM) of the right order, so that they are in the same units and are comparable. Overall, it is found that coefficients for most terms are close to zero except for the SC3 configuration at the DE stage (p-value < 0.05). Here, the first order and second order terms are more important than the third order. This sensitivity is also apparent in the experimental data where SC3 was seen to have enhanced proliferation with increased crosslinking.

4.3.5 Pancreatic differentiation in the alginate array

We next evaluated the sensitivity of hESC differentiation on substrate conditions and culture configuration influenced. We have previously reported that increasing substrate stiffness enhances DE differentiation, and suppresses PP differentiation in bulk alginate capsules, formed by dropwise addition of alginate into a cation solution [159]. In the current report, synthesis of the alginate array system allows us to investigate such effects with finer resolution, along with inducing multi-parametric perturbations by simultaneously varying stiffness and culture configuration. Encapsulated hESCs were first induced to the DE stage (Figure 4.3B), and differentiation was evaluated by SOX17 and FOXA2 protein immunostaining. Figure 4.7A presents the protein expression levels quantified using the LICOR Odyssey platform, and normalized to DNA.

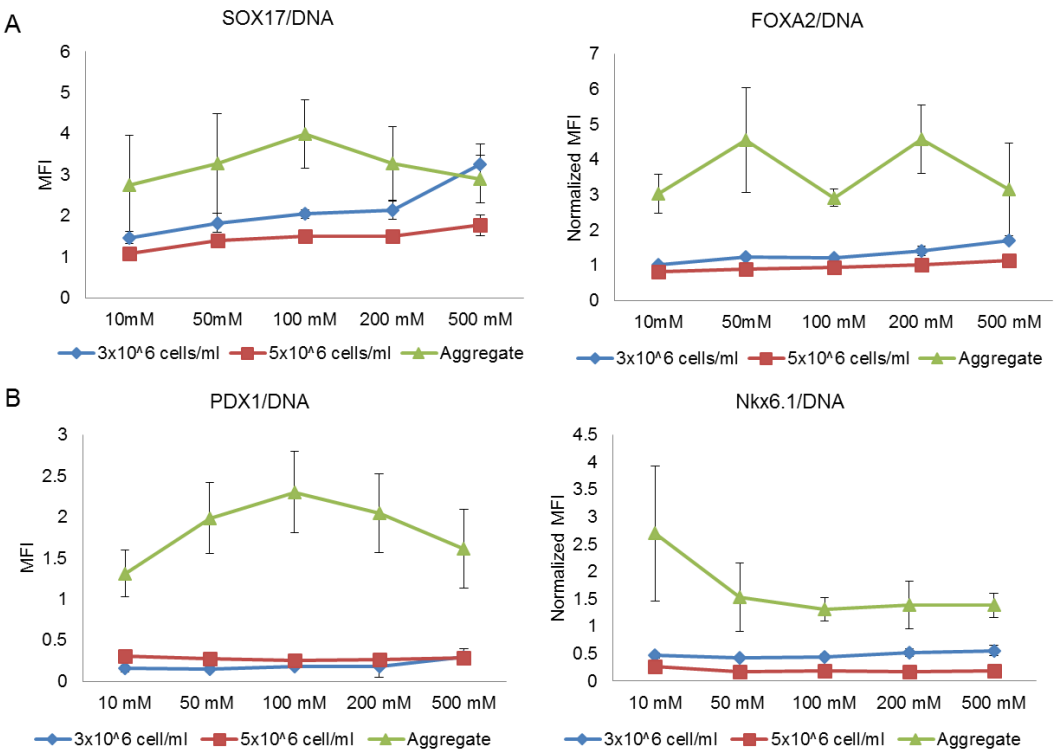

Figure 4.7. Analysis of DE and PP stage differentiation as alginate crosslinking and culture configuration is varied.

(A) Quantification SOX17 and FOXA2 protein expression after DE differentiation for single cells encapsulated at 3 or $5x10^6$ cells/ml and preformed aggregates; encapsulated using 10, 50, 100, 200, and 500 mM $BaCl_2$. (B) Quantification PDX1 and Nkx6.1 protein expression after PP stage differentiation for single cells encapsulated at 3 or $5x10^6$ cells/ml and preformed aggregates; encapsulated using 10, 50, 100, 200, and 500 mM $BaCl_2$. Ki67 expression of each array spot was normalized the cellular DNA content within the array spot. Each crosslinking and culture configuration condition represents the average of n=5 array spots.

Overall, both SOX17 and FOXA2 were observed to have a similar response to the exposed perturbations. SC5 showed a slight increase in SOX17/DNA (~1 – 1.7) and FOXA2/DNA (~0.8 – 1.1) as substrate stiffness was increased. The same trend was observed for SC3, however, the

expression of SOX17 and FOXA2/DNA was higher for each stiffness, as compared to SC5. Interestingly, cells encapsulated as preformed aggregates showed considerably higher expression of SOX17/DNA and FOXA2/DNA, as compared to cells encapsulated as single cells. However, aggregates showed an increase in SOX17/DNA expression as stiffness increased up to the 100 mM BAlg condition, and then began to decrease as stiffness was further increased. While FOXA2/DNA was significantly higher in aggregates compared to single cells, the trend in protein expression as stiffness was increased was less clear.

Having confirmed germ layer commitment, we next analyzed the sensitivity of pancreatic differentiation to perturbations in substrate and culture configurations. Pancreatic differentiation was analyzed by quantifying the expression levels of PDX1 and Nkx6.1 proteins, both vital markers of the progenitor population required for downstream β cell commitment. As illustrated in Figure 4.7B, while SC5 showed higher expression of PDX1/DNA as compared to SC3, pancreatic differentiation of single cells was insensitive to changes in substrate properties. Similarly, expression of Nkx6.1/DNA for SC3 and SC5 showed slight variations as stiffness was increased, but essentially remained unchanged as stiffness increased. Unlike that seen with PDX1, SC3 showed higher Nkx6.1/DNA expression as compared to SC5. Consistent with DE differentiation, preformed aggregates showed significantly higher pancreatic phenotype as compared to single cell encapsulation. Additionally, PDX1/DNA expression in encapsulated aggregates was more sensitive to substrate conditions: it increased as stiffness was increased up to the 100 mM BAlg condition, and then decreased as stiffness was further increased. Nkx6.1/DNA expression for preformed aggregates was significantly higher than both SC3 and SC5, consistent with the expression of DE stage makers and with PDX1 expression. Similar to PDX1, Nkx6.1 expression for preformed aggregates was also sensitive to substrate properties,

but the nature was slightly different. While PDX1 peaked around 100 mM concentration, NKX6.1 expression was highest at 10mM concentration and dropped beyond that with increasing crosslinking. Taken together, these results indicate that differentiation is sensitive to both culture configuration and substrate properties during each stage of pancreatic differentiation.

In order to evaluate this sensitivity using quantitative metrics, we next performed a statistical analysis to quantify the importance of substrate properties on the differentiation of the encapsulated hPSCs. Again, the cation concentration was chosen as the independent variable, but now the differentiation markers were chosen as the response variables. This includes SOX17 and FOXA2 protein expression at the DE stage, and PDX1 and Nkx6.1 protein expression at the PP stage. Figure 4.8 shows the regression coefficients for the differentiation markers at the DE and PP stages.

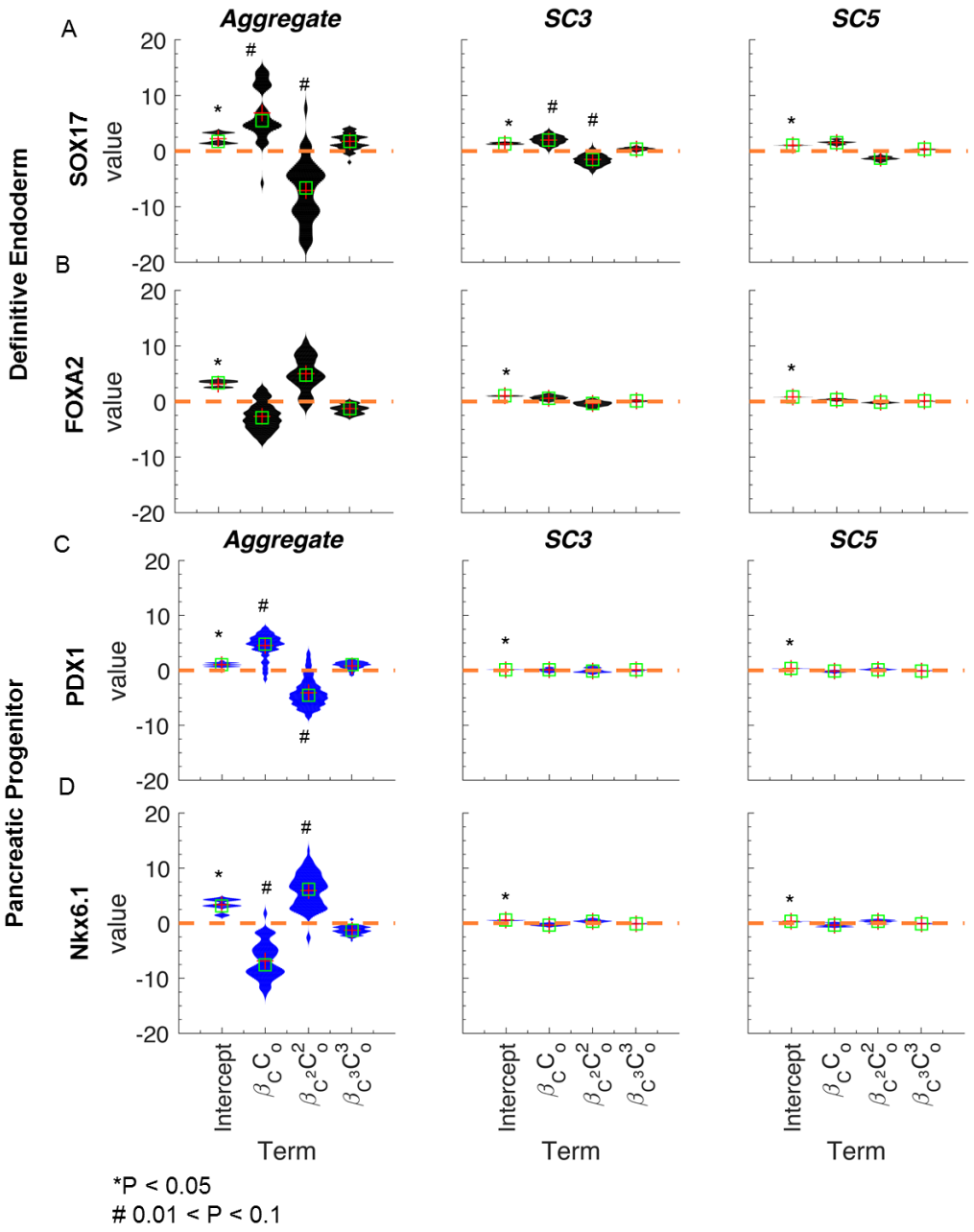

Figure 4.8. Significance of cation concentration in determining differentiation for each culture configuration.

(A-B) DE stage and (C-D) PP stage. The mean and median of the distributions in the violin plot are shown as red crosses and green squares. The p-values of the F-statistic are given for the significant terms. *P < 0.05 and # 0.01 < P < 0.1

Again, only those bootstrap samples for which the R squared values ranged from 0.5 to 0.95 are shown. For the DE markers SOX17 (Figure 4.8A) and FOXA2 (Figure 4.8B), the influence of substrate properties are more pronounced in the aggregate configuration than the other configurations. However, the p-values over the bootstrap samples are in a wider range ($0.01 < p\text{-value} < 0.1$). Similar observations can be made for the PP stage markers PDX1 (Figure 4.8C) and Nkx6.1 (Figure 4.8D). There is a minor effect of concentration in the SC3 configuration at the DE stage.

4.3.6 Statistical analysis to identify best predictors of proliferation and differentiation

The above analysis shows a somewhat disparate effect of substrate properties on proliferation and differentiation. While cation concentration most significantly affected the proliferation of SC3 cells, for differentiations the aggregate cultures were most sensitive to substrate properties. Thus in order to resolve the combined effect of multiple parameters (substrate properties and culture configuration) on proliferation and differentiation, a multiple regression with two independent variables was performed (Equation 1.2). Cation concentration was chosen as a continuous variable as done in Figures 6 and 8. Culture configuration being a categorical variable was encoded as follows: aggregates as ‘config 1’, SC3 as ‘config 2’ and SC5 as ‘config 3’. During regression, a simple coding scheme was used with ‘config 1’ as the reference level with respect to which the regression coefficients were calculated. Therefore, the regression model measures the influence of deviation of config 2 and 3, from this reference level. In the reduced form, the model equation contains third order polynomials to describe the dependence on cation concentration (substrate effect), linear terms for culture configurations and bi-linear terms for interaction between cation concentration and culture configuration. To compare the

relative importance of configuration vs. cation concentration, the p-values of the regression terms will be used. The violin plots in Figure 4.9 show a distribution of coefficients of each regression term for the proliferation and differentiation markers, each term brought to the same units.

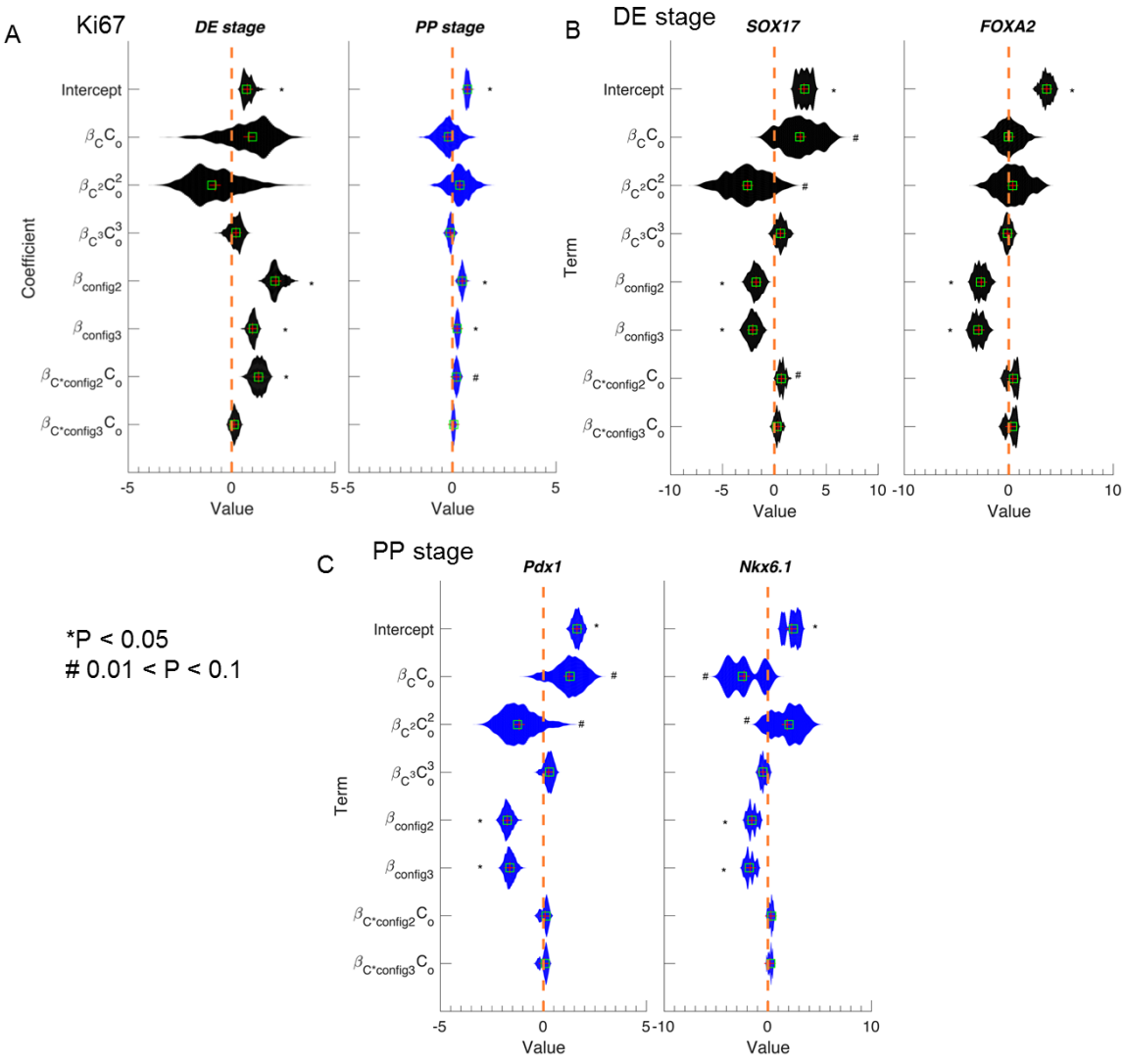

Figure 4.9. Influence of configuration and stiffness in determining proliferation and differentiation. (A) Proliferation marker at DE and PP stage, (B) DE stage markers, (C) PP stage markers. The mean and median of the distributions in the violin plot are shown as red crosses and green squares. The p-values of the F-statistic are given for the significant terms. *P < 0.05 and # 0.01 < P < 0.1

Figure 4.9A shows the coefficients for the proliferation marker Ki67 at DE and PP stage. Overall, the configuration terms are found to be most important (Intercept and config 2 and 3) at both stages. Additionally, the interaction of config 2 and concentration shows a secondary importance at the DE (also seen from Figure 4.6). This term was less significant at the PP stage. Overall, these results also indicate that the contributions of each term to the proliferation marker are reduced after the DE stage.

For the differentiation markers SOX17 and FOXA2 at the DE stage, and PDX1 and Nkx6.1 at the PP stage (Figure 4.9B and C), the configuration terms were again important (p-value < 0.05), while the concentration terms showed a range of significance values (0.01 < p-value < 0.1). The interaction between config 2 and concentration was still seen for SOX17 in a number of regression models, but this interaction was lost for other differentiation markers. Overall, this indicates that culture configuration is the primary determinant of the average expression of the proliferation and differentiation markers, while cation concentration (and hence stiffness) fine-tunes the expression around the average levels.

4.4 DISCUSSION

The objective of this study is to quantitatively evaluate the effect of combinatorial perturbations of cell microenvironment on the pancreatic differentiation of hESCs, conducted in a 3D configuration. The implementation of a high-throughput alginate-based 3D microarray platform allowed simultaneous variation of both hydrogel crosslinking, as a well as culture configuration (in this study, single cells or preformed aggregates). Translation of hPSCs to clinic for regenerative cell therapy will require its large scale propagation, along with functional

differentiation. In addition, encapsulation in a retrievable device is a necessity in current clinical trials, in particular for diabetes therapy [173]. Hence, in our 3D alginate array platform we evaluated the sensitivity of hESC proliferation and differentiation on encapsulation and substrate parameters. By integrating regression analysis with quantitative imaging, we identified that proliferation and differentiation were sensitive to substrate stiffness in the array at lower seeding densities, while cell aggregates were not. When simultaneously varying cell density, cell culture configuration, and substrate stiffness, we identified that hESC proliferation and differentiation were most strongly sensitive to configuration. Thus, in the current study, we report the variations of alginate crosslinking and culture configuration which are most amenable to proliferation and pancreatic differentiation of hESCs.

The alginate array is constructed by first spotting a barium/PLL solution in the desired array configuration onto nitrocellulose coated tissue culture plastic. The solution is allowed to dry before spotting the cell-alginate solution directed on top of the cation spot. The physical stimuli imparted on the cells were directly controlled by the barium concentration used. We have previously identified the range of barium alginate stiffness, specifically 4-7 kPa, which was supportive of hESC growth and pancreatic differentiation in alginate hydrogel capsules [159]. Reproduction of the same stiffness range in the current array platform required higher Ba^{2+} concentrations as compared to the alginate capsules. For example, in capsules, crosslinking with 10 mM $BaCl_2$ results in approximately 4 kPa stiffness, while 150 mM $BaCl_2$ was necessary to achieve this same stiffness in the array. This difference in cation concentration needed to match the alginate stiffness in the two platforms are likely due to differences in gelation kinetics: while alginate capsules are formed by external gelation, the alginate array is primarily by internal gelation. For example, we have previously reported the alginate hydrogel stiffness to be ~1 kPa

for a 1.0% alginate crosslinked with 48 mM $CaCO_3$ using internal gelation [117]; while Morch et al. have shown that alginate of the same type and concentration, crosslinked with 50 mM $CaCl_2$ resulted in hydrogels of ~10 kPa [36]. Since different gelation methodologies could result in the different hydrogel stiffness, in the current study we chose to adjust the cation concentration in order to reproduce the desired stiffness range conducive to hESC growth and pancreatic differentiation.

The primary advantage of the array platform is it allows simultaneous perturbation of multiple parameters. We first used the platform to evaluate the effect of hydrogel crosslinking and culture configuration on the viability and growth of hESCs during pancreatic differentiation. Encapsulation of single cells, both 3 and $5x10^6$ cells/ml, and aggregates showed high viability after pancreatic induction. Encapsulated single cells grew into large viable cell colonies by the end of differentiation; however, for both SC3 and SC5, the number of viable cells decreased with increasing alginate crosslinking. This same trend was observed in our previous report using alginate capsules [159]. Interestingly, however, the viability of encapsulated preformed aggregates was unaffected by alginate crosslinking. This suggests that formation of preformed hESC aggregates prior to encapsulation resulted in a more robust starting population for differentiation. Encapsulation of single cells showed considerable cell death after encapsulation and during differentiation; however, both single cells and aggregates conditions showed good viability by the end of pancreatic differentiation. This suggests that single cells are more sensitive to encapsulation conditions and differentiation, even in the presence of Y-27632, while aggregates were more robust.

Cell proliferation potential during pancreatic differentiation within the array was analyzed by Ki67 staining after the DE and PP stage, and quantified using the LICOR Odyssey

scanner. Overall, it was observed that under all tested conditions the cells were more proliferative at the end of DE stage, compared to the PP stage. This is expected, since as hPSCs undergo differentiation and approach maturation, their proliferative potential begins to decrease. However, comparison across the tested conditions showed distinct differences. At the DE stage, as substrate stiffness was increased, Ki67 expression increased for both the SC3 and SC5 conditions, albeit only slightly for SC5. A similar trend was observed at the PP stage for both single cell conditions, while the aggregate condition showed no change in Ki67 expression as stiffness was increased. Although our platform is in 3D, a number of studies on 2D substrates have similarly shown that cell proliferation increases as substrate stiffness is increased [174-177]. While expression of the proliferation maker increased with stiffness, cell growth was deceased as stiffness increased, as shown by a decrease in DNA content, due to the hydrogel physically inhibiting cell expansion. Similar results have been seen in alginate encapsulated breast cancer cells [178], neural stem cells [179], and hESC-derived pancreatic cells [159]. The importance of substrate stiffness on hESC proliferation during pancreatic differentiation was better resolved using a regression analysis. While studying the influence of cation concentration (hence, substrate stiffness), it was seen that the proliferation marker was not affected significantly by the cation concentration, except in the SC3 conditions at the DE stage. Since the relationship of Ki67 with hydrogel crosslinking in the SC3 condition was significant, it indicates that fine-tuning the stiffness will be beneficial at lower cell densities, with increasing stiffness favoring proliferation, especially at the DE stage. This relationship comes without loss of DE differentiation potential; however, cell number is decreased from the physical inhibition of growth as crosslinking increases. At the PP stage, increasing cation concentration will not be beneficial for increasing proliferation.

While differentiation was influenced by substrate stiffness at both the DE and PP stages, the trends were less clear. At the DE stage, while SOX17 and FOXA2 expression in the SC5 condition were not sensitive to changes in substrate stiffness, they were sensitive to changes in substrate stiffness in the SC3 condition. For the aggregate condition, while the trend was not clear for FOXA2 expression, SOX17 expression increased as stiffness increased until the 100 mM condition, after which it began to decrease. However, the regression analysis showed that the effect of crosslinking on differentiation at the DE stage was only significant in the SC3 condition for SOX17. Similarly, the regression analysis identified that the effect of substrate stiffness on differentiation at the PP stage was only significant in the aggregate condition, while the single cell conditions were not. PDX1 expression increased until the 100 mM condition, after which expression decreased. Nkx6.1 was highest at the lowest stiffness condition of 10 mM, after which the expression deceased and reached steady state by the 100 mM condition. Schaffer et al. showed that the delineation between endocrine and exocrine cells during beta cell development is controlled in part by the expression of Nkx6.1 and PtF1a [180]. High expression of Nkx6.1 results in the repression of Ptf1a, leading to endocrine commitment. Previously, for alginate encapsulation of hESCs, we saw an increase in Ptf1a expression as alginate stiffness was increased [159]. Thus, the decrease in Nkx6.1 expression as alginate stiffness is increased could indicate a commitment to the exocrine pancreas as stiffness is increased. This is further supported by the decrease in PDX1 expression after the 100 mM conditions, as PDX1 expression has been shown to decrease as the exocrine pancreas develops [180]. However, in the presence of experimental variability, the influence of hydrogel crosslinking to pancreatic differentiation was only significant in the aggregate condition, within the alginate array platform.

While only slight effects were observed to be significant when considering only substrate stiffness, performing a multiple regression analysis on both substrate stiffness and configuration identified the significant contributions to proliferation and differentiation. Conditions with lower seeding density were more proliferative for all alginate crosslinking conditions and at all stages of differentiation. Wu et al. observed that hPSC proliferation was decreased as cell density was increased in adherent cultures [181]. Similarly, while not in hPSCs, Stephan et al. showed that Ki67 expression was decreased in adult human intervertebral disc cells encapsulated in alginate, as seeding density was increased [182]. From the LIVE/DEAD images, the higher seeding density of the SC5 condition, resulted in slightly larger aggregates by the end of the DE stage compared to SC3, and considerably larger aggregates by the end of the PP stage. When encapsulated single cells undergo expansion, they form small cell aggregates within the alginate hydrogel. As these cells continue to grow, the propensity for aggregate coalescence is higher in the SC5 condition since more cells are present and more densely packed in the hydrogel, resulting in the larger aggregates observed after PP induction. Hence, the higher seeding density led to larger aggregates during culture, which in turn may have caused the decrease in proliferation, as seen by lower Ki67 expression. Interestingly, however, encapsulation of preformed aggregates showed lower Ki67 expression than either single cells condition at both the DE and PP stages, for all stiffness conditions. Nelson et al. have shown that endothelial and smooth muscle cell proliferation in 2D was inhibited by decreasing cell spreading as cells become crowded [183]. Gray et al. have shown that endothelial cell proliferation was increased when in contact with only one other cell, but was inhibited when in contact with two or more cells [184]. Thus, is it is possible that preaggregation of the hESCs prior to encapsulation, resulted in locally minimal cell spreading, which in turn limited the proliferative capacity within

the hydrogel. Combined with the physical inhibition of cell growth imparted by the hydrogel stiffness, cell proliferation of preformed aggregates was minimized.

Similar to what was seen with proliferation, culture configuration significantly influenced the differentiation potential at both the DE and PP stages, and while the effect of crosslinking was present, it was weak. Differentiation was most sensitive to changes in culture configuration, while alginate crosslinking had a secondary effect in certain cases. At the DE stage, the SC3 condition showed higher SOX17 and FOXA2 protein expression as compared to the SC5 condition for all stiffness conditions. However, SOX17 and FOXA2 expression in preformed aggregates was significantly higher than both the SC3 and SC5 conditions. This suggests that formation of tight cell-cell contacts from pre-aggregation prior to encapsulation may be promoting differentiation. This is supported by Tang et al., who have shown in 2D that the extent of mesenchymal stem cell osteogenic and adipogenic differentiation increases as cell-cell contact was increased [185]. While encapsulation of single cells in the SC3 and SC5 conditions eventually form aggregates as well, aggregates form primarily from confined single cell division, thus forcing cell aggregation over time as cells proliferate. This indicates that formation of hESC aggregates prior to encapsulation is more supportive of differentiation at the DE stage than when cells form aggregates from single cells through cell proliferation. The same trends were observed at the PP stage as that seen at the DE stage. Encapsulation of preformed aggregates showed higher PDX1 and Nkx6.1 protein expression, as compared to either the SC3 or SC5 conditions, suggesting that preformed aggregates as the starting population are more supportive of differentiation. Toyoda et al. have shown that an increase in cell density supported pancreatic differentiation of hESCs in adherent culture, and that aggregation of cells strongly enhanced pancreatic bud differentiation [161]. While we did not see the strong increase in differentiation

as cell density was increased in our 3D alginate array, we have observed a similar effect of cell aggregates strongly supporting differentiation. In future, we could focus efforts on finding optimal culture configurations for hPSC proliferation and differentiation in large scale biomanufacturing, while using hydrogel properties which are most supportive of bioreactor culture.

4.5 CONCLUSIONS

The objective of this chapter was to use alginate-based 3D microarray platform, to simultaneously evaluate the effect of culture configuration and alginate crosslinking on the directed differentiation of hESCs to the pancreatic lineage. While the effect of hydrogel crosslinking was shown to be minimal on proliferation of hESCs encapsulated as single cells, the effect was significant in the aggregate configuration. Encapsulation of single cells in the array showed higher growth and proliferation than aggregates during differentiation. However, single cells were more susceptible to apoptosis as compared to aggregates. Finally, the pancreatic differentiation of hESCs was sensitive to both crosslinking and culture configuration, although it was more strongly sensitive to the latter. While slight changes in pancreatic differentiation were observed as crosslinking in the array was varied, cells encapsulated as aggregates showed significantly higher levels of differentiation as compared to cells encapsulated as single cells.

5.0 ENGINEERED PEPTIDE MODIFIED HYDROGEL PLATFORM FOR BIOMANUFACTURING OF HUMAN PLURIPOTENT STEM CELLS

5.1 INTRODUCTION

Having demonstrated in Aims 1 and 2 that alginate hydrogel capsules provided a permissive and supportive environment for hPSC propagation and differentiation to pancreatic islet cell types, our next step was to consider large scale expansion for clinical translation. A vital step in the path to clinical translation of laboratory scale scientific advances in hPSCs is to implement reproducible, scalable culture and differentiation protocols. The primary criterion for hPSC scale up platforms is the maintenance of high viability and proliferation without compromising pluripotency and differentiation potency. However, a critical requirement for hPSC survival and proliferation is maintaining cell-cell contact, failing which results in dissociation induced apoptosis. This requirement significantly restricts options for scalable cultures, which has inspired novel avenues for hPSC scale-up.

With maintenance of cell-cell contact being critical for hPSC survival, these cells are commonly cultured and propagated as colonies on adherent 2D substrates. The most commonly used method employs propagation on tissue culture plastic coated with Matrigel, an animal derived ECM protein cocktail [186]. However, being animal derived and expensive, this limits the scalability for use in cellular therapy applications [70]. Suspension culture systems, on the

other hand, are intrinsically better suited for scalable cultures because of geometric scalability. Current methods of suspension cultures of hPSCs include microcarrier culture [187, 188] and cell aggregate culture [189, 190]. Microcarrier culture offers the unique advantage of scaling up adherent hPSCs. While uniquely suited for hPSCs, this platform possesses a high propensity for undesirable cell clustering, along with problematic separation of cells from the carrier. Currently the most promising scalable platform is aggregate-based suspension culture of single cell inoculation with ROCK inhibition, which supports long-term cell survival in an undifferentiated state [191-198]. Key challenges with the current suspension cultures are (i) maintaining homogeneity of cell aggregates and (ii) accounting for the uncontrolled shear stress on the surface of aggregates. Specifically, the response of hPSCs to shear stress varies with cell lines, hence reducing the versatility of the platform [198, 199]. Overcoming these shortcomings will be highly critical in establishing a robust and controlled stem cell biomanufacturing platform.

Maintaining tight cell-cell contact is indispensable for hPSC survival and proliferation; the absence of which results in ROCK pathway activation, actomyosin hyperactivation, and ultimately dissociation induced apoptosis. ROCK inhibition is by far the most commonly used procedure for single cell hPSC cultures, however, this only partially rescues the dissociation induced apoptosis [200]. Specifically, hPSCs treated with ROCK inhibitor can still result in over 50% cell death upon dissociation [78]. The Rho/ROCK signaling cascade is initiated by dissociation of the transmembrane glycoprotein E-cadherin, a primary homophilic adhesion molecule responsible for hPSC survival [79] (Figure 5.1).

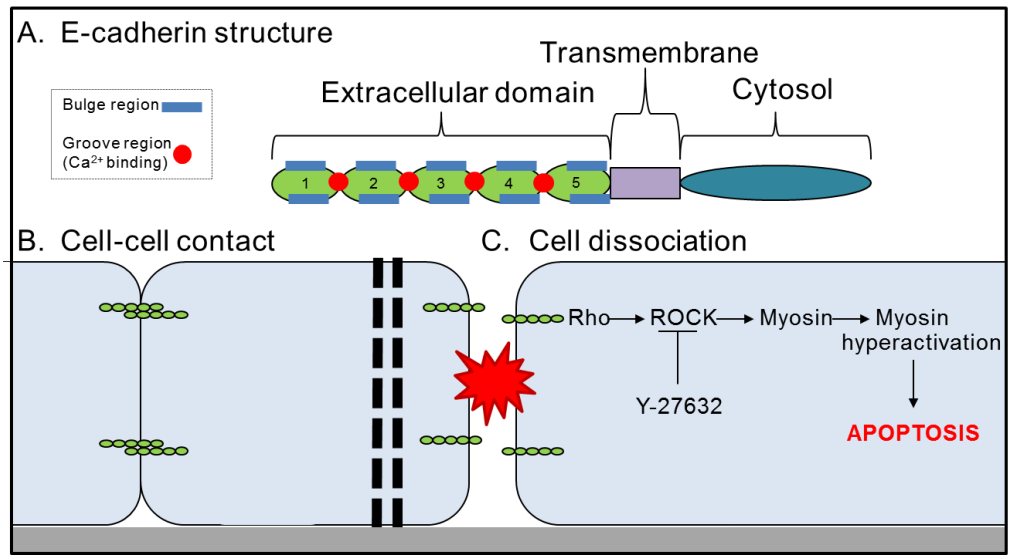

Figure 5.1: Schematic of E-cadherin binding between two hESCs.

A) E-Cadherin protein. B) Trans dimerization of E-Cadherin in the presence of cell-cell contact. C) Dissociation induced apoptosis of hESCs.

Hence, an alternative strategy to improve cell viability is to directly target E-cadherin [201]. To this end, the extracellular domain of E-cadherin has been successfully used to replace Matrigel in adherent cultures of hPSCs [202]. Recently, there has been extensive advancement in designing xeno-free, chemically defined substrates for 2D adherent cultures of hPSCs. A highly promising avenue has been to replace Matrigel with recombinant proteins such as laminin [68], a primary constituent of Matrigel, or vitronectin [69]. While this approach to produce hPSCs will comply with FDA regulations for cell therapy applications, the production of xeno-free recombinant proteins is highly expensive. This again places more limitations on transitioning hPSC culture to large scale applications due to the enormous cost. Therefore, there has been attempts to design synthetic peptides to replace the bioactive region of full protein; mimicking the bioactive regions of integrin's with synthetic peptides has recently been successfully shown in 2D adherent

cultures of hPSC [203-205]. However, it is not obvious how critical integrin junction is for hPSC viability. In this study we have accordingly designed synthetic peptides to mimic E-cadherin, primarily because it is critical for hESC survival. We have designed a biomimetic alginate substrate which mimics the role of E-cadherin during cell-cell binding. Alginate was chosen as the support substrate since it has been previously demonstrated to be suitable for hPSC propagation and differentiation. Additionally, alginate is easily modified with peptides using simple water soluble carbodiimide chemistry [206]. Our ultimate goal is to synthesize a biomimetic hydrogel for cell encapsulation for propagation in the large scale bioreactor setting; in this work we evaluated the E-cadherin mimicking peptides in 2D adherent culture. To this end, while informing optimal parameters for a future 3D platform, the 2D E-cadherin mimicking substrate developed in this chapter has commercial potential to replace current animal-derived substrates.

E-cadherin dimerizes through completion of a trans interaction between adjacent EC1 domains which contains either a 'bulge' region consisting of a conserved HAV peptide sequence or 'groove' regions through the ADT sequence [207-209] (Figure 5.1A). These and other sequences, based on overlapping dimers of various EC1-5 domains, have resulted in a variety of sequences that result in binding of E-cadherin of various cell types [207, 210, 211]. The EC1 domain has been previously shown to be the primary E-cadherin subunit involved in cell-cell contact [212, 213]. Thus, we focused on this region to mimic E-cadherin binding using short synthetic peptides. We used peptide sequences based on the active domain of the bulge and groove region of the EC1 domain for production of our biomimetic E-cadherin mimicking alginate hydrogels (Table 1).

Table 1. E-cadherin mimicking peptides and sequences.

Name	Sequence	Description
HAV10	LFSHAVSSNG	Groove EC1 10 peptide
HAV6	SHAVSS	Groove EC1 6 peptide
ADT10	QGADTPPVGV	Bulge EC1 10 peptide
ADT6	ADTPPV	Bulge EC1 6 peptide

Previous work using these peptide sequences has focused on sequestration of E-cadherin binding sites to increase intracellular porosity [207, 214-216]. On the other hand, N-cadherin-derived HAV peptide enhanced MSC chondrogenesis in conjunction with methacrylated hyaluronic acid [217]. The same substrate was recently shown to enhance osteogenesis of hMSCs [218]. The HAV motif from the EC1 domain of N-cadherin is highly conserved across other types of cadherin's, and thus as previously mentioned, the same HAV domain is also present in the EC1 domain of E-cadherin. However, these peptides have never been evaluated for use with pluripotent stem cells.

We hypothesized that the extracellular E-cadherin domain of hPSCs will bind to the synthetic peptides of the biomimetic alginate to retain single-cell viability and clonogenicity. Hence, the objective of this study was to functionalize alginate hydrogels with synthetic peptides mimicking E-cadherin and evaluate peptide performance in promoting cell attachment, viability, maintaining pluripotency, and differentiation potential. We observed that alginate conjugated with HAV and ADT based peptides supported initial cell attachment and hPSC propagation. Cells propagated on the peptide modified substrates maintained good pluripotency and differentiation potential, as shown by gene and protein analysis.

5.2 MATERIALS AND METHODS

5.2.1 hPSC Culture

Undifferentiated (UD) H1 hESCs (WiCell) were maintained on hESC-qualified Matrigel (BD Biosciences) coated tissue culture plastic for 5–7 days in mTeSR1 (StemCell Technologies) at 37°C and 5% CO_2 before passaging. Experiments were performed with p55-p85 hESCs.

5.2.2 Thin Alginate Hydrogel formation and peptide conjugation

The alginate hydrogels were formed prior to peptide attachment. The culture well was coated with a thin layer of 1.1% (w/v) low viscosity alginate (Sigma-Aldrich) with 0.2% (v/v) gelatin (Sigma-Aldrich), which was allowed to dry overnight. 20 mM $BaCl_2$ was used to rehydrate and simultaneously cross link the alginate in a thin hydrogel covering the bottom of the culture well. Peptide conjugation was done using water soluble carbodiimide chemistry [206]. Alginate hydrogels were activated by incubating with 20 mM/10 mM EDC/NHS in buffer containing 0.3 M 2-(N-morpholino) ethanesulfonic acid (MES) and 0.1 M NaCl, for 15 min. The peptides were then added and incubated overnight at 4ºC to allow for peptide conjugation to the carbonyl groups of the alginate hydrogel. After conjugation, peptide modified hydrogels were washed with 0.9% saline prior to seeding cells.

Confirmation of peptide conjugation to the alginate hydrogels was done using the BCA assay, according to manufacturer's instructions. Briefly, peptide conjugated alginate hydrogels were incubated with BCA reagent at 60ºC for 30 min. The resulting supernatant absorbance analyzed using a Synergy 2 multi-mode Microplate Reader (BioTek, Winooski, VT, USA).

5.2.3 Cell Attachment

For cell attachment studies to the peptide modified hydrogels, hESC were first labeled with DiD according to manufactures instruction, a fluorescent lipophilic dye, which is incorporated in the cell membrane. hESC were treated with 10 μm Y-27632 (R&D Systems, Minneapolis, MIN) for 2 hours prior to harvesting by Accutase (Invitrogen) treatment for 5-7 min. For cell attachment, studies were performed in a 48 well plate, seeded with 50,000 cells/well. Cell attachment was analyzed 24 hours after seeding. First, total cell number per well was quantified using the LI-COR Odyssey scanner and Image Studio software to obtain the total possible MFI. Dead and unattached cells were washed away and the number of attached cells per well was again quantified using the LI-COR Odyssey scanner Image Studio software. Cell attachment data was presented as percent attachment by normalizing the attached cell MFI to the total cell MFI for each peptide and peptide concentration.

5.2.4 LIVE/DEAD Assay

LIVE/DEAD (Life Technologies) viability assay was performed according to manufacturer's instructions.

5.2.5 Cell Expansion

To determine cell expansion, cellular metabolism was assayed on cells attached to alginate conjugated with 50 μg/ml of each peptide using the CellTiter 96 ® AQ_{ueous} One Solution Cell Proliferation Assay (MTS) after 1 and 6 days of culture, according to manufacturer's

instructions. Briefly, cells were incubated with the MTS solution at a 1:5 v/v dilution for 3 hours at 37ºC. Absorbance intensity of the supernatant at 490 nm was measured using a Synergy 2 multi-mode Microplate Reader. Fold expansion was determined by normalizing the day 6 absorbance by the day 1 absorbance, for cells grown on each peptide-conjugated alginate substrate.

5.2.6 Directed Differentiation

hESC seeded on the peptide modified alginate hydrogels were propagated for 4 days in mTeSR1 with 10 µm Y-27632 prior to DE induction. DE was induced using 100 ng/ml ActivinA (R&D Systems) with 25 ng/ml Wnt3A (R&D Systems) for 4 days.

5.2.7 Quantitative Reverse Transcriptase Polymerase Chain Reaction

mRNA was isolated using the NucleoSpin RNA II kit (Macherey-Nagel, Bethlehem, PA). cDNA was obtained using ImpromII Reverse Transcription (Promega, Madison, WI). Each PCR reaction contained 5 µl SYBR Green Master Mix (Agilent, Santa Clara, CA), 2 µl nuclease free H2O, 2 µl primer, and 1µl cDNA. Samples were normalized to the house keeping gene GAPDH and analyzed relative to UD hESCs using the ΔΔCt method. Gene expression was measured with quantitative polymerase chain reaction (qRT-PCR) using an MX3005P system (Agilent).

5.2.8 Immunostaining

Cells were fixed with 4% formaldehyde for 20 min, and were permeabilized with 0.1% Triton-X (Sigma) in 0.9 % saline for 5 min. A blocking step with 10% donkey serum in 0.9 % saline was done for 1 hour. For primary antibody staining, we used goat anti-Nanog (1:200 dilution, Cell Signaling, Danvers, MA). The incubation time for primary antibodies was done overnight at 4°C. Cells were incubated with the secondary antibody for 45 min at room temperature. For secondary antibody staining, we used anti-goat Alexafluor 488 (1:500 dilution). Cells were washed three times with 0.9 % saline (5-10 min) before mounting on slides with hardening mounting medium containing DAPI (Vectashield, Vector laboratory). Imaging was done using a Nikon A1 confocal microscope.

5.2.9 Statistical Analysis

Statistical significance comparing multiple groups was determined using one-way ANOVA, with Tukeys or Games-Howell post hoc testing for homogeneous or inhomogeneous variance, respectively. Probability values at $P < 0.05$(*) and $P < 0.01$ (**) indicated statistical significance.

5.3 RESULTS

5.3.1 Substrate Design and Characterization

A thin alginate hydrogel was created by first coating tissue culture wells with a 1.1% alginate solution, allowing this coating to dry, and finally rehydrating the dried alginate using 20 mM $BaCl_2$ (Figure 5.2A).

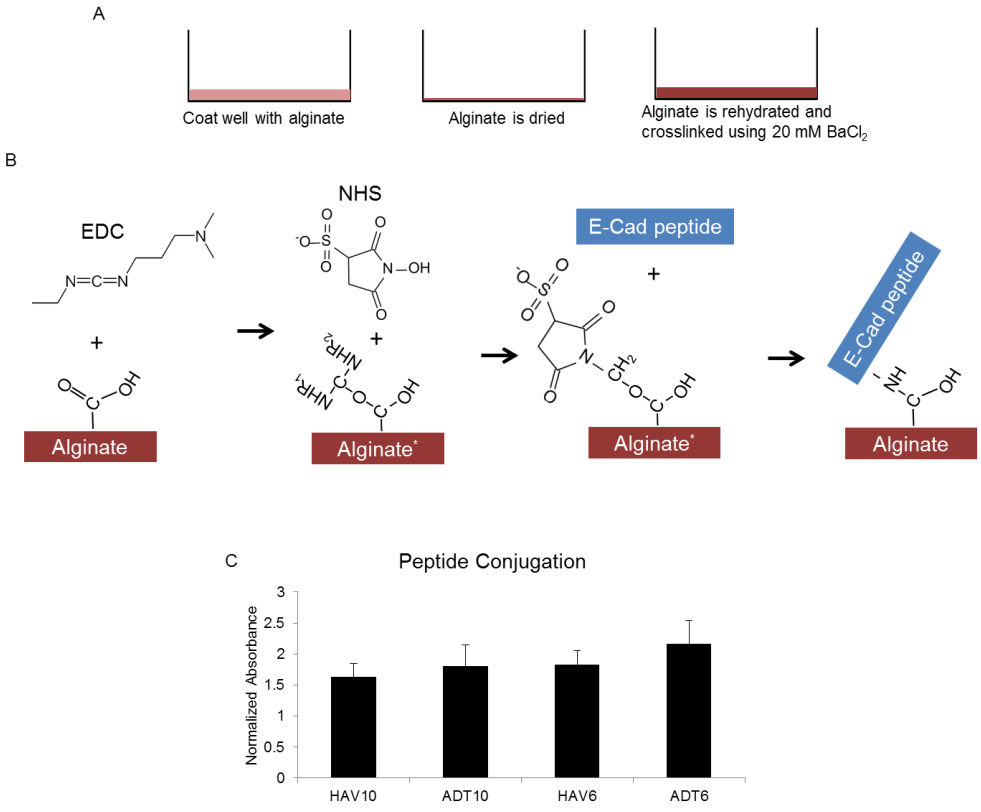

Figure 5.2. Schematic of peptide conjugated alginate hydrogel and characterization.

A) Schematic of alginate hydrogel formation in a well plate. B) Carbodiimide chemistry was used to activate the carboxylic acid groups on alginate, forming a peptide bond with the N-terminus of the desired peptide. C). BCA protein assay analysis confirming the attachment of the peptides to alginate.

The $BaCl_2$ crosslinks the alginate as it is being rehydrated, which resulted in a thin alginate hydrogel that covered the entire culture surface, thus preventing cells from getting underneath the gel between the tissue culture plastic and hydrogel. Peptide conjugation was achieved by first activating the alginate hydrogel using 20/10 mM EDC/NHS (Figure 5.2B). The EDC activates the carbonyl groups of the alginate back bone, forming an unstable o-Acylisourea intermediate. This intermediate is stabilized by the addition of the NHS, forming a reactive sulfo-NHS ester group on the carboxylic acid groups of the alginate substrate, allowing for peptide bond formation with the N-terminus of the e-cadherin peptides.

Peptide conjugation to the alginate hydrogel was confirmed using the BCA assay (Figure 5.2C). The peptide bonds between the amino acids in the peptides cause the reduction of Cu^{+2} in the BCA reagent to Cu^{+1}. This chelates the BCA reagent, and thus, in the presence of the peptide-conjugated hydrogels, results in a colorimetric detection of the attached peptides, quantified using absorbance spectroscopy. The presence of the conjugated peptide was represented as the absorbance from each peptide conjugated hydrogel, normalized to the absorbance of the alginate hydrogel alone. A similar level of absorbance was detected for each peptide and ranged from 1.6 to 2.2-fold increase in absorbance as compared to alginate alone, for HAV10 and ADT6 conjugated hydrogel respectively.

5.3.2 hESC Attachment to Peptide Conjugated Alginate hydrogel

Having confirmed peptide conjugation to the alginate hydrogel, our first step was to analyze cell attachment to each peptide conjugated substrate. Peptide concentration during conjugation was varied from 0 µg/ml (EDC/NHS activation of alginate alone) to 500 µg/ml. hPSCs were treated with Y-27632 prior to harvesting, and seeded as single cells on the alginate conjugated with

HAV10, ADT10, HAV6, and ADT6. As steric hindrance could significantly influence cellular access to the peptide, both a short (6 amino acids) and long (10 amino acids) variant of peptides mimicking the bulge (ADT) and groove (HAV) regions of E-cadherin, were examined. Prior to seeding, cells were labeled using DiD, a lipophilic fluorescent dye, which is incorporated into the cell membrane. After 1 day, cell attachment was quantified for each tested condition using the LI-COR Odyssey scanner. Percent cell attachment was determined by scanning the signal for total seeded cells (prior to wash) and attached cells (post-wash) and normalizing the attached cell MFI to the total cell MFI, for each peptide and peptide concentration (Figure 5.3A).

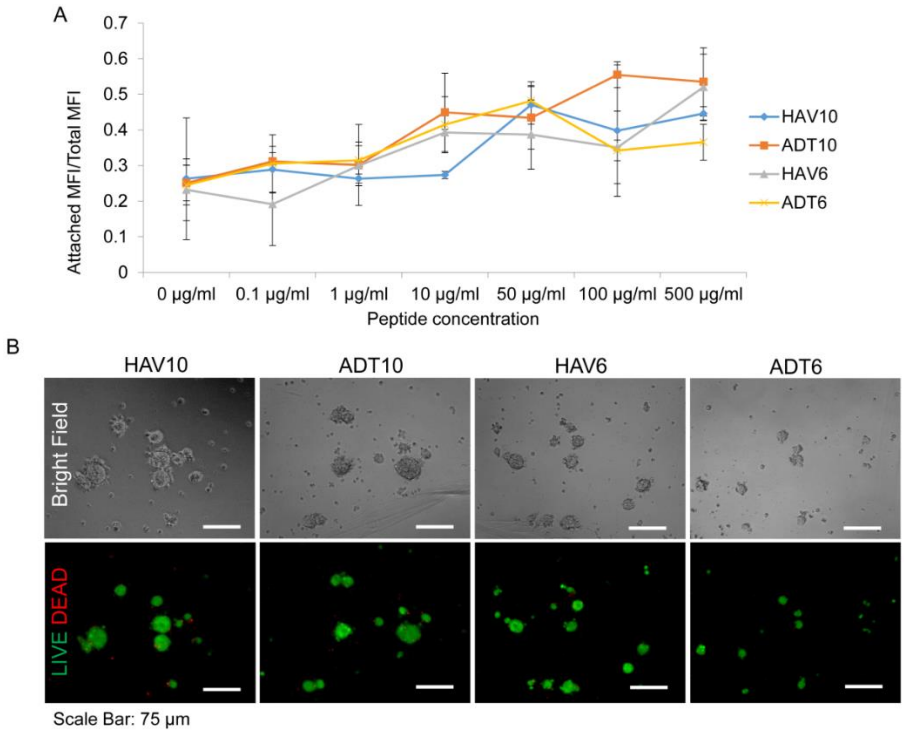

Figure 5.3. Cell attachment to e-cadherin peptide modified alginate.

(A) Percent cell attachment after 1 day, determined by normalizing attached cell MFI by total cell MFI. Cell attachment was analyzed for each peptide, conjugated at 0 – 500 µg/ml. (B) LIVE/DEAD analysis for cell attached to each peptide modified hydrogel, conjugated with 50 µg/ml.

For each peptide, as concentration was increased, cell attachment correspondingly increased. Cell attachment to the HAV10 and ADT6 substrates peaked at the 50 µg/ml condition, after which attachment decreased slightly or was unchanged. Cell attachment to the HAV10 conjugated substrate was essentially unchanged from the control, until a sharp increase in attachment was observed at the 50 µg/ml condition. Cells attached to the ADT10 substrate continuously increased as peptide concentration was increased, and showed the highest cell attachment among all peptides, at all concentrations except 50 µg/ml. Interestingly, while the HAV6 conjugated substrate only showed higher cell attachment than the HAV10 substrate at concentrations less than 100 µg/ml, at the highest concentration of 500 µg/ml it showed higher cell attachment than HAV6 and HAV10 and was on par with ADT10. Figure 5.3B shows representative day 1 LIVE/DEAD images of cells attached to alginate conjugated with 50 µg/ml for each peptide. While cells were plated as single cells, upon attachment and interaction with the E-cadherin mimicking substrates, they quickly began to form small, rounded colonies when in contact with peptide modified alginate. Thus, hPSCs showed a concentration dependent attachment to peptide modified alginate, and each peptide performed similarly when considering cell attachment. While there was quantitative differences in cell attachment in individual peptides, cell morphology appeared similar in all the tested conditions.

5.3.3 hESC Viability and expansion potential after propagation

Having confirmed and quantified initial cell attachment, we next wanted to evaluate how the E-cadherin mimicking substrates support hPSC propagation. Cell viability and morphology were analyzed after 6 days of propagation using the LIVE/DEAD assay, on each of the peptide modified alginate hydrogels, again conjugated with 0.1 – 500 µg/ml of each peptide (Figure 5.4).

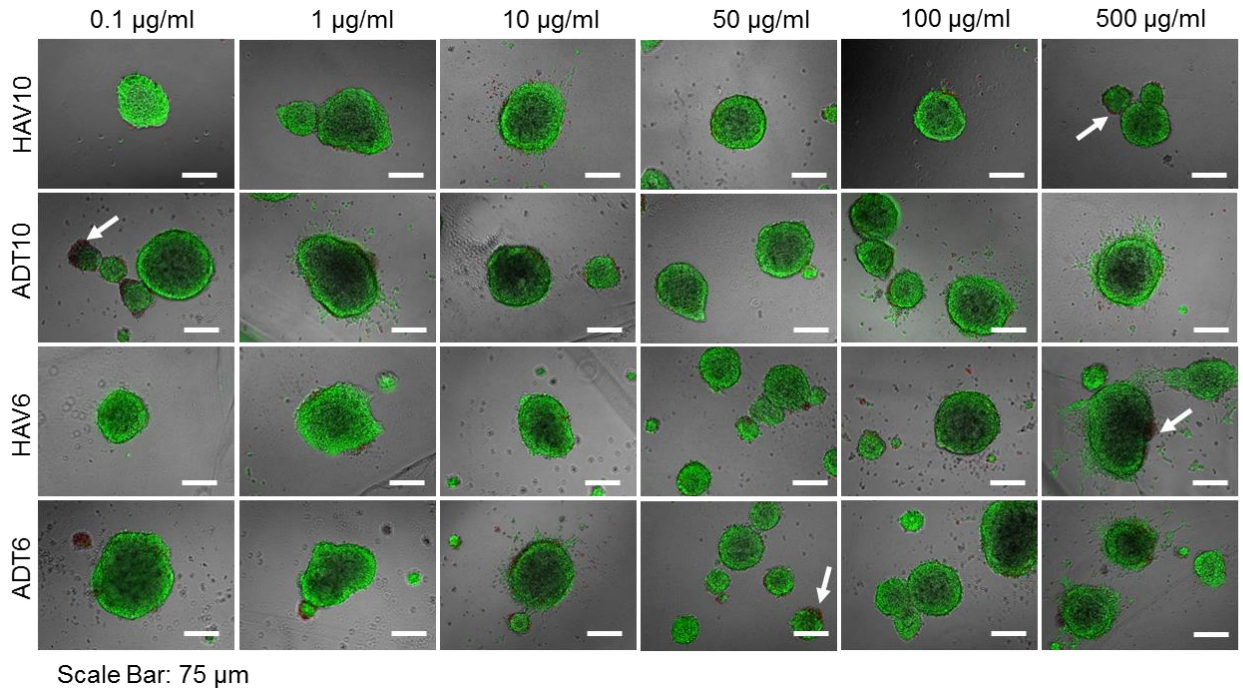

Figure 5.4. Cell viability and morphology after 6 days of propagation for each peptide, conjugated at 0 – 500 µg/ml.

White arrows indicate apoptotic single cells observed on the periphery of some colonies after propagation.

High cell viability was observed on all peptides and no dependence of viability on peptide concentration was observed. For the most part, apoptotic colonies were not observed after the 6 days of propagation, however a small number of apoptotic cells were observed on the periphery of colonies in some conditions. Additionally, a small population of apoptotic single cells was observed, which appeared to have shed off the colonies during culture, or died initially during the seeding step. For each peptide, at all concentrations tested, the colony size increased during the 6 days propagation period, and retained the characteristic round and uniform hPSC colony morphology. However, the colonies appeared to have slightly "domed" or "pancake"-like

morphology, as shown by darker regions in the center of the colony in the microscopy images, indicating that the hPSC colonies were thicker in the center as compared to the edges. While little to no difference in colony size or diameter was observed when comparing across each peptide, colony size did appear to change in response to peptide concentration. For the most part though, larger colonies were observed at the lower peptide concentrations, and as concentration was increased, there appeared to be a higher occurrence of small colonies, although larger colonies were still observed.

Since high cell expansion is necessary to generate clinically relevant numbers of hPSCs, we next quantified the expansion potential of hPSCs grown on each peptide. Expansion potential was determined by normalizing cell number after 6 days of propagation, by day 1 cell number using MTS. Figure 5.5 shows hPSC expansion potential on alginate modified with 50 μg/ml of each peptide.

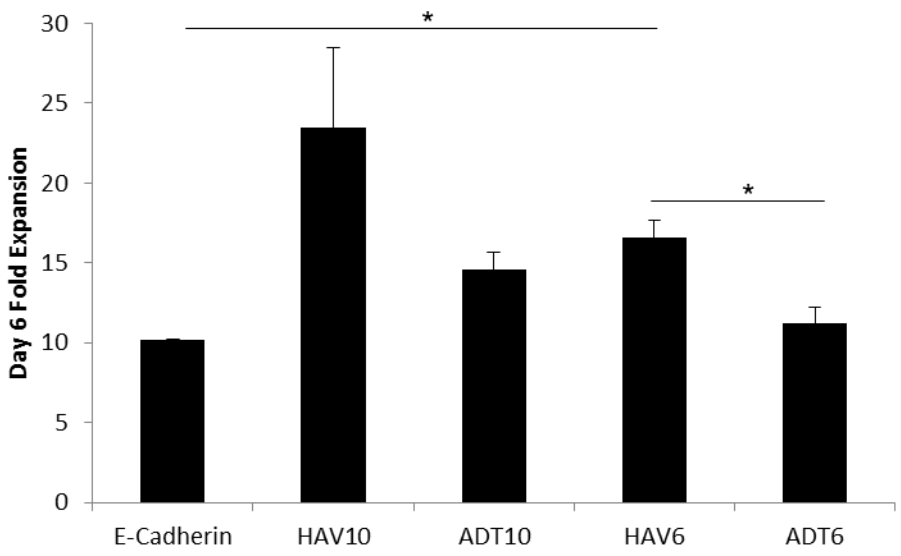

Figure 5.5. Day 6 hPSC expansion potential on recombinant e-cadherin, or alginate conjugated with each peptide. n=3, results were considered significant if *P<0.05, **P<0.01.

The highest expansion was observed with hPSCs grown on HAV10 substrates, showing an approximately 23-fold expansion. Interestingly, while still high, cells propagated on recombinant E-cadherin protein showed only a 10-fold expansion over 6 days of propagation. ADT10 conjugated alginate also showed higher expansion than E-cadherin, with an approximately 14 fold expansion. HAV6 and ADT6 showed a similar trend as the longer peptides, although expansion was lower in magnitude, with a 16 and 11-fold expansion, respectively. Taken together, it is clear that the E-cadherin mimicking substrates can support hPSC proliferation, and high expansion potential.

5.3.4 hESC Pluripotency on Peptide Modified Substrate

Having confirmed the substrates supported attachment and propagation of hPSCs, our next step was to analyze the maintenance of hPSC pluripotency after propagation. hPSC pluripotency is the ability to become any cell type in the body, and along with self-renewal, is the defining characteristic of hPSCs. The maintenance of pluripotency is required for the downstream of hPSC for differentiation into any functions cell type, for cell therapy applications. As cell attachment and propagation did not change considerably when alginate was conjugated with peptide concentrations higher than 50 µg/ml, this condition was chosen to evaluate hPSC pluripotency for each peptide. hPSCs were seeded on alginate conjugated with 50 µg/ml of HAV10, ADT10, HAV6, or ADT, and propagated for 6 days. Again, cell morphology was similar across each peptide, and appeared to have similar morphology to the typical hPSC colony (Figure 5.6A).

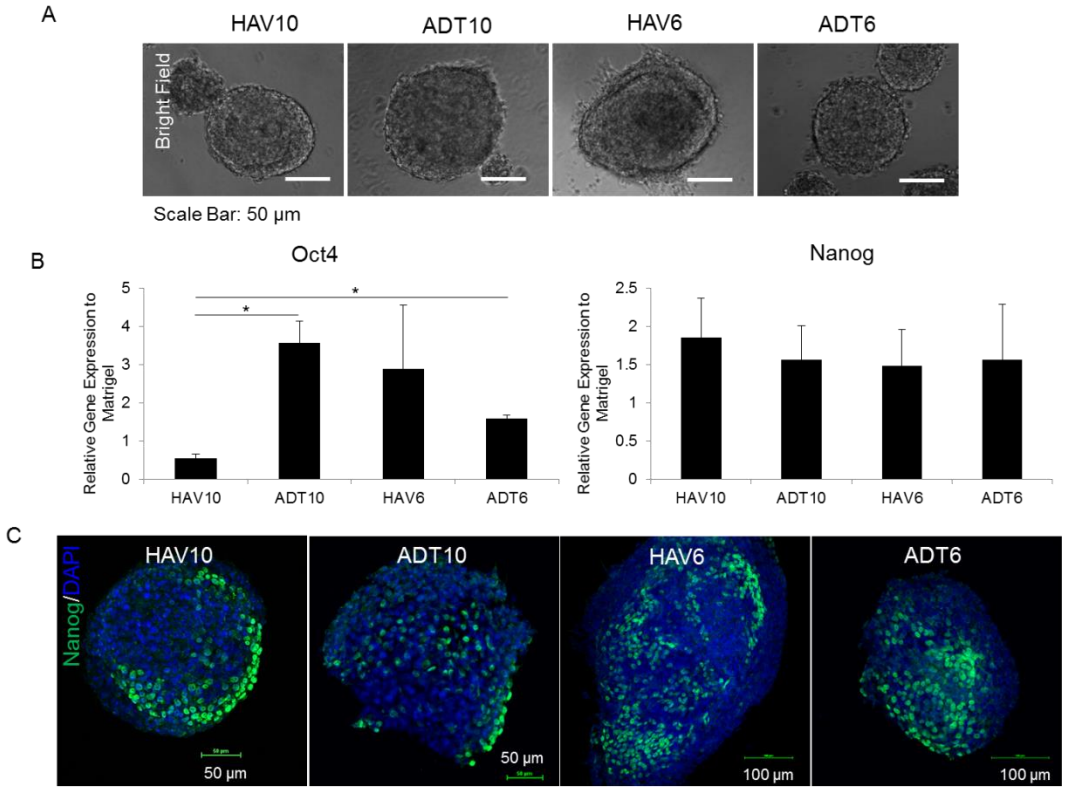

Figure 5.6. hPSC pluripotency after propagation on the peptide modified alginate substrate.

(A) Phase contrast images of hPSC morphology after 6 days of propagation on alginate modified with 50 µg/ml of HAV10, ADT10, HAV6, or ADT6. (B) Gene expression analysis of OCT4 and Nanog. n=3, results were considered significant if *P<0.05, **P<0.01. (C) Nanog immunostaining of hPSC colonies propagated on each peptide conjugated substrate.

Pluripotency was first analyzed by qRT-PCR for gene expression of OCT4 and Nanog, and was shown relative to cells propagated on Matrigel (Figure 5.6B). Cells propagated on HAV10 substrates showed an approximately 2-fold down regulation of OCT4 compared to Matrigel controls; however, expression of Nanog was slightly upregulated. On the other hand, cells cultured on HAV6 showed a 2 and 1.5 fold upregulation of OCT4 and Nanog, respectively,

compared to Matrigel. The ADT10 modified substrate had the highest upregulation of pluripotency markers, which showed a 3 and 1.5-fold upregulation of OCT4 and Nanog respectively, compared to Matrigel. Cells propagated on ADT10 showed significantly higher expression of OCT4, as compared to cells on HAV10. Similarly, ADT6 also retained good pluripotency with expression of OCT4 and Nanog on par with Matrigel, as showed significantly higher OCT4 expression compared to HAV10. Next, maintenance of pluripotency was confirmed by protein immunostaining for Nanog (Figure 5.6C). Cells positive for Nanog were observed in hPSC colonies propagated on each of the peptide modified substrates. Thus, it is clear that hESCs grown on each E-cadherin mimicking substrate retained high pluripotency, which were comparable to, and even higher, than the Matrigel control.

5.3.5 hESC Differentiation Potential

Having confirmed that hPSCs maintained high pluripotency after being propagated on the E-cadherin mimicking substrates, the next question was if the differentiation potency was also maintained. To evaluate differentiation potential, cells were induced toward the definitive endoderm (DE) germ layer. Differentiation was analyzed after hPSCs were propagated on alginate modified with each of the peptides, and subsequently induced to the DE stage. Figure 5.7A shows gene expression analysis of SOX17 after DE induction, which showed a strong upregulation for cells grown on HAV10 (~15000-fold) and ADT10 (~13700-fold), as compared to undifferentiated hESC controls.

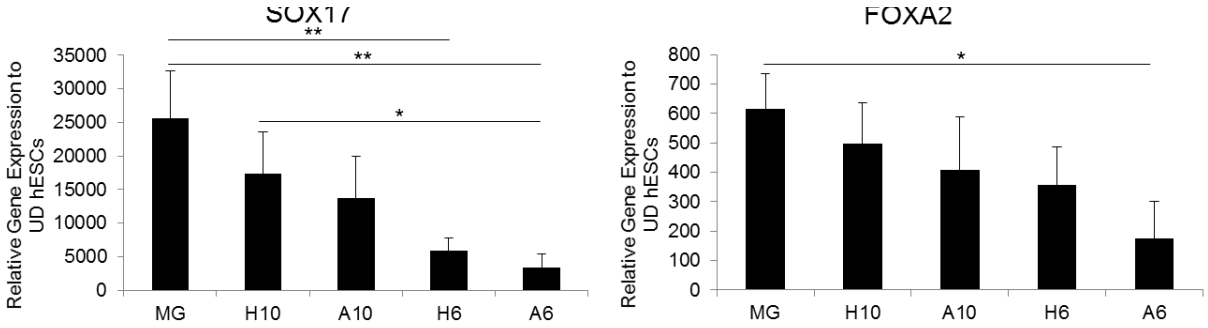

Figure 5.7. Differentiation potential of hESCs propagated on e-cadherin peptide mimicking substrates.

hPSCs were induced to the definitive endoderm stage using chemical induction. qRT-PCR was used to analyze the relative gene expression of SOX17 and FOXA2 for cell grown on each peptide conjugated hydrogel. n=3, results were considered significant if *P<0.05, **P<0.01.

Although still highly upregulated, expression of SOX17 on the shorter peptides HAV6 and ADT6 showed an upregulation of 5900 and 3400-fold respectively, compared to undifferentiated controls. While cells grown on the Matrigel controls showed a 25000-fold upregulation of SOX17, cells grown on the HAV10 and ADT10 peptide modified substrates showed no statistical difference compared to Matrigel. Likewise, gene expression analysis of FOXA2 showed a similar trend, although of a lower magnitude, with fold increases of 497, 409, 355, and 174 for HAV10, ADT10, HAV6, and ADT6, respectively. Again, however, there was no statistical difference between cells differentiated on Matrigel, as compared to HAV10 or ADT10 based substrates. These findings indicate successful induction of hESC to the DE stage, confirming cells propagated on the peptide modified substrates retained differentiation potency.

5.3.6 Cell Attachment and Pluripotency using Peptide combinations

In analysis performed thus far, specific peptide has specific advantages. For example, while ADT10 appeared to support the highest initial cell attachment, and retained the highest pluripotency's, HAV10 showed the highest expansion potential and level of differentiation. Hence, we next examined if attachment, viability, and pluripotency further improved by conjugating alginate with a combination of peptides. Thus, Alginate was conjugated with HAV10 + ADT10, HAV10 + ADT6, ADT10 + HAV6, or ADT6 + HAV6, using 50 µg/ml for each peptide. Single cell hPSCs were seeded on each substrate, and attachment and cell viability were evaluated after 1 day (Figure 5.8).

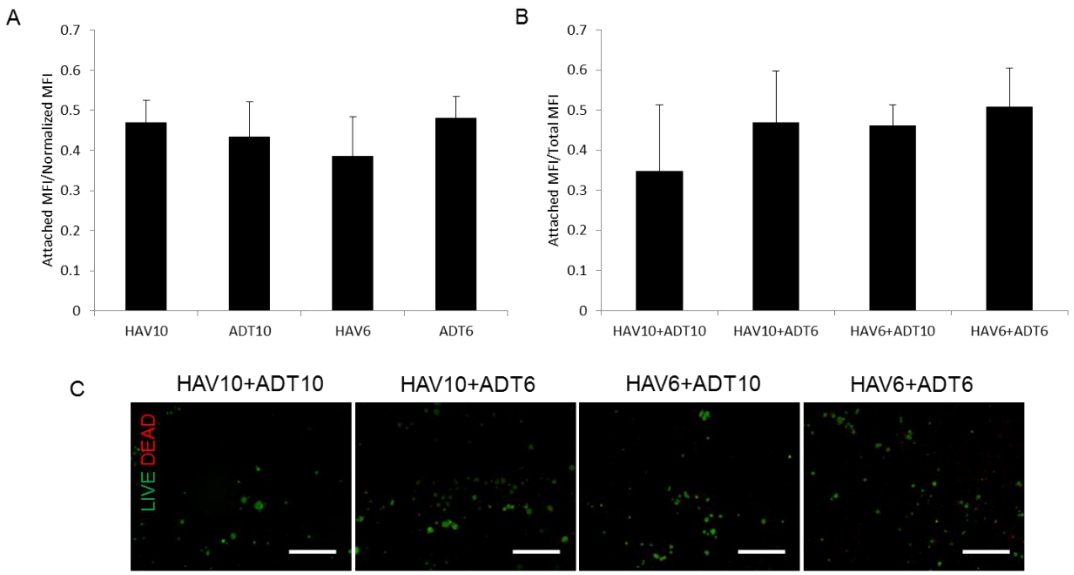

Figure 5.8. Day 1 hPSC attachment to alginate modified with HAV and ADT peptides.

(A) Day 1 attachment on alginate conjugated with 50 µg/ml of each peptide individually. (B) Day 1 attachment to alginate conjugated with combination of each peptide, each conjugated at 50 µg/ml. (C) LIVE/DEAD images of cell attached to alginate conjugated with peptide combination. Scale bar is 450 µm.

Both attachment and cell viability for each peptide combination was similar to that seen when individual peptides were conjugated alone. Specifically, cell attachment ranged from 0.38 - 0.48 % attachment for individual peptides, and similarly, cell attachment with peptide combinations ranged from 0.35 – 0.5 %. Thus, conjugation of peptide combination did not significantly alter attachment from single peptides.

While cell attachment was not changed considerably by conjugating alginate with peptide combinations, it did have an effect on hPSC pluripotency. Previously, we observed that OCT4 expression was down regulated compared to Matrigel on HAV10 substrates, while OCT4 expression was actually upregulated on and ADT10 substrates. Interestingly, when HAV10 and ADT10 were combined, OCT4 expression was upregulated by 2-fold compared to Matrigel controls (Figure 5.9).

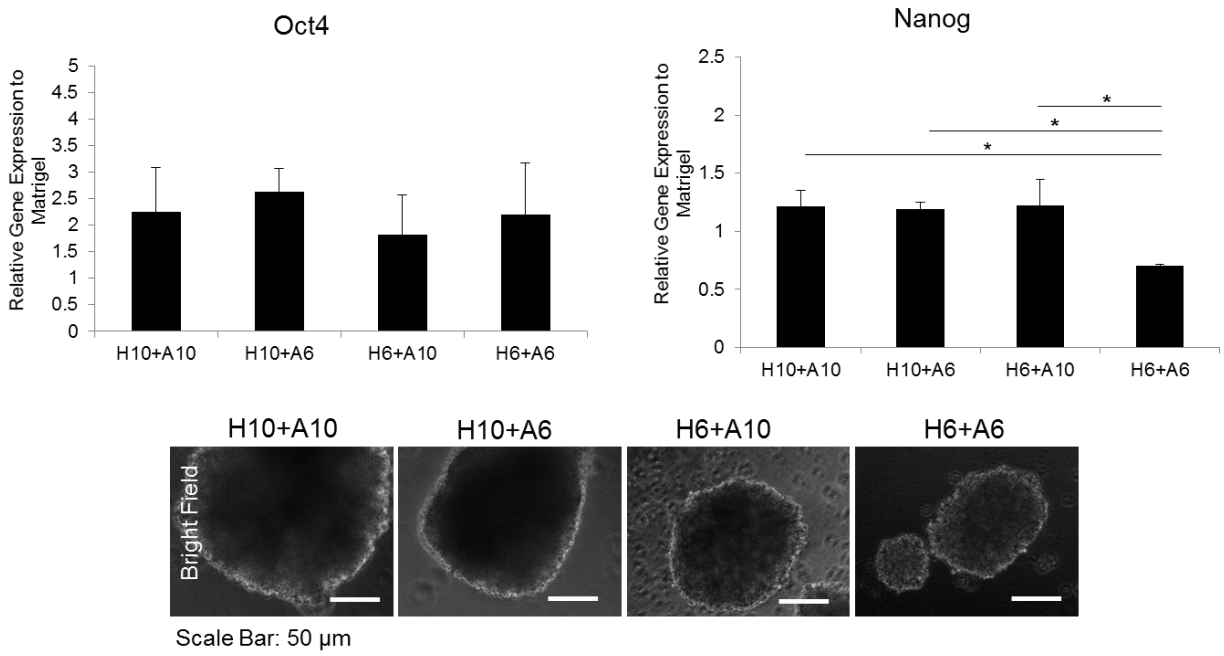

Figure 5.9. hPSC pluripotency after propagation on alginate modified with combination of HAV and ADT peptides.

All other peptide combinations showed OCT4 expression to be on par with the Matrigel controls. Similarly, each peptide combination showed Nanog expression to be on par with the Matrigel control, with the exception of the HAV6 + ADT6 conditions. When the peptides were combined during conjugation, the resulting Nanog expression was slightly down regulated, while the peptides showed a slight upregulation when conjugated individually. Taken together, while cell attachment was unaffected by combining the peptide, an increase in pluripotency was observed with some combinations.

5.4 DISCUSSION

The objective of this chapter was to incorporate synthetic peptides mimicking E-cadherin into a hydrogel substrate for the single cell culture of hPSCs. The use of a low cost synthetic peptide based substrate for hPSC culture can directly be used as a replacement for current expensive animal derived platforms, such as Matrigel. The use of E-cadherin based peptides has the potential to mitigate hPSC death occurring when these cells are cultured as single cells. This platform can then be further extended to 3D culture for biomanufacturing of hPSC in the bioreactor setting. Thus, the requirements for meeting these goals will be to develop a platform that (1) is low cost, (2) supports single hPSC attachment and viability, (3) maintains hPSC pluripotency, and (4), retains hPSC differentiation potential. In the synthesis of this platform, we have evaluated each of these criteria using 4 peptide sequences which mimic the EC1 domain of E-cadherin. We observed that each peptide supported both good initial attachment and viability, as well as hPSC propagation. While hPSCs maintained pluripotency and differentiation potential on most peptide-conjugated substrates, some dependence on peptide length and type was observed. Hence, in this chapter we have shown for the first time that E-cadherin mimicking synthetic peptides can be used for the culture and differentiation of hPSCs.

To evaluate this platform's ability to promote single cell viability, our first step was to evaluate attachment as a function of peptide type and concentration. Previous reports have shown that synthetic peptides containing the bioactive regions of ECM proteins, such as laminin and vitronectin, support good hPSC attachment and pluripotency [204, 205, 219]. Additionally, the use of the full E-cadherin protein has successfully been used to replace Matrigel for hPSC propagation and self-renewal [220]. However, it was unclear if synthetic peptides mimicking only the EC1 domain of E-cadherin could also support hPSC attachment. Our findings showed

that alginate conjugated with each of the tested peptides supported single hPSC attachment. Cell attachment increased as peptide concentration was increased and was similar for HAV10, ADT10, HAV6, and ADT6 conjugated substrates. This is in contrast to a previous report which found that E-cadherin alone did not support single hPSC attachment and clonal expansion, but required a combination of E-cadherin with ECM, in this case, laminin fragments [221]. Similarly, while not shown with hPSCs, previous work with hMSCs showed that methacrylated hyaluronic acid hydrogels conjugated with a HAV containing N-cadherin peptide supported hMSC attachment, as well as chondrogenesis [217] and osteogenesis [218]. Again, these substrates engaged cell-cell contacts through the N-cadherin peptide and cellular cadherin's, as well as integrin's through the hyaluronic acid. It is unclear whether the N-cadherin peptide alone is responsible, or if a combination with integrin is necessary. In this work, however, attachment could occur without additional ECM components, and was dependent on peptide concentration, although only a slight dependence on peptide type and length was observed.

We next evaluated whether the combined conjugation of peptides from both the bulge and groove region of the EC1 domain of E-cadherin could improve cellular attachment. Our results showed that using a combination of HAV and ADT peptides, did not result in an increase in cell attachment, as compared to single peptides. These results are similar to previous reports, which have shown that a combination of peptides from the bulge and groove region did not increase the inhibition of tight intracellular cell-cell junctions on CaCo-2 and MDCK cells, as compared to individual peptide [222, 223]. However, these studies combined the peptides by linking them together, forming a single peptide with bioactive domains from both regions. In our system, we conjugated a combination of single HAV and ADT peptides to the alginate substrate. Additionally, the previous studies required the peptides to be in solution, as opposed to being

attached to the culture surface. However, taken together, our findings, as well as the previous reports, clearly indicate that engaging both the bulge and groove region is not required to invoke a cellular response. Thus, the use of fused HAV-ADT peptides, or a combination of single HAV and ADT peptides, did not enhance peptide performance, as compared to individual HAV or ADT peptides.

E-cadherin peptides supported good initial cell attachment, however supporting long term culture and high cell expansion is also required. Cells propagated for a period of 6 days showed good viability on each peptide modified substrate, however there appeared to be little to no effect of peptide concentration on hPSC propagation. hPSC expansion potential on the peptide-modified alginate will provide insight as to how this system can perform when transitioned to large scale bioprocessing. Initial studies using Matrigel coated microcarriers achieved a 20-fold expansion of hPSCs [224, 225]. Here, we observed that hPSCs propagated on our substrate achieved an approximately 15-23-fold expansion, which was comparable to these previous studies. Interestingly, we observed that hPSC propagated on the full E-cadherin protein supported only a 10-fold expansion. Taken together, these results show that E-cadherin peptide-modified substrates support high cell attachment, proliferation and cell expansion.

While supporting cell attachment is critical in evaluating peptide performance, the long term goal of this work will be to incorporate these peptides in alginate in the 3D setting, and thus ensuring cell-peptide interaction. The evaluation of pluripotency after propagation on the E-cadherin peptide substrates is of critical importance for informing the optimal settings for future 3D platforms. Nagaoka et al. showed that hPSCs passaged and cultured as colonies on human recombinant E-cadherin substrates maintained pluripotency and self-renewal [220]. Herein however, the hPSC starting population being plated on peptide-conjugated substrates consisted

of single cells and not colonies, which is more advantageous for large scale bioprocessing. Analysis of the pluripotency genes OCT4 and Nanog showed clear differences in peptide performance, which appeared to be dependent on peptide type and length. Specifically, OCT4 and Nanog expression was down regulated 2-fold and upregulated 1.9-fold, respectively, on the HAV10 substrate. However, hPSCs propagated on the ADT10 substrates showed a 3.6 and 1.6-fold upregulation of OCT4 and Nanog, respectively. Interestingly, while no effect was seen on cell attachment, cells propagated on alginate conjugated with a combination of HAV10 and ADT10, showed an OCT4 upregulated by 2.2-fold. Thus, the addition of ADT10 appeared to rescue the pluripotency of hPSCs propagated on HAV10 alone. This indicates that while both the bulge and groove region of E-cadherin was not required for cell attachment, it may be advantageous for maintenance of hPSC pluripotency.

Maintaining pluripotency is essential for large scale bioprocessing and production of clinically relevant cells number; however, the maintenance of good differentiation potential is also required for cell therapy applications. Previously, it has been shown that an acrylate surface modified with ECM based peptides not only supported hESC self-renewal, but also supported cardiomyocyte differentiation [219]. To evaluate the differentiation potential on our E-cadherin peptide modified substrate, we evaluated hPSC germ layer induction to the DE stage after propagation on alginate conjugated with each of the E-cadherin peptides. The DE layer gives rise to a number of functional cell types, such as insulin producing cells and hepatocytes, all of which are in high demand for cellular therapy [70]. The DE gene markers SOX17 and FOXA2 were highly upregulated on each of the four substrates; however, HAV10 and ADT10-conjugated substrates showed the best performance. While cells grown on Matrigel coated TCP showed slightly higher expression of the DE markers, the level of differentiation on E-cadherin peptides

was comparable to the gold standard control. This data supports similar findings in a previous report, although in mESCs, which found that a recombinant E-cadherin substrate supported endoderm differentiation [226]. Thus, it is clear that E-cadherin peptides can also strongly support directed differentiation of hPSCs.

5.5 CONCLUSIONS

Previous reports have indicated that cell-cell contact through E-cadherin is critical for hPSC viability and pluripotency. To that end, it has also been shown that recombinant E-cadherin protein can support hPSC colony attachment, pluripotency, and differentiation. However production of recombinant human E-cadherin is highly expensive and will serve as a major bottleneck in the translation from lab scale hPSC culture to large scale biomanufacturing. In this chapter, we showed that short, inexpensive, synthetic peptides derived from E-cadherin can be used in place of the full E-cadherin protein. Peptide-modified alginate substrates supported good initial cell attachment, viability after propagation, and have an expansion potential on par with recombinant E-cadherin. More importantly, however, hPSCs cultured on this substrate maintained high pluripotency and differentiation potential. Future studies will focus on incorporating the E-cadherin peptides into alginate capsules in 3D. Peptide functionalized hydrogel capsules will provide a controlled environment for hPSC survival, propagation, and differentiation, while isolating the hPSC colonies from external stresses associated with bioreactor hydrodynamics.

6.0 OVERALL CONCLUSIONS AND FUTURE WORK

The overall goal of this work was to establish a directly transplantable 3D culture platform that would support hPSC proliferation and viability, good pancreatic differentiation, and have the capacity for immunoisolation. Having established alginate as a suitable platform for differentiation in Chapters 2-4, we further evaluated its modification to support single hPSC culture for large scale biomanufacturing applications in Chapter 5. We established that alginate could support the pancreatic differentiation of hPSCs, and then e-cadherin mimicking alginate substrates could also support single hPSC attachment, pluripotency, and differentiation. Taken together, this work shows the potential for alginate encapsulation to be a viable platform for large scale biomanufacturing of undifferentiated hPSCs, which can be directly differentiated after propagation. This has a great potential to alleviate current bottle necks in hPSC biomanufacturing for cell therapy applications

6.1 AIM 1: ALGIANTE ENCAPSULATION AS A PLATFORM FOR THE PANCREATIC DIFFERENTIATION OF HPSCS

Alginate encapsulation has been utilized for decades for the encapsulation of pancreatic islets because it supports islet viability, and can immunoisolate the encapsulated cells from the immune system post implantation [5, 12-22]. This eliminates the need for regular

immunosuppression, which ultimately leads to a more complete treatment and cure to T1D, and can provide better patient quality of life. Thus, our objective in Aim 1 (Chapter 2) was to evaluate alginate as a platform for the pancreatic differentiation of hPSCs, which then has the potential to be directly transplanted for T1D treatment. In this work, we established that while encapsulation of a predifferentiated DE population resulted in the best differentiation, the yield of viable cells upon mature differentiation was limited. However, encapsulation of undifferentiated hPSC resulted in a high cell viability, and enhanced the pancreatic differentiation of hPSC compared to the gold standard 2D Matrigel controls.

In 2014, seminal work by the Melton lab established a new pancreatic differentiation protocol for hPSCs, capable of generating mature, functional glucose responsive β cells in vitro [46]. The protocol established in our lab (Figure 2.1A) when the work in Chapter 2 was completed, was adapted from a prior protocol by D'Amour [227]. Our protocol was also capable of generating glucose responsive β cells from hPSC in vitro; however, these cells were polyhormonal, indicating immaturity. Thus, future work related to AIM 1 will be to evaluate the pancreatic differentiation protocol established by Melton, under calcium alginate encapsulation. The key finding of this differentiation protocol was the generation of glucose responsive hPSC-derived islets in vitro. Since we perceived a low level of glucose responsiveness using our differentiation protocol with alginate encapsulation, which we had not achieved in 2D culture, we can anticipate the observation of enhanced performance when using this updated differentiation protocol. While it will be important to demonstrate physiological levels of glucose responsiveness in vitro, the next step will be implantation of alginate encapsulated hPSC-derived islets in a mouse model.

In Aim 1, we have demonstrated that alginate encapsulation can improve the pancreatic differentiation of hPSCs, compared to 2D controls. In addition to our work, it has also been shown that alginate encapsulation enhanced the differentiation of hPSCs to midbrain dopamine neurons [55], and hESC-derived male germ-like cells [228], compared to traditional 2D culture. Additional future work for this Aim could include applying alginate encapsulation as a differentiation platform for other tissues-based functional cell types, such as thymus, liver, kidney, intestinal, or lung cells, to generate desirable cells for cell replacement therapy.

6.2 AIM 2: THE EFFECT OF ALGIANTE CAPSULE PROPERTIES ON THE PANCREATIC DIFFRENTIATION OF HPSCS

Stem cell differentiation is traditionally achieved by addition of soluble chemical factors in a stage wise fashion, mimicking stages of in vivo development. These chemical factors, including proteins and small molecules, modulate key signaling pathways, resulting in stem cell specification to the desired lineage. However, during embryonic development, both soluble and insoluble cues drive development and lineage specification [229]. Thus, countless studies over the last decade have shown that insoluble differentiation cues can also strongly influence stem cell differentiation in vitro [57, 114-120] . These insoluble cues include substrates stiffness, cell-cell interactions, and cell-ECM interactions. In Aim 1 of this work, we clearly established that the pancreatic differentiation of hPSCs was significantly improved when done under alginate encapsulation, as compared to TCP. In Aim 2, we further investigated this by varying alginate crosslinking, and thus the resulting stiffness, and investigated how directed pancreatic differentiation was influenced. Interestingly, we observed a biphasic response to differentiation

as stiffness was increased, depending on the stage of differentiation. An increase in alginate stiffness supported DE stage differentiation; however, it suppressed differentiation at the PP stage. Signaling analysis identified that increased alginate stiffness enhanced TGFβ signaling, which is responsible for DE specification, but is also detrimental during downstream PP stage differentiation.

The above results were for a single controlled perturbation; however, we further wanted to evaluate the effects of multiple simultaneous perturbations on the pancreatic differentiation of hPSCs. To enable this, in the second part of Aim 2 (Chapter 4) we designed a 3D alginate array platform for the high throughput investigation of multiple simultaneous non-soluble differentiation cues on the directed pancreatic differentiation of hPSCs. We again varied alginate stiffness by varying crosslinking concentration, but in Chapter 4 we introduced the effect of culture configuration (cell-cell contact) by encapsulating cells as single cells or as preformed aggregates. Using statistical analysis, we identified that while cell proliferation and differentiation showed a slight dependence on alginate stiffness, they were more strongly influenced by culture configuration during directed differentiation. These studies are the first to demonstrate, to the best of our knowledge, the importance of insoluble differentiation cues during the pancreatic differentiation of hPSC. The general consensus in the field of hPSC differentiation is that the effect of insoluble cues is secondary to soluble cues, because key signaling pathways are being directly modulated by the added soluble factors. However, in this work, we have clearly shown that the insoluble differentiation cues can enhance the effect of soluble cues during pancreatic differentiation of hPSCs. Encapsulation offers clear advantages for implantation and large scale bioprocessing, and thus, balancing the effects of insoluble and soluble cues to identify synergistic ranges of both will be critically important.

For future work, it will be important to include additional insoluble cues utilizing the alginate array platform. Specifically, it has been previously shown that ECM proteins can strongly influence stem cell differentiation [151-153]. In our own lab, we have seen that the pancreatic differentiation of hPSCs was responsive to different organ derived ECM proteins (liver, heart, or pancreas). Evaluating the response of encapsulated hPSCs while varying the alginate stiffness, culture configuration, and ECM proteins in the alginate, will further inform optimal hydrogel setting to achieve optimal differentiation. Additionally, the establishment of the Melton protocol was developed using hPSC aggregates in suspension culture. While this platform included cell-cell contact, it will be interesting to determine if the current "gold-standard" differentiation protocols by the Melton group can be further optimized if done in conjunction with multiple combinations of insoluble cues. This will yield the development of an effective in vitro differentiation protocol that more closely mimics pancreatic development, leading to potential higher yields of differentiated cells, and better functionality for cell therapy and drug testing. The alginate array platform developed in this work can be used to simultaneously vary both physical and chemicals differentiation factors.

Additional future work for this Aim should include evaluating the effect of varying alginate composition and concentration, as well as cation type. Previous reports have shown that varying alginate composition, specifically G/M ratio [31], or concentration [61], can influence cell response. Although it has been established that increasing the G content of alginate, or alginate concentration will results in an increase in alginate stiffness after crosslinking, it will be interesting to decouple alginate stiffness and cation concentration. Specifically, if the same hydrogel stiffness is achieved separately by varying alginate composition/concentration, and keeping cation concentration constant, or keeping alginate composition/concentration constant

and increasing cation concentration, will the effect on proliferation and differentiation of encapsulated cells be the same. Additionally, in chapter 3 of this work, barium was chosen because it produces a more robust gel, which will maintain hydrogel integrity better than calcium alginate hydrogel after long term culture. However, barium has been shown to be toxic in the body, and thus minimizing barium concentration could improve future cell-therapy applicability. It has previously been shown that alginate cross linked with 50 mM $CaCl_2$, in combination with a lower concentration of 1 mM $BaCl_2$ supported islet encapsulation [132]. It will thus be interesting to evaluate if a combination of calcium and barium can be used to achieve optimal hydrogel stiffness for the pancreatic differentiation of hPSCs, while minimizing barium concentration.

Finally, in Aim 2 we have focused on biomaterial properties which best support the pancreatic differentiation of hPSCs. However, in this work we were unable to further evaluate the in vivo applicability or biocompatibility of the selected optimal alginate stiffness. Vegas et al. have recently shown that hPSC-derived β-cells encapsulated in intriazole–thiomorpholine dioxide modified alginate, crosslinked with $BaCl_2$, showed good biocompatibility and long-term glycemic control after implantation [230]. The hPSC-derived β-cells in this study were encapsulated after differentiation, and were not differentiated under encapsulation. However, our goal is to use alginate encapsulation as a differentiation platform, which is directly transplantable. The Vegas et al. study identified that barium alginate can support cell functionality and in vivo biocompatibility. However, as the alginate encapsulation parameters are varied to support differentiation, the effect on post implantation functionality and biocompatibility should be investigated. Specifically, it will be important to evaluate a range of

supportive alginate compositions, and balance which parameters support both good pancreatic differentiation, but also long term viability, functionality, and biocompatibility post implantation.

6.3 AIM3: PEPTIDE MODIFIED ALGINATE FOR THE PROPAGATION AND DIFFERENTATION OF HESC

Clinical translation of hPSC-derived functional cells requires the use of large scale culture techniques to meet clinically relevant cell numbers. The use of 3D cell culture techniques, in combination with bioreactors, has the potential to satisfy future biomanufacturing needs for hPSC therapy to achieve commercial success. However, current lab scale technologies being utilized for hPSC propagation require cells to be passaged as colonies to maintain cell-cell contact, and employ the use of highly expensive Matrigel to support cell attachment and pluripotency. While recent work has focused on developing xeno-free platforms by replacing Matrigel with synthetic human recombinant proteins, these techniques are still highly expensive. The use of short synthetic peptides which mimic the bioactive region of key ECM proteins have been shown to support hPSC propagation and self-renewal when cultured as colonies. However, for large scale bioprocessing, the use of hPSCs in a single cell format is highly advantageous. Additionally, treatment with ROCK inhibitor will support upwards of 50% viability after dissociation, but there is a significant loss of the starting population, severely limiting the commercial applicability of hPSC-based cell therapy. In the final Aim of this work (Chapter 5), our goal was thus to develop a low cost, xeno-free substrate, which can support single hPSC culture. Dissociation induced apoptosis is triggered by loss of cell-cell e-cadherin binding, thus we developed an alginate hydrogel based substrate, conjugated with synthetic e-cadherin-based

peptides which mimic cell-cell contact. In Chapter 5, we demonstrated that the peptide modified alginate supported cell attachment in a concentration dependent manner, propagation, and high expansion potential. Additionally, after propagation on the developed substrate, hPSCs retained good pluripotency and differentiation potency.

While the ultimate goal of Aim 3 was to investigate peptide performance to inform optimal parameters for use in 3D, the developed 2D platform also has commercial potential. Successful translation from the lab scale protocols to the clinic requires that low cost xeno-free platforms are used from the initial conception of the work. Merely switching from Matrigel to a xeno-free platform immediately prior to clinical testing is problematic, as the use of animal derived products may cause cross contamination with animal pathogens [231]. Specifically, the efficiency of maintaining hPSC pluripotency and differentiation cannot be assumed to be equivalent on one substrate, versus another. The culture and development of hPSC differentiation protocols must be done considering the supporting substrate from the start, especially when the ultimate goal is transitioning from the lab setting to large scale bioprocessing. Thus, a low cost xeno-free platform for lab scale research, which can support single cell culture, is in high demand. For future work, additional analysis of hPSC expansion and maintenance of pluripotency over multiple serial passages will be required. Additionally, herein we have tested differentiation potency using simple DE germ layer commitment. Further in depth analysis, not only to mesoderm and ectoderm germ layers, but also to functional mature cell types, will be required for this platform to compete with Matrigel or recombinant protein-based substrates.

Furthermore, although the work in Aim 3 focused on evaluation of e-cadherin peptides in 2D, our ultimate goal is to develop a 3D platform for large scale biomanufacturing. As mentioned previously, current large scale biomanufacturing techniques for hPSCs primarily

includes cells grown on microcarriers, or as cellular aggregates, in the bioreactor setting. However, both of these approaches have significant draw backs, including susceptibility to cell over-aggregation and hydrodynamic shear forces imparted by the bioreactor. Thus, additional future work for Aim 3 should focus on using the findings in Chapter 5 to inform optimal parameters for the 3D peptide conjugated alginate platform. Alginate encapsulation will serve to protect the hPSCs from over-aggregation and hydrodynamic shear forces, and inclusion of the e-cadherin peptide could significantly improve single cell viability, and thus promote cellular expansion potential. Determination of optimal parameters should include peptide sequence and length, as well as concentration. Initial work should focus on peptide conjugation to alginate in solution prior to hydrogel formation, including material characterization [206]. It should also focus on the in vitro performance on hPSC viability, expansion, pluripotency, and differentiation, under encapsulation in the developed hydrogel. Upon establishment of supporting each of these at the lab scale, the next step will be to incorporate the use of a bioreactor.

Putatively, although alginate encapsulation will protect cells from over aggregation and hydrodynamic shear forces, the alginate parameters which support hPSC viability and expansion will need to be balanced with those that support capsule robustness in the bioreactor. Thus, future work concerning the use of peptide modified alginate in the bioreactor should determine alginate G/M ratio, cation chemistry and cation concentration supporting single cell viability and clonal expansion of encapsulated hPSCs. The objective should be to design alginate capsules that are suitable for withstanding the stress and hydrodynamic perturbations inherent in scaled up stirred suspension culture system. This will result in identification of key biophysical parameters necessary for alginate capsule structural stability in such systems.

Taken together in totality, the findings described in this dissertation represent a significant leap forward in the understanding of the application of biomaterial based hPSC propagation and differentiation platforms. We have shown alginate encapsulation supports strong hPSC pancreatic differentiation, but is highly sensitive to biomaterials parameters and culture configuration. The results of this dissertation thus strongly indicate that optimal parameters for hPSCs must be balanced with those parameters which support large-scale bioprocessing for cell therapy applications.

BIBLIOGRAPHY

[1] Daneman, D., Type 1 diabetes. The Lancet, 2006. **367**(9513): p. 847-858.

[2] Shapiro, A.M.J., et al., Islet Transplantation in Seven Patients with Type 1 Diabetes Mellitus Using a Glucocorticoid-Free Immunosuppressive Regimen. New England Journal of Medicine, 2000. **343**(4): p. 230-238.

[3] Efrat, S. and H.A. Russ, Making beta cells from adult tissues. Trends in endocrinology and metabolism: TEM, 2012. **23**(6): p. 278-85.

[4] O'Sullivan, E.S., et al., Rat islet cell aggregates are superior to islets for transplantation in microcapsules. Diabetologia, 2010. **53**(5): p. 937-45.

[5] Dufrane, D., et al., Six-month survival of microencapsulated pig islets and alginate biocompatibility in primates: proof of concept. Transplantation, 2006. **81**(9): p. 1345-53.

[6] Lim, F. and A.M. Sun, Microencapsulated Islets as Bioartificial Endocrine Pancreas. Science, 1980. **210**(4472): p. 908-910.

[7] Scharp, D.W. and P. Marchetti, Encapsulated islets for diabetes therapy: History, current progress, and critical issues requiring solution. Advanced Drug Delivery Reviews, 2014. **67-68**: p. 35-73.

[8] Beck, J., et al., Islet encapsulation: strategies to enhance islet cell functions. Tissue engineering, 2007. **13**(3): p. 589-99.

[9] Lee, K.Y. and D.J. Mooney, Alginate: Properties and biomedical applications. Progress in Polymer Science, 2012. **37**(1): p. 106-126.

[10] Wilson, J.L. and T.C. McDevitt, Stem cell microencapsulation for phenotypic control, bioprocessing, and transplantation. Biotechnology and bioengineering, 2013. **110**(3): p. 667-82.

[11] S, M., S. Ja, and S. M, Regenerative Medicine and Tissue Engineering for the Treatment of Diabetes, in Tissue Engineering for Tissue and Organ Regeneration, D. Eberli, Editor 2011, InTech: Rijeka. p. Ch. 19.

[12] O'Sullivan, E., et al., Rat islet cell aggregates are superior to islets for transplantation in microcapsules. Diabetologia, 2010. **53**(5): p. 937-945.

[13] Lim, F. and A. Sun, Microencapsulated islets as bioartificial endocrine pancreas. Science, 1980. **210**(4472): p. 908-910.

[14] Oshea, G.M. and A.M. Sun, Encapsulation of Rat Islets of Langerhans Prolongs Xenograft Survival in Diabetic Mice. Diabetes, 1986. **35**: p. A82-A82.

[15] Duvivier-Kali, V.F., et al., Complete protection of islets against allorejection and autoimmunity by a simple barium-alginate membrane. Diabetes, 2001. **50**(8): p. 1698-705.

[16] Hoesli, C.A., et al., Reversal of diabetes by βTC3 cells encapsulated in alginate beads generated by emulsion and internal gelation. Journal of Biomedical Materials Research Part B: Applied Biomaterials, 2012. **100B**(4): p. 1017-1028.

[17] Scharp, D.W. and P. Marchetti, Encapsulated islets for diabetes therapy: History, current progress, and critical issues requiring solution. Advanced Drug Delivery Reviews, 2013(0).

[18] Steele, J.A.M., et al., Therapeutic cell encapsulation techniques and applications in diabetes. Advanced Drug Delivery Reviews, 2013(0).

[19] Tuch, B.E., et al., Safety and Viability of Microencapsulated Human Islets Transplanted Into Diabetic Humans. Diabetes care, 2009. **32**(10): p. 1887-1889.

[20] Jacobs-Tulleneers-Thevissen, D., et al., Sustained function of alginate-encapsulated human islet cell implants in the peritoneal cavity of mice leading to a pilot study in a type 1 diabetic patient. Diabetologia, 2013. **56**(7): p. 1605-1614.

[21] Li, N., et al., Engineering islet for improved performance by optimized reaggregation in alginate gel beads. Biotechnology and applied biochemistry, 2016.

[22] Lacy, P.E., et al., Maintenance of normoglycemia in diabetic mice by subcutaneous xenografts of encapsulated islets. Science, 1991. **254**(5039): p. 1782-4.

[23] Nishimura, M., et al., Effects of encapsulated porcine islets on glucose and C-peptide concentrations in diabetic nude mice 6 months after intraperitoneal transplantation. Xenotransplantation, 2017.

[24] Maiti, S., et al., Adipic acid dihydrazide treated partially oxidized alginate beads for sustained oral delivery of flurbiprofen. Pharmaceutical Development and Technology, 2009. **14**(5): p. 461-470.

[25] Bouhadir, K.H., E. Alsberg, and D.J. Mooney, Hydrogels for combination delivery of antineoplastic agents. Biomaterials, 2001. **22**(19): p. 2625-2633.

[26] Silva, E.A. and D.J. Mooney, Effects of VEGF temporal and spatial presentation on angiogenesis. Biomaterials, 2010. **31**(6): p. 1235-1241.

[27] Chan, A.W. and R.J. Neufeld, Tuneable semi-synthetic network alginate for absorptive encapsulation and controlled release of protein therapeutics. Biomaterials, 2010. **31**(34): p. 9040-9047.

[28] Balakrishnan, B., et al., Evaluation of the effect of incorporation of dibutyryl cyclic adenosine monophosphate in an in situ-forming hydrogel wound dressing based on oxidized alginate and gelatin. Biomaterials, 2006. **27**(8): p. 1355-1361.

[29] Rabbany, S.Y., et al., Continuous Delivery of Stromal Cell-Derived Factor-1 From Alginate Scaffolds Accelerates Wound Healing. Cell Transplantation, 2010. **19**(4): p. 399-408.

[30] Huang, X., et al., Microenvironment of alginate-based microcapsules for cell culture and tissue engineering. Journal of bioscience and bioengineering, 2012. **114**(1): p. 1-8.

[31] Wilson, J.L., et al., Alginate encapsulation parameters influence the differentiation of microencapsulated embryonic stem cell aggregates. Biotechnology and bioengineering, 2014. **111**(3): p. 618-31.

[32] Zimmermann, H., S.G. Shirley, and U. Zimmermann, Alginate-based encapsulation of cells: past, present, and future. Current diabetes reports, 2007. **7**(4): p. 314-20.

[33] Stabler, C., et al., The effects of alginate composition on encapsulated betaTC3 cells. Biomaterials, 2001. **22**(11): p. 1301-10.

[34] Siti-Ismail, N., et al., The benefit of human embryonic stem cell encapsulation for prolonged feeder-free maintenance. Biomaterials, 2008. **29**(29): p. 3946-52.

[35] Bohari, S.P., D.W. Hukins, and L.M. Grover, Effect of calcium alginate concentration on viability and proliferation of encapsulated fibroblasts. Bio-medical materials and engineering, 2011. **21**(3): p. 159-70.

[36] Morch, Y.A., et al., Effect of Ca2+, Ba2+, and Sr2+ on alginate microbeads. Biomacromolecules, 2006. **7**(5): p. 1471-80.

[37] Chan, E.S., et al., Effect of formulation of alginate beads on their mechanical behavior and stiffness. Particuology, 2011. **9**(3): p. 228-234.

[38] Balamurugan, A.N., et al., Prospective and challenges of islet transplantation for the therapy of autoimmune diabetes. Pancreas, 2006. **32**(3): p. 231-43.

[39] Bradley, J.A., E.M. Bolton, and R.A. Pedersen, Stem cell medicine encounters the immune system. Nature Reviews Immunology, 2002. **2**(11): p. 859-871.

[40] Segev, H., et al., Differentiation of Human Embryonic Stem Cells into Insulin-Producing Clusters. STEM CELLS, 2004. **22**(3): p. 265-274.

[41] Xu, X., et al., Endoderm and Pancreatic Islet Lineage Differentiation from Human Embryonic Stem Cells. Cloning and Stem Cells, 2006. **8**(2): p. 96-107.

[42] Baharvand, H., et al., Generation of insulin-secreting cells from human embryonic stem cells. Development, Growth & Differentiation, 2006. **48**(5): p. 323-332.

[43] D'Amour, K.A., et al., Production of pancreatic hormone-expressing endocrine cells from human embryonic stem cells. Nat Biotech, 2006. **24**(11): p. 1392-1401.

[44] Jaramillo, M., et al., Potential for pancreatic maturation of differentiating human embryonic stem cells is sensitive to the specific pathway of definitive endoderm commitment. PloS one, 2014. **9**(4): p. e94307.

[45] Jaramillo, M., et al., Endothelial Cells Mediate Islet-Specific Maturation of Human Embryonic Stem Cell-Derived Pancreatic Progenitor Cells. Tissue engineering. Part A, 2014.

[46] Pagliuca, F.W., et al., Generation of functional human pancreatic beta cells in vitro. Cell, 2014. **159**(2): p. 428-39.

[47] Rezania, A., et al., Reversal of diabetes with insulin-producing cells derived in vitro from human pluripotent stem cells. Nature Biotechnology, 2014. **32**(11): p. 1121-33.

[48] Cogger, K. and M.C. Nostro, Recent advances in cell replacement therapies for the treatment of type 1 diabetes. Endocrinology, 2015. **156**(1): p. 8-15.

[49] Maguire, T., et al., Alginate-PLL microencapsulation: Effect on the differentiation of embryonic stem cells into hepatocytes. Biotechnology and Bioengineering, 2006. **93**(3): p. 581-591.

[50] Li, L., et al., Neural lineage differentiation of embryonic stem cells within alginate microbeads. Biomaterials, 2011. **32**(20): p. 4489-4497.

[51] Wang, N., et al., Alginate encapsulation technology supports embryonic stem cells differentiation into insulin-producing cells. Journal of Biotechnology, 2009. **144**(4): p. 304-312.

[52] Siti-Ismail, N., et al., The benefit of human embryonic stem cell encapsulation for prolonged feeder-free maintenance. Biomaterials, 2008. **29**(29): p. 3946-3952.

[53] Dean, S.K., et al., Differentiation of Encapsulated Embryonic Stem Cells After Transplantation. Transplantation, 2006. **82**(9): p. 1175-1184 10.1097/01.tp.0000239518.23354.64.

[54] Chayosumrit, M., B. Tuch, and K. Sidhu, Alginate microcapsule for propagation and directed differentiation of hESCs to definitive endoderm. Biomaterials, 2010. **31**(3): p. 505-514.

[55] Kim, J., P. Sachdev, and K. Sidhu, Alginate microcapsule as a 3D platform for the efficient differentiation of human embryonic stem cells to dopamine neurons. Stem Cell Research, 2013. **11**(3): p. 978-989.

[56] Hunt, N.C., et al., 3D culture of human pluripotent stem cells in RGD-alginate hydrogel improves retinal tissue development. Acta biomaterialia, 2017. **49**: p. 329-343.

[57] Engler, A.J., et al., Matrix elasticity directs stem cell lineage specification. Cell, 2006. **126**(4): p. 677-89.

[58] Zoldan, J., et al., The influence of scaffold elasticity on germ layer specification of human embryonic stem cells. Biomaterials, 2011. **32**(36): p. 9612-21.

[59] Discher, D.E., D.J. Mooney, and P.W. Zandstra, Growth factors, matrices, and forces combine and control stem cells. Science, 2009. **324**(5935): p. 1673-7.

[60] Higuchi, A., et al., Physical cues of cell culture materials lead the direction of differentiation lineages of pluripotent stem cells. Journal of Materials Chemistry B, 2015. **3**(41): p. 8032-8058.

[61] Lee, B.H., B. Li, and S.A. Guelcher, Gel microstructure regulates proliferation and differentiation of MC3T3-E1 cells encapsulated in alginate beads. Acta biomaterialia, 2012. **8**(5): p. 1693-702.

[62] Banerjee, A., et al., The influence of hydrogel modulus on the proliferation and differentiation of encapsulated neural stem cells. Biomaterials, 2009. **30**(27): p. 4695-4699.

[63] Strand, B.L., A.E. Coron, and G. Skjak-Braek, Current and Future Perspectives on Alginate Encapsulated Pancreatic Islet. Stem cells translational medicine, 2017. **6**(4): p. 1053-1058.

[64] Robinton, D.A. and G.Q. Daley, The promise of induced pluripotent stem cells in research and therapy. Nature, 2012. **481**(7381): p. 295-305.

[65] Kriks, S., et al., Dopamine neurons derived from human ES cells efficiently engraft in animal models of Parkinson's disease. Nature, 2011. **480**(7378): p. 547-51.

[66] Chong, J.J., et al., Human embryonic-stem-cell-derived cardiomyocytes regenerate non-human primate hearts. Nature, 2014. **510**(7504): p. 273-7.

[67] Maruotti, J., et al., Small-molecule-directed, efficient generation of retinal pigment epithelium from human pluripotent stem cells. Proceedings of the National Academy of Sciences of the United States of America, 2015. **112**(35): p. 10950-5.

[68] Rodin, S., et al., Clonal culturing of human embryonic stem cells on laminin-521/E-cadherin matrix in defined and xeno-free environment. Nature communications, 2014. **5**: p. 3195.

[69] Braam, S.R., et al., Recombinant vitronectin is a functionally defined substrate that supports human embryonic stem cell self-renewal via alpha V beta 5 integrin. Stem Cells, 2008. **26**(9): p. 2257-2265.

[70] Jenkins, M.J. and S.S. Farid, Human pluripotent stem cell-derived products: advances towards robust, scalable and cost-effective manufacturing strategies. Biotechnology journal, 2015. **10**(1): p. 83-95.

[71] Simaria, A.S., et al., Allogeneic cell therapy bioprocess economics and optimization: single-use cell expansion technologies. Biotechnology and bioengineering, 2014. **111**(1): p. 69-83.

[72] Want, A.J., et al., Large-scale expansion and exploitation of pluripotent stem cells for regenerative medicine purposes: beyond the T flask. Regenerative medicine, 2012. **7**(1): p. 71-84.

[73] Oh, S.K.W., et al., Long-term microcarrier suspension cultures of human embryonic stem cells. Stem cell research, 2009. **2**(3): p. 219-230.

[74] Gerecht-Nir, S., S. Cohen, and J. Itskovitz-Eldor, Bioreactor cultivation enhances the efficiency of human embryoid body (hEB) formation and differentiation. Biotechnology and bioengineering, 2004. **86**(5): p. 493-502.

[75] Abbasalizadeh, S. and H. Baharvand, Technological progress and challenges towards cGMP manufacturing of human pluripotent stem cells based therapeutic products for allogeneic and autologous cell therapies. Biotechnology Advances, 2013. **31**(8): p. 1600-1623.

[76] Lock, L.T. and E.S. Tzanakakis, Expansion and Differentiation of Human Embryonic Stem Cells to Endoderm Progeny in a Microcarrier Stirred-Suspension Culture. Tissue Engineering Part A, 2009. **15**(8): p. 2051-2063.

[77] Fridley, K.M., M.A. Kinney, and T.C. McDevitt, Hydrodynamic modulation of pluripotent stem cells. Stem Cell Research & Therapy, 2012. **3**.

[78] Watanabe, K., et al., A ROCK inhibitor permits survival of dissociated human embryonic stem cells. Nat Biotechnol, 2007. **25**(6): p. 681-6.

[79] Li, L., S.A. Bennett, and L. Wang, Role of E-cadherin and other cell adhesion molecules in survival and differentiation of human pluripotent stem cells. Cell Adh Migr, 2012. **6**(1): p. 59-70.

[80] Lanza, R.P., et al., Transplantation of encapsulated canine islets into spontaneously diabetic BB/Wor rats without immunosuppression. Endocrinology, 1992. **131**(2): p. 637-42.

[81] O'Shea, G.M., M.F.A. Goosen, and A.M. Sun, Prolonged survival of transplanted islets of Langerhans encapsulated in a biocompatible membrane. Biochimica et Biophysica Acta (BBA) - Molecular Cell Research, 1984. **804**(1): p. 133-136.

[82] Maki, T., et al., Treatment of Diabetes by Xenogeneic Islets Without Immunosuppression: Use of a Vascularized Bioartificial Pancreas. Diabetes, 1996. **45**(3): p. 342-347.

[83] Iwata, H., et al., Evaluation of Microencapsulated Islets in Agarose-Gel as Bioartificial Pancreas by Studies of Hormone-Secretion in Culture and by Xenotransplantation. Diabetes, 1989. **38**: p. 224-225.

[84] Leung, A., et al., Tissue transplantation by stealth—Coherent alginate microcapsules for immunoisolation. Biochemical Engineering Journal, 2010. **48**(3): p. 337-347.

[85] Shen, F., et al., Mechanically enhanced microcapsules for cellular gene therapy. Journal of biomedical materials research. Part B, Applied biomaterials, 2009. **90**(1): p. 350-61.

[86] Hillberg, A.L., et al., Improving alginate-poly-L-ornithine-alginate capsule biocompatibility through genipin crosslinking. Journal of biomedical materials research. Part B, Applied biomaterials, 2013. **101**(2): p. 258-68.

[87] Jaramillo, M. and I. Banerjee, Endothelial cell co-culture mediates maturation of human embryonic stem cell to pancreatic insulin producing cells in a directed differentiation approach. Journal of visualized experiments : JoVE, 2012(61).

[88] Watanabe, K., et al., A ROCK inhibitor permits survival of dissociated human embryonic stem cells. Nat Biotech, 2007. **25**(6): p. 681-686.

[89] Heiligenstein, S., et al., In vitro and in vivo characterization of nonbiomedical- and biomedical-grade alginates for articular chondrocyte transplantation. Tissue engineering. Part C, Methods, 2011. **17**(8): p. 829-42.

[90] Thomas, F.T., et al., Anoikis, extracellular matrix, and apoptosis factors in isolated cell transplantation. Surgery, 1999. **126**(2): p. 299-304.

[91] Rezania, A., et al., Maturation of human embryonic stem cell-derived pancreatic progenitors into functional islets capable of treating pre-existing diabetes in mice. Diabetes, 2012. **61**(8): p. 2016-29.

[92] Bruin, J.E., et al., Maturation and function of human embryonic stem cell-derived pancreatic progenitors in macroencapsulation devices following transplant into mice. Diabetologia, 2013. **56**(9): p. 1987-98.

[93] Cozar-Castellano, I., et al., Molecular Control of Cell Cycle Progression in the Pancreatic β-Cell. Endocrine Reviews, 2006. **27**(4): p. 356-370.

[94] Tuch, B.E., T.C. Hughes, and M.D. Evans, Encapsulated pancreatic progenitors derived from human embryonic stem cells as a therapy for insulin-dependent diabetes. Diabetes/metabolism research and reviews, 2011. **27**(8): p. 928-32.

[95] Martín, F., et al., Mechanisms of glucose hypersensitivity in beta-cells from normoglycemic, partially pancreatectomized mice. Diabetes, 1999. **48**(10): p. 1954-1961.

[96] Ungrin, M.D., et al., Reproducible, ultra high-throughput formation of multicellular organization from single cell suspension-derived human embryonic stem cell aggregates. Plos One, 2008. **3**(2): p. e1565.

[97] Nair, R., et al., Gene Expression Signatures of Extracellular Matrix and Growth Factors during Embryonic Stem Cell Differentiation. PLoS ONE, 2012. **7**(10): p. e42580.

[98] Brafman, D.A., et al., Regulation of endodermal differentiation of human embryonic stem cells through integrin-ECM interactions. Cell death and differentiation, 2013. **20**(3): p. 369-81.

[99] Jones, L.E., et al., Comprehensive analysis of matrix metalloproteinase and tissue inhibitor expression in pancreatic cancer: increased expression of matrix metalloproteinase-7 predicts poor survival. Clinical cancer research : an official journal of the American Association for Cancer Research, 2004. **10**(8): p. 2832-45.

[100] Singh, A.M., et al., Signaling Network Crosstalk in Human Pluripotent Cells: A Smad2/3-Regulated Switch that Controls the Balance between Self-Renewal and Differentiation. Cell Stem Cell, 2012. **10**(3): p. 312-326.

[101] Conery, A.R., et al., Akt interacts directly with Smad3 to regulate the sensitivity to TGF-beta-induced apoptosis. Nature Cell Biology, 2004. **6**(4): p. 366-372.

[102] Remy, I., A. Montmarquette, and S.W. Michnick, PKB/Akt modulates TGF-beta signalling through a direct interaction with Smad3. Nature Cell Biology, 2004. **6**(4): p. 358-365.

[103] Richardson, T., P.N. Kumta, and I. Banerjee, Alginate Encapsulation of Human Embryonic Stem Cells to Enhance Directed Differentiation to Pancreatic Islet-Like Cells. Tissue engineering. Part A, 2014.

[104] Darrabie, M.D., W.F. Kendall, and E.C. Opara, Effect of alginate composition and gelling cation on microbead swelling. Journal of microencapsulation, 2006. **23**(6): p. 613-21.

[105] Wang, X.W. and H.G. Spencer, Calcium alginate gels: Formation and stability in the presence of an inert electrolyte. Polymer, 1998. **39**(13): p. 2759-2764.

[106] Schneider, S., et al., Intraportal transplantation of allogenic pancreatic islets encapsulated in barium alginate beads in diabetic rats. Artificial organs, 2003. **27**(11): p. 1053-6.

[107] Safley, S.A., et al., Biocompatibility and immune acceptance of adult porcine islets transplanted intraperitoneally in diabetic NOD mice in calcium alginate poly-L-lysine microcapsules versus barium alginate microcapsules without poly-L-lysine. Journal of diabetes science and technology, 2008. **2**(5): p. 760-7.

[108] Veiseh, O., et al., Size- and shape-dependent foreign body immune response to materials implanted in rodents and non-human primates. Nature materials, 2015. **14**(6): p. 643-51.

[109] Herrero, E.P., E.M. Del Valle, and M.A. Galan, Immobilization of mesenchymal stem cells and monocytes in biocompatible microcapsules to cell therapy. Biotechnology progress, 2007. **23**(4): p. 940-5.

[110] Penolazzi, L., et al., Encapsulation of mesenchymal stem cells from Wharton's jelly in alginate microbeads. Tissue engineering. Part C, Methods, 2010. **16**(1): p. 141-55.

[111] Gaetani, P., et al., Adipose-derived stem cell therapy for intervertebral disc regeneration: an in vitro reconstructed tissue in alginate capsules. Tissue engineering. Part A, 2008. **14**(8): p. 1415-23.

[112] Estes, B.T., et al., Isolation of adipose-derived stem cells and their induction to a chondrogenic phenotype. Nature Protocols, 2010. **5**(7): p. 1294-1311.

[113] Dean, S.K., et al., Differentiation of encapsulated embryonic stem cells after transplantation. Transplantation, 2006. **82**(9): p. 1175-84.

[114] Keung, A.J., et al., Soft microenvironments promote the early neurogenic differentiation but not self-renewal of human pluripotent stem cells. Integrative biology : quantitative biosciences from nano to macro, 2012. **4**(9): p. 1049-58.

[115] Eroshenko, N., et al., Effect of substrate stiffness on early human embryonic stem cell differentiation. Journal of biological engineering, 2013. **7**(1): p. 7.

[116] Hazeltine, L.B., et al., Temporal impact of substrate mechanics on differentiation of human embryonic stem cells to cardiomyocytes. Acta Biomaterialia, 2014. **10**(2): p. 604-12.

[117] Candiello, J., et al., Early differentiation patterning of mouse embryonic stem cells in response to variations in alginate substrate stiffness. Journal of biological engineering, 2013. **7**(1): p. 9.

[118] Jaramillo, M., et al., Inducing endoderm differentiation by modulating mechanical properties of soft substrates. Journal of tissue engineering and regenerative medicine, 2015. **9**(1): p. 1-12.

[119] Task, K., et al., Systems level approach reveals the correlation of endoderm differentiation of mouse embryonic stem cells with specific microstructural cues of fibrin gels. Journal of the Royal Society, Interface / the Royal Society, 2014. **11**(95): p. 20140009.

[120] Zhang, X.N., et al., Analysis of Regulatory Network Involved in Mechanical Induction of Embryonic Stem Cell Differentiation. PloS one, 2012. **7**(4).

[121] Musah, S., et al., Glycosaminoglycan-binding hydrogels enable mechanical control of human pluripotent stem cell self-renewal. ACS nano, 2012. **6**(11): p. 10168-77.

[122] Candiello, J., et al., Biomechanical properties of native basement membranes. The FEBS journal, 2007. **274**(11): p. 2897-908.

[123] Otonkoski, T., et al., Unique basement membrane structure of human pancreatic islets: implications for beta-cell growth and differentiation. Diabetes, obesity & metabolism, 2008. **10 Suppl 4**: p. 119-27.

[124] Riopel, M. and R. Wang, Collagen matrix support of pancreatic islet survival and function. Frontiers in bioscience, 2014. **19**: p. 77-90.

[125] Goh, S.K., et al., Perfusion-decellularized pancreas as a natural 3D scaffold for pancreatic tissue and whole organ engineering. Biomaterials, 2013. **34**(28): p. 6760-6772.

[126] Singh, A.M., et al., Signaling network crosstalk in human pluripotent cells: a Smad2/3-regulated switch that controls the balance between self-renewal and differentiation. Cell stem cell, 2012. **10**(3): p. 312-26.

[127] Cho, C.H.H., et al., Inhibition of activin/nodal signalling is necessary for pancreatic differentiation of human pluripotent stem cells. Diabetologia, 2012. **55**(12): p. 3284-3295.

[128] Afrikanova, I., et al., Inhibitors of Src and Focal Adhesion Kinase Promote Endocrine Specification IMPACT ON THE DERIVATION OF beta-CELLS FROM HUMAN PLURIPOTENT STEM CELLS. Journal of Biological Chemistry, 2011. **286**(41): p. 36042-36052.

[129] Dennler, S., et al., Induction of sonic hedgehog mediators by transforming growth factor-beta: Smad3-dependent activation of Gli2 and Gli1 expression in vitro and in vivo. Cancer research, 2007. **67**(14): p. 6981-6.

[130] Sugimoto, M., et al., What is the nature of pancreatic consistency? Assessment of the elastic modulus of the pancreas and comparison with tactile sensation, histology, and occurrence of postoperative pancreatic fistula after pancreaticoduodenectomy. Surgery, 2014. **156**(5): p. 1204-1211.

[131] EPA, Toxicological Review of Barium and Compounds. Cincinnati, OH: Unitied States Environmental Protection Agency, 2005: p. 1-57.

[132] Qi, M., et al., Survival of human islets in microbeads containing high guluronic acid alginate crosslinked with Ca2+ and Ba2+. Xenotransplantation, 2012. **19**(6): p. 355-64.

[133] Kelly, O.G., et al., Cell-surface markers for the isolation of pancreatic cell types derived from human embryonic stem cells. Nature Biotechnology, 2011. **29**(8): p. 750-U114.

[134] Kroon, E., et al., Pancreatic endoderm derived from human embryonic stem cells generates glucose-responsive insulin-secreting cells in vivo. Nature Biotechnology, 2008. **26**(4): p. 443-52.

[135] Sui, L., et al., Transplantation of Human Embryonic Stem Cell-Derived Pancreatic Endoderm Reveals a Site-Specific Survival, Growth, and Differentiation. Cell Transplantation, 2013. **22**(5): p. 821-830.

[136] Tuch, B.E., T.C. Hughes, and M.D.M. Evans, Encapsulated pancreatic progenitors derived from human embryonic stem cells as a therapy for insulin-dependent diabetes. Diabetes-Metabolism Research and Reviews, 2011. **27**(8): p. 928-932.

[137] Narayanan, K., et al., Extracellular matrix-mediated differentiation of human embryonic stem cells: differentiation to insulin-secreting beta cells. Tissue engineering. Part A, 2014. **20**(1-2): p. 424-33.

[138] Saha, S., et al., TGFbeta/Activin/Nodal pathway in inhibition of human embryonic stem cell differentiation by mechanical strain. Biophysical journal, 2008. **94**(10): p. 4123-33.

[139] Saha, S., et al., Inhibition of human embryonic stem cell differentiation by mechanical strain. Journal of cellular physiology, 2006. **206**(1): p. 126-37.

[140] Allen, J.L., M.E. Cooke, and T. Alliston, ECM stiffness primes the TGFbeta pathway to promote chondrocyte differentiation. Molecular biology of the cell, 2012. **23**(18): p. 3731-42.

[141] Song, K., et al., Novel roles of Akt and mTOR in suppressing TGF-beta/ALK5-mediated Smad3 activation. The EMBO journal, 2006. **25**(1): p. 58-69.

[142] Remy, I., A. Montmarquette, and S.W. Michnick, PKB/Akt modulates TGF-beta signalling through a direct interaction with Smad3. Nature cell biology, 2004. **6**(4): p. 358-65.

[143] Nostro, M.C., et al., Stage-specific signaling through TGF beta family members and WNT regulates patterning and pancreatic specification of human pluripotent stem cells (vol 138, pg 861, 2011). Development, 2011. **138**(7): p. 1445-1445.

[144] Guo, T.X., et al., Factors Expressed by Murine Embryonic Pancreatic Mesenchyme Enhance Generation of Insulin-Producing Cells From hESCs. Diabetes, 2013. **62**(5): p. 1581-1592.

[145] Lopez-Carballo, G., et al., Activation of the phosphatidylinositol 3-kinase/Akt signaling pathway by retinoic acid is required for neural differentiation of SH-SY5Y human neuroblastoma cells. The Journal of biological chemistry, 2002. **277**(28): p. 25297-304.

[146] Gittes, G.K., Developmental biology of the pancreas: a comprehensive review. Developmental biology, 2009. **326**(1): p. 4-35.

[147] Shevde, L.A. and R.S. Samant, Nonclassical hedgehog-GLI signaling and its clinical implications. International journal of cancer. Journal international du cancer, 2014. **135**(1): p. 1-6.

[148] Mih, J.D., et al., A Multiwell Platform for Studying Stiffness-Dependent Cell Biology. Plos One, 2011. **6**(5).

[149] Ankam, S., et al., Substrate topography and size determine the fate of human embryonic stem cells to neuronal or glial lineage. Acta biomaterialia, 2013. **9**(1): p. 4535-45.

[150] Pan, F., et al., Topographic effect on human induced pluripotent stem cells differentiation towards neuronal lineage. Biomaterials, 2013. **34**(33): p. 8131-9.

[151] Flaim, C.J., S. Chien, and S.N. Bhatia, An extracellular matrix microarray for probing cellular differentiation. Nature methods, 2005. **2**(2): p. 119-25.

[152] Derda, R., et al., High-Throughput Discovery of Synthetic Surfaces That Support Proliferation of Pluripotent Cells. Journal of the American Chemical Society, 2010. **132**(4): p. 1289-1295.

[153] Zhang, D. and K.A. Kilian, Peptide microarrays for the discovery of bioactive surfaces that guide cellular processes: a single step azide-alkyne "click" chemistry approach. Journal of Materials Chemistry B, 2014. **2**(27): p. 4280-4288.

[154] Gobaa, S., et al., Artificial niche microarrays for probing single stem cell fate in high throughput. Nature methods, 2011. **8**(11): p. 949-55.

[155] Ranga, A., et al., 3D niche microarrays for systems-level analyses of cell fate. Nature communications, 2014. **5**: p. 4324.

[156] Yang, F., et al., Combinatorial extracellular matrices for human embryonic stem cell differentiation in 3D. Biomacromolecules, 2010. **11**(8): p. 1909-14.

[157] Lee, M.Y., et al., Three-dimensional cellular microarray for high-throughput toxicology assays. Proceedings of the National Academy of Sciences of the United States of America, 2008. **105**(1): p. 59-63.

[158] Fernandes, T.G., et al., Three-dimensional cell culture microarray for high-throughput studies of stem cell fate. Biotechnology and bioengineering, 2010. **106**(1): p. 106-18.

[159] Richardson, T., et al., Capsule stiffness regulates the efficiency of pancreatic differentiation of human embryonic stem cells. Acta biomaterialia, 2016.

[160] Lee, L.H., et al., Micropatterning of human embryonic stem cells dissects the mesoderm and endoderm lineages. Stem cell research, 2009. **2**(2): p. 155-62.

[161] Toyoda, T., et al., Cell aggregation optimizes the differentiation of human ESCs and iPSCs into pancreatic bud-like progenitor cells. Stem cell research, 2015. **14**(2): p. 185-197.

[162] Lei, Y. and D.V. Schaffer, A fully defined and scalable 3D culture system for human pluripotent stem cell expansion and differentiation. Proceedings of the National Academy of Sciences of the United States of America, 2013. **110**(52): p. E5039-48.

[163] Chen, V.C., et al., Scalable GMP compliant suspension culture system for human ES cells. Stem cell research, 2012. **8**(3): p. 388-402.

[164] Richardson, T., P.N. Kumta, and I. Banerjee, Alginate encapsulation of human embryonic stem cells to enhance directed differentiation to pancreatic islet-like cells. Tissue engineering. Part A, 2014. **20**(23-24): p. 3198-211.

[165] Kutner, M.H., Applied linear statistical models. 5th ed. The McGraw-Hill/Irwin series operations and decision sciences2005, Boston: McGraw-Hill Irwin. xxviii, 1396 p.

[166] Efron, B. and R. Tibshirani, An introduction to the bootstrap. Monographs on statistics and applied probability1993, New York: Chapman & Hall. xvi, 436 p.

[167] Mathew, S., et al., Analysis of alternative signaling pathways of endoderm induction of human embryonic stem cells identifies context specific differences. Bmc Systems Biology, 2012. **6**: p. 154.

[168] Gong, H.B., et al., In Vivo Imaging of Xenograft Tumors Using an Epidermal Growth Factor Receptor-Specific Affibody Molecule Labeled with a Near-infrared Fluorophore. Neoplasia, 2010. **12**(2): p. 139-U59.

[169] Tong, R., et al., Polylactide Nanoparticles Containing Stably Incorporated Cyanine Dyes for In Vitro and In Vivo Imaging Applications. Microscopy Research and Technique, 2010. **73**(9): p. 901-909.

[170] Tichauer, K.M., et al., In Vivo Quantification of Tumor Receptor Binding Potential with Dual-Reporter Molecular Imaging. Molecular Imaging and Biology, 2012. **14**(5): p. 584-592.

[171] Task, K., et al., Systems level approach reveals the correlation of endoderm differentiation of mouse embryonic stem cells with specific microstructural cues of fibrin gels. Journal of the Royal Society Interface, 2014. **11**(95).

[172] Mathew, S., et al., Analysis of alternative signaling pathways of endoderm induction of human embryonic stem cells identifies context specific differences. Bmc Systems Biology, 2012. **6**.

[173] Stock, P.G. and M.S. German, A Path to Insulin Independence: "The End of the Beginning". Cell stem cell, 2016. **18**(4): p. 431-433.

[174] Califano, J.P. and C.A. Reinhart-King, Substrate Stiffness and Cell Area Predict Cellular Traction Stresses in Single Cells and Cells in Contact. Cellular and molecular bioengineering, 2010. **3**(1): p. 68-75.

[175] Chowdhury, F., et al., Soft substrates promote homogeneous self-renewal of embryonic stem cells via downregulating cell-matrix tractions. Plos One, 2010. **5**(12): p. e15655.

[176] Fu, J., et al., Mechanical regulation of cell function with geometrically modulated elastomeric substrates. Nature methods, 2010. **7**(9): p. 733-6.

[177] Ghosh, K., et al., Cell adaptation to a physiologically relevant ECM mimic with different viscoelastic properties. Biomaterials, 2007. **28**(4): p. 671-9.

[178] Cavo, M., et al., Microenvironment complexity and matrix stiffness regulate breast cancer cell activity in a 3D in vitro model. Scientific reports, 2016. **6**: p. 35367.

[179] Banerjee, A., et al., The influence of hydrogel modulus on the proliferation and differentiation of encapsulated neural stem cells. Biomaterials, 2009. **30**(27): p. 4695-9.

[180] Schaffer, A.E., et al., Nkx6 Transcription Factors and Ptf1a Function as Antagonistic Lineage Determinants in Multipotent Pancreatic Progenitors. Developmental Cell, 2010. **18**(6): p. 1022-1029.

[181] Wu, J., Y. Fan, and E.S. Tzanakakis, Increased Culture Density Is Linked to Decelerated Proliferation, Prolonged G1 Phase, and Enhanced Propensity for Differentiation of Self-

Renewing Human Pluripotent Stem Cells. Stem Cells and Development, 2014. **24**(7): p. 892-903.

[182] Stephan, S., W.E. Johnson, and S. Roberts, The influence of nutrient supply and cell density on the growth and survival of intervertebral disc cells in 3D culture. European cells & materials, 2011. **22**: p. 97-108.

[183] Nelson, C.M. and C.S. Chen, Cell-cell signaling by direct contact increases cell proliferation via a PI3K-dependent signal. FEBS letters, 2002. **514**(2-3): p. 238-42.

[184] Gray, D.S., et al., Engineering amount of cell-cell contact demonstrates biphasic proliferative regulation through RhoA and the actin cytoskeleton. Experimental Cell Research, 2008. **314**(15): p. 2846-2854.

[185] Tang, J., R. Peng, and J. Ding, The regulation of stem cell differentiation by cell-cell contact on micropatterned material surfaces. Biomaterials, 2010. **31**(9): p. 2470-6.

[186] Ludwig, T.E., et al., Feeder-independent culture of human embryonic stem cells. Nature methods, 2006. **3**(8): p. 637-646.

[187] Serra, M., et al., Improving expansion of pluripotent human embryonic stem cells in perfused bioreactors through oxygen control. Journal of Biotechnology, 2010. **148**(4): p. 208-215.

[188] Chen, A.K.L., et al., Critical microcarrier properties affecting the expansion of undifferentiated human embryonic stem cells. Stem Cell Research, 2011. **7**(2): p. 97-111.

[189] Kehoe, D.E., et al., Scalable stirred-suspension bioreactor culture of human pluripotent stem cells. Tissue engineering. Part A, 2010. **16**(2): p. 405-21.

[190] Schulz, T.C., et al., A scalable system for production of functional pancreatic progenitors from human embryonic stem cells. Plos One, 2012. **7**(5): p. e37004.

[191] Abbasalizadeh, S., et al., Bioprocess development for mass production of size-controlled human pluripotent stem cell aggregates in stirred suspension bioreactor. Tissue Eng Part C Methods, 2012. **18**(11): p. 831-51.

[192] Amit, M., et al., Dynamic suspension culture for scalable expansion of undifferentiated human pluripotent stem cells. Nat Protoc, 2011. **6**(5): p. 572-9.

[193] Chen, V.C., et al., Scalable GMP compliant suspension culture system for human ES cells. Stem Cell Res, 2012. **8**(3): p. 388-402.

[194] Krawetz, R., et al., Large-scale expansion of pluripotent human embryonic stem cells in stirred-suspension bioreactors. Tissue Eng Part C Methods, 2010. **16**(4): p. 573-82.

[195] Olmer, R., et al., Long term expansion of undifferentiated human iPS and ES cells in suspension culture using a defined medium. Stem Cell Res, 2010. **5**(1): p. 51-64.

[196] Olmer, R., et al., Suspension culture of human pluripotent stem cells in controlled, stirred bioreactors. Tissue Eng Part C Methods, 2012. **18**(10): p. 772-84.

[197] Singh, H., et al., Up-scaling single cell-inoculated suspension culture of human embryonic stem cells. Stem Cell Res, 2010. **4**(3): p. 165-79.

[198] Zweigerdt, R., et al., Scalable expansion of human pluripotent stem cells in suspension culture. Nat Protoc, 2011. **6**(5): p. 689-700.

[199] Wang, Y., L. Cheng, and S. Gerecht, Efficient and scalable expansion of human pluripotent stem cells under clinically compliant settings: a view in 2013. Ann Biomed Eng, 2014. **42**(7): p. 1357-72.

[200] Kurosawa, H., Application of Rho-associated protein kinase (ROCK) inhibitor to human pluripotent stem cells. J Biosci Bioeng, 2012. **114**(6): p. 577-81.

[201] Rodin, S., et al., Clonal culturing of human embryonic stem cells on laminin-521/E-cadherin matrix in defined and xeno-free environment. Nat Commun, 2014. **5**: p. 3195.

[202] Nagaoka, M., et al., Culture of human pluripotent stem cells using completely defined conditions on a recombinant E-cadherin substratum. BMC Dev Biol, 2010. **10**: p. 60.

[203] Melkoumian, Z., et al., Synthetic peptide-acrylate surfaces for long-term self-renewal and cardiomyocyte differentiation of human embryonic stem cells. Nature Biotechnology, 2010. **28**(6): p. 606-U95.

[204] Deng, Y., et al., Long-term self-renewal of human pluripotent stem cells on peptide-decorated poly(OEGMA-co-HEMA) brushes under fully defined conditions. Acta biomaterialia, 2013. **9**(11): p. 8840-50.

[205] Higuchi, A., et al., Long-term xeno-free culture of human pluripotent stem cells on hydrogels with optimal elasticity. Scientific reports, 2015. **5**: p. 18136.

[206] Rowley, J.A., G. Madlambayan, and D.J. Mooney, Alginate hydrogels as synthetic extracellular matrix materials. Biomaterials, 1999. **20**(1): p. 45-53.

[207] Sinaga, E., et al., Increasing paracellular porosity by E-cadherin peptides: discovery of bulge and groove regions in the EC1-domain of E-cadherin. Pharm Res, 2002. **19**(8): p. 1170-9.

[208] Chappuis-Flament, S., Multiple cadherin extracellular repeats mediate homophilic binding and adhesion. The Journal of Cell Biology, 2001. **154**(1): p. 231-243.

[209] Renaud-Young, M. and W.J. Gallin, In the first extracellular domain of E-cadherin, heterophilic interactions, but not the conserved His-Ala-Val motif, are required for adhesion. J Biol Chem, 2002. **277**(42): p. 39609-16.

[210] Kobayashi, N., et al., Inhibition of e-cadherin-mediated homotypic adhesion of Caco-2 cells: a novel evaluation assay for peptide activities in modulating cell-cell adhesion. J Pharmacol Exp Ther, 2006. **317**(1): p. 309-16.

[211] Chen, T., et al., E-cadherin-mediated cell-cell contact is critical for induced pluripotent stem cell generation. Stem Cells, 2010. **28**(8): p. 1315-25.

[212] Boggon, T.J., et al., C-cadherin ectodomain structure and implications for cell adhesion mechanisms. Science, 2002. **296**(5571): p. 1308-13.

[213] Parisini, E., et al., The crystal structure of human E-cadherin domains 1 and 2, and comparison with other cadherins in the context of adhesion mechanism. Journal of molecular biology, 2007. **373**(2): p. 401-11.

[214] Kiptoo, P., et al., Enhancement of drug absorption through the blood-brain barrier and inhibition of intercellular tight junction resealing by E-cadherin peptides. Mol Pharm, 2011. **8**(1): p. 239-49.

[215] Makagiansar, I.T., et al., Improving the selectivity of HAV-peptides in modulating E-cadherin-E-cadherin interactions in the intercellular junction of MDCK cell monolayers. Pharm Res, 2001. **18**(4): p. 446-53.

[216] Noe, V., et al., Inhibition of adhesion and induction of epithelial cell invasion by HAV-containing E-cadherin-specific peptides. J Cell Sci, 1999. **112 (Pt 1)**: p. 127-35.

[217] Bian, L.M., et al., Hydrogels that mimic developmentally relevant matrix and N-cadherin interactions enhance MSC chondrogenesis. Proceedings of the National Academy of Sciences of the United States of America, 2013. **110**(25): p. 10117-10122.

[218] Zhu, M.L., et al., Hydrogels functionalized with N-cadherin mimetic peptide enhance osteogenesis of hMSCs by emulating the osteogenic niche. Biomaterials, 2016. **77**: p. 44-52.

[219] Melkoumian, Z., et al., Synthetic peptide-acrylate surfaces for long-term self-renewal and cardiomyocyte differentiation of human embryonic stem cells. Nature Biotechnology, 2010. **28**(6): p. 606-10.

[220] Nagaoka, M., et al., Culture of human pluripotent stem cells using completely defined conditions on a recombinant E-cadherin substratum. Bmc Developmental Biology, 2010. **10**.

[221] Rodin, S., et al., Clonal culturing of human embryonic stem cells on laminin-521/E-cadherin matrix in defined and xeno-free environment. Nature communications, 2014. **5**.

[222] Sinaga, E., et al., Increasing paracellular porosity by E-cadherin peptides: discovery of bulge and groove regions in the EC1-domain of E-cadherin. Pharmaceutical research, 2002. **19**(8): p. 1170-9.

[223] Kiptoo, P., et al., Enhancement of Drug Absorption through the Blood-Brain Barrier and Inhibition of Intercellular Tight Junction Resealing by E-Cadherin Peptides. Molecular Pharmaceutics, 2011. **8**(1): p. 239-249.

[224] Bardy, J., et al., Microcarrier suspension cultures for high-density expansion and differentiation of human pluripotent stem cells to neural progenitor cells. Tissue engineering. Part C, Methods, 2013. **19**(2): p. 166-80.

[225] Ting, S., et al., An intermittent rocking platform for integrated expansion and differentiation of human pluripotent stem cells to cardiomyocytes in suspended microcarrier cultures. Stem cell research, 2014. **13**(2): p. 202-213.

[226] Haque, A., et al., The effect of recombinant E-cadherin substratum on the differentiation of endoderm-derived hepatocyte-like cells from embryonic stem cells. Biomaterials, 2011. **32**(8): p. 2032-42.

[227] D'Amour, K.A., et al., Production of pancreatic hormone-expressing endocrine cells from human embryonic stem cells. Nature Biotechnology, 2006. **24**(11): p. 1392-401.

[228] Lim, J.J., et al., Three-Step Method for Proliferation and Differentiation of Human Embryonic Stem Cell (hESC)-Derived Male Germ Cells. Plos One, 2014. **9**(4).

[229] Higuchi, A., et al., Physical Cues of Biomaterials Guide Stem Cell Differentiation Fate. Chemical Reviews, 2013. **113**(5): p. 3297-3328.

[230] Vegas, A.J., et al., Long-term glycemic control using polymer-encapsulated human stem cell-derived beta cells in immune-competent mice. Nature Medicine, 2016. **22**(3): p. 306-311.

[231] Tannenbaum, S.E., et al., Derivation of xeno-free and GMP-grade human embryonic stem cells--platforms for future clinical applications. Plos One, 2012. **7**(6): p. e35325.